THE PULSE RADIOLYSIS OF ALKYL IODIDES AND OXYGEN IN THE GAS PHASE

BY

JORGE E. RAMIREZ

A DISSERTATION PRESENTED TO THE GRADUATE COUNCIL OF
THE UNIVERSITY OF FLORIDA
IN PARTIAL FULFILLMENT OF THE REQUIREMENTS FOR THE
DEGREE OF DOCTOR OF PHILOSOPHY

UNIVERSITY OF FLORIDA

1981

Dedicated to

my parents Luis and Anita

and my nephews Ray and David

ACKNOWLEDGMENTS

The author expresses his sincere appreciation to his research director, Prof. Robert J. Hanrahan, and Prof. M. Luis Muga for their advice, encouragement, and friendship throughout this work. He also thanks Prof. Phillip M. Achey for the many stimulating and candid conversations.

Special thanks are given to Kelley St. Charles, Bob Doyle, and Dawit Teclemariam for their friendship and assistance, especially when "the going got tough," on and off the field.

Special appreciation is given to John Kurtz, Mike Collins, and John Pooser for their friendship and all the "red, white, and blue."

His deepest thanks are given to the WGAS gang in Miami, Robert Pridgen, Nestor Herrera, Martin Miller, Lynn McCullough, and especially Joe Benitoa for the "best years of our lives."

Above all, the author expresses his deepest love and gratitude to his father and mother and his brothers and their families whose love and understanding made this work possible.

Thanks to Frank Ramos for making many of the drawings in this text.

Thanks Wil.

TABLE OF CONTENTS

Page

ACKNOWLEDGMENTS iii

LIST OF TABLES v

LIST OF FIGURES vi

ABSTRACT ix

I. INTRODUCTION 1

A. Foreward 1
B. Review of Previous Work 2

II. EXPERIMENTAL APPARATUS AND PROCEDURES 10

A. Monochromators and Light Transport Apparatus 10
B. Optical Efficiencies 27
C. Reaction Cells 34
D. Spectrophotometry 43
E. Lamp Systems 49
F. Febetron 706 System 74
G. Transient Recorder and Computer System 77
H. Computer Programs 80
I. Reagents and Their Purification 82
J. Sample Preparation 84
K. Sample Irradiation 87

III. THE GAS PHASE PULSE RADIOLYSIS OF ALKYL IODIDES 89

A. Experimental Results 89
B. Discussion 101

IV. FORMATION OF GROUND STATE OZONE IN THE PULSE RADIOLYSIS OF OXYGEN 105

A. Experimental Results 105
B. Discussion 110

APPENDIX PULSE RADIOLYSIS COMPUTER PROGRAMS 119

REFERENCES 127

BIOGRAPHICAL SKETCH 135

LIST OF TABLES

Table Page

1 I^* Quenching Rates by RI 95

2 I^* Quenching Rates by the Medium 98

3 I^* Fraction and Branching Ratios 100

LIST OF FIGURES

Figure		Page
1	Entrance and exit slit system flange adaptation to the Jarrell-Ash monochromator	12
2	Coupling arrangement from the lamp flange to the entrance slit flange (Fig. 1)	13
3	Exit slit flange adapter flange and window mechanism for connecting the exit slit flange to the PMT housing, Model 3262, for end-on PMTs	15
4	Quartz rod light pipe guides and housing	17
5	Nylon guides	18
6	Lead shields for PMT photocathodes in the Pacific Precision Instruments PMT housings	20
7	Single-pass cell arrangement for VUV work	22
8	Vacuum extension flange and lens focusing arrangement ..	23
9	McPherson 218 exit window flange and window	25
10	High vacuum pumping system for the McPherson 218 monochromator	26
11	University of Florida Pulse Radiolysis System	28
12	90^{o} optical configuration using a 10 or 7.5 cm focal length parabolic mirror	29
13	Iodine discharge lamp spectrum with nitrogen flushing of the optical path	32
14	Iodine discharge lamp spectrum with helium flushing of the optical path	33
15	Single-pass cell with six equal flange ports	35
16	Multiple-pass reaction cell arrangement for visible and UV studies	38

LIST OF FIGURES (continued)

Figure Page

17 Multiple-pass reaction cell mirror system with MgF_2 coated first surface aluminum mirrors 39

18 Reaction cell-Febetron 706 face plate coupling mechanism 41

19 Complete assembly of the reaction cell flange onto the Febetron face plate 42

20 Photomultiplier tube base schematic used with EMI 9750 QB and 9856B PMTs and Model 3262 housing 46

21 Photomultiplier tube base schematic used with EMI 9783B side window PMT and Model 3150 housing 48

22 Lamp system 51

23 Evenson cavity 53

24 Microwave discharge lamp bodies 56

25 Lamp window and coupling flange 57

26 Iodine emission spectrum from the microwave discharge lamp using a sodium salicylate fluorescent screen to cut off stray visible light from other orders 62

27 Iodine discharge lamp spectrum after 5 minutes of active pumping on the McPherson 218 64

28 Iodine discharge lamp spectrum after 10 minutes of active pumping on the McPherson 218 65

29 Chemical compound absorption interference in the spectral range 170 to 190 nm (Fig. 26) 66

30 Absorption band for 2.5 torr methyl iodide in the 200 nm region 67

31 Emission spectrum of OH from the microwave discharge lamp 69

32 Mercury lamp system in DC operation mode 70

33 Hg lamp intensity versus time for various input sensitivities of the transient recorder with the reaction cell evacuated 72

LIST OF FIGURES (continued)

Figure Page

34 Hg lamp intensity versus time for two initial oxygen pressures and vacuum in the reaction cell at 1 VFS transient recorder input sensitivity 73

35 Febetron 706 system 76

36 Vacuum line and pumping system 85

37 Graphical display of optical signal versus time for a single Febetron pulse 90

38 Graphical display of optical signal versus time for three Febetron pulses summed into the buffer 91

39 Curve fit of data from Fig. 38 93

40 Pulse radiolysis of methyl iodide with 180 torr argon 96

41 Pulse radiolysis of trifluoromethyl iodide with 575 torr argon 97

42 Computer calculation for I* deactivation, intermediates, and products 103

43 Ozone absorption growth monitored at 253.7 nm following the pulse radiolysis of 750 torr O_2 106

44 Dosimetry: Ozone yield in the pulse radiolysis of oxygen measured at 253.7 nm 107

45 First-order plot of ozone absorption growth (Fig. 43) following the pulse radiolysis of 750 torr O_2 108

46 Ground vibrational state ozone formation rate versus O_2 pressure 111

47 Computer calculation for a=b=0.2 and c=0.6 113

48 Computer calculation for a=0.1, b=0.6, and c=0.3 115

Abstract of Dissertation Presented to the Graduate Council
of the University of Florida in Partial Fulfillment of the Requirements
for the Degree of Doctor of Philosophy

THE PULSE RADIOLYSIS OF ALKYL IODIDES AND OXYGEN IN THE GAS PHASE

By

Jorge E. Ramirez

December, 1981

Chairman: Dr. R.J. Hanrahan
Major Department: Chemistry

A pulse radiolysis facility for the study of fast chemical kinetics in the gas phase, based on a Febetron 706 electron beam accelerator, has been established at the University of Florida Radiation Chemistry Laboratories. Maximum accelerator specifications are 600 keV electron energy, 8000 amps, and 10 joules per pulse; pulse width is 3 nanoseconds (FWHM). Hardware has been developed for studies in the ultraviolet and vacuum ultraviolet regions using absorption spectrophotometry.

Parameters relevant to a linear electron beam initiated atomic iodine laser, which would lase on the transition $5^{2}P_{1/2}$ $(I^{*}) \rightarrow 5^{2}P_{3/2}$ (I), have been investigated by pulse radiolysis. Kinetic data for the parent compound quenching of I^{*} were obtained by variation of the parent compound pressure at constant buffer gas pressure and observing I^{*} decay rates versus time. Deactivation rate constants for the perfluoroalkyl iodides were found to be much lower than for alkyl iodides (in cm^{3}/molec s): CH_3I, $2.0 \pm 0.1 \times 10^{-13}$; C_2H_5I, $5.0 \pm 0.3 \times 10^{-13}$; CF_3I, $8.8 \pm 1.5 \times 10^{-16}$; C_2F_5I, $9.7 \pm 1.0 \times 10^{-15}$; i-$C_3F_7I$, $1.7 \pm 0.1 \times 10^{-15}$; C_4F_9I, $1.8 \pm 0.1 \times 10^{-14}$.

The extent of population inversion was investigated by measuring initial excited state and ground state atomic iodine concentrations and calculating the branching ratio, $[I']_0/[I]_0$: CH_3I, 2.7; CF_3I, 3.8; C_2F_5I, 2.7; i-C_3F_7I, 3.2; C_4F_9I, 1.8. Perfluoromethyl iodide showed the largest population inversion from electron beam irradiation.

Using formation of O_3 from O_2 as the dosimeter (G = 13.8 molecules/100 eV for ozone), energy deposited per electron pulse in 750 torr O_2 was 7.3×10^{18} eV/g. Spectrophotometric detection of ozone utilized the 253.7 nm Hg line.

The rate of formation of ground vibrational state ozone in the pulse radiolysis of oxygen was followed using the 253.7 nm Hg line. The rate of formation was found to be nearly second-order with a rate constant of $4.1 \pm 0.4 \times 10^{-15}$ cm^3/molec s. It is formed from direct combination of oxygen atoms and oxygen molecules and from collisional quenching of vibrationally excited ozone and/or an electronically excited ozone precursor, probably ozone ($^3B_2$).

I. INTRODUCTION

A. Foreward

The establishment of a pulse radiolysis system was undertaken to expand the chemical kinetics facilities of the University of Florida Radiation Chemistry Laboratory. Major efforts were made to design the system for the greatest versatility for the studies undertaken as well as for possible future studies.

Pulse radiolysis is a technique for studying the kinetics of species involved in the fast elementary steps of a reaction process following sample irradiation by a short pulse of ionizing radiation. In general, the transient species are of major interest. The direct study of fast processes has two basic requirements. First, the process must be initiated in a time scale which is shorter than or comparable to the process being observed. Second, the process to be observed must have associated with it some detectable change in one or more physical parameters.

To meet the first requirement, the pulse radiolysis system was developed around a Febetron 706 electron beam (e-beam) accelerator. A maximum 8 kiloamp beam of maximum 600 keV electrons in a pulse duration of 3 nanoseconds (FWHM) could be delivered for sample irradiation. The second requirement must be met by the chemical system chosen for study.

To aid the study of fast chemical processes, a microcomputer-based data acquisition system was coupled to the pulse radiolysis system. The computer system was used to acquire, analyze, and store data.

The chemical studies of alkyl iodides and perfluoroalkyl iodides, relevant to the atomic iodine laser, were undertaken to help elucidate previous photolysis work. Also, since the flash photolysis and pulse radiolysis techniques are very similar, previous studies served as references as to the validity of data acquired during the development of the pulse radiolysis system.

The oxygen-ozone studies were undertaken to establish a chemical dosimeter for our Febetron 706 system.

B. Review of Previous Work

Pulse radiolysis

At the University of Florida Radiation Chemistry Laboratory there has been a continuous interest in the reaction kinetics and mechanisms of simple alkyl halide systems.[1-5] Of particular interest in these studies has been the identity and reactivity of important transient species.

Historically, pulse radiolysis was first developed to study intermediates which had been postulated in radiation initiated chemical reaction systems.[6-8] Though the technique was developed by radiation chemists, it was quickly employed for the study of transients of broader chemical interest.[8-11] The developmental work on pulse radiolysis was carried out on liquid phase systems. The use of liquid systems was dictated by the availability of only high-energy low-current accelerators. Densities of liquids were convenient for sufficient interaction of the system under study with the ionizing radiation (greater than 2 MeV), in order to deposit enough energy to provide an observable concentration of transient species. In order for gases to absorb enough energy from high-energy electron beams, high pressure systems (10-100 atm) were initially used.[12-14] Gas phase work at an atmosphere or less was made possibly by advances in detection techniques and the development of high pulse current accelerators like the Febetron 706.[14]

In principle, pulse radiolysis is similar to flash photolysis. The photoflash and photodissociation of molecules is replaced by a short pulse of high-energy electrons with subsequent excitation and ionization of the molecules by electron impact. Subsequent dissociation can occur by unimolecular decomposition or by collision with other atoms or molecules. The important properties of the electron pulse are its maximum energy, pulse current, time profile, cross-sectional homogeneity, and divergence.

The maximum electron energy is directly related to the e-beam's penetration in a reaction cell; therefore, it must be large enough to sufficiently irradiate the chemical system. The concentration of the species of interest is directly related to the number of interactions between the chemical system and the e-beam. This is determined by the pulse current. For convenient time resolution of the observed signal the time profile of the pulse must be shorter than the half-life of the transient of interest. The cross-sectional homogeneity and the divergence of the beam are important for uniform irradiation of the chemical system. This helps ensure optical sampling of a homogeneous reaction region.

In its present form, the technique of pulse radiolysis requires a high level of experimental sophistication.[10,13-16] Spectrophotometric detection techniques have replaced less sensitive spectrophotographic detection techniques.[14] The efficiency of the optical system is of great importance for observation of useful signals. Although similar e-beam sources have been used in previous studies, the associated optical systems were customized for each individual laboratory.

The optical systems were designed with two major considerations. First, optical throughput to the detector had to be maximized in order to achieve the best signal-to-noise ratios possible.[14,17] Second, due to sources of noise associated with pulsed electron beam sources, simple optical concepts took on elaborate physical designs in order to appropriately shield the photodetector and electronic circuitry.[10,14]

A desire to carry out studies in the ultraviolet (UV) and vacuum ultraviolet (VUV) regions further complicated the optical spectrophotometry systems. Specific attention had to be given to the properties of the optical materials and detectors at these wavelengths. Optical system throughput efficiencies were especially important in these regions.[18-20]

In order to facilitate data acquisition and reduction, on-line computer systems have been developed at various levels of sophistication.[21-24] These systems have greatly reduced the time required for data analysis. The quantity and quality of the data processed in a given time were greatly increased by the use of on-line computers.[22]

The pulse radiolysis system in our laboratory was designed to carry out low pressure (atmospheric and below) gas phase studies in the UV and VUV. Once operational, the system was used to study transients important in the operation of an iodine atom chemical laser.

Alkyl iodides-atomic iodine studies

Laser action on the atomic transition

$$5\ ^2P_{1/2}\ (I^*) \rightarrow 5\ ^2P_{3/2}\ (I), \qquad \text{I-1}$$

where I* represents the excited state atom and I represents the ground state atom, at 1.315 microns, was first reported by Kasper and Pimentel.[25] Further studies raised interest in the dynamics of the photolysis of alkyl iodides.[26] Of main importance to the lasing action of the systems is the production efficiency of the excited state atom, I*, its rate of deactivation, and the the initial branching ratio. The initial branching ratio is the ratio of initial concentrations of excited state atoms to ground state atoms,

$$\Phi = [I^*]_0\ /\ [I]_0\ . \qquad \text{I-2}$$

In the cases where the branching ratio is large and where other threshold requirements necessary for lasing are met, a high laser gain may be achieved.

Since the above transition is electric dipole forbidden, the mean radiative lifetime of the excited state is relatively long (0.13s).[27] Spin orbit relaxation by emission or by collisional quenching competes with chemical reaction of I*. If collisional quenching and chemical reaction are slow relative to emission, then a population inversion may be maintained and the excited atom population can initiate and propagate stimulated emission in a laser cavity.

Further interest in the alkyl iodide systems was generated when it was confirmed that the branching ratio was large for the photolysis of several alkyl iodides.[28] These studies were carried out using the kinetic spectrophotographic detection technique and suffered from parent alkyl iodide absorption interference in the region of interest, especially in the VUV.[29,30]

Several gas phase studies of the photolysis of alkyl iodide systems have been carried out.[31-46] Also, gas phase radiation chemical studies of these systems have been carried out.[1,23,47] Many of these studies were directly stimulated by the need to understand the energetics and kinetics of potential atomic iodine laser systems.[28,32-39,41-45] Specific interest[36,39,44] was further stimulated by the possibility of initiating thermonuclear fusion by laser irradiation using the photoinitiated atomic iodine laser.[48-53]

In general, most of these studies have used detection of I* by absorption in the UV (206.2 nm) and VUV (179.9 nm) and by its emission at 1.315 microns in the infrared (IR). The more sensitive spectrophotometric technique[17,37] has replaced the spectrophotographic technique[42] in the absorption experiments. IR detection[43,45] is still a very useful technique for emission studies[40] and compliments the absorption studies.

Mass spectrometric analyses of flash[34] and laser[32] photodissociated fragments have also been carried out. The latter study yielded much information about the energy distribution of the nascent photofragments following laser photolysis of methyl iodide at 266 nm.

Laser gain studies have yielded pressure dependent information about the atomic iodine laser[46] as well as kinetic data on I* deactivation.[39]

In recent studies,[32-39,41-46] except where laser photolysis[32,35] and VUV photolysis[33] were used, photoinitiation was carried out with broadband flash lamps emitting in the 200-300 nm absorption band of the perfluoroalkyl and alkyl iodides.[29,30] The use of high energy linear e-beams (pulse radiolysis) as the initiating source for the study of deactivation rate constants has only been reported by this laboratory,[23] although electron transverse discharge excitation of the atomic iodine laser has been previously reported and modeled.[53,54]

More recently the use of a solar pumped iodine laser for power transmission in space has been modeled[55] and tested.[56] These, as well as the high power lasers,[48,51] used the perfluoroalkyl iodides as the source of atomic iodine. Although many studies have been made of alkyl iodides, far less work has been done on the perfluoroalkyl iodides and thus, in general, literature values of rate constants used in modeling of the laser contained many discrepancies.[53]

Studies of the alkyl and perfluoroalkyl iodides have been carried out using the pulse radiolysis system in this laboratory. These results were compared, where appropriate, to other established results.

Oxygen-ozone studies

The reaction of oxygen atoms with molecular oxygen has been of considerable interest in the study of the atmosphere.[57-59] Similarly the dynamics of ozone decomposition has been investigated because of its importance in atmospheric chemistry.[60] The ozone formation reaction is also important in the radiation chemistry of oxygen-containing systems.

The reaction

$$O + O_2 + M \rightarrow O_3 + M \qquad \text{I-3}$$

has been extensively investigated.[58,59,61-78] Recent methods used in these studies have included direct observation of ozone formation in the Hartley band region (200-300 nm)[79,80] via fast absorption spectroscopy using pulse radiolysis[61-64,71-73] and flash photolysis[62,74-77]; flash photolysis-resonance fluorescence[59,78]; time-resolved infrared detection of vibrationally excited ozone[74,75]; and direct observation of oxygen atom disappearance via atomic resonance absorption.[58,65,66]

The oxygen-ozone system was reinvestigated in the course of setting-up the pulse radiolysis facility in our laboratory, primarily because it is a convenient gas-phase dosimeter which has been studied with a similar high dose-rate e-beam accelerator.[63] Since the ground state of ozone could be monitored conveniently with an intense mercury resonance lamp, it was convenient to carry out some kinetic studies along with the observations needed for the dosimetry work.

The time-resolved behavior of the absorption spectrum of ozone in the 200-350 nm region was first observed by Hochanadel et al.[62] They attributed absorption at wavelengths other than at the normal ozone ground state maximum near 260 nm to vibrationally excited ground state ozone formed in Reaction I-3 with molecular oxygen as the third body. Riley and Cahill observed a second absorption maximum near 315 nm which they interpreted as a transient species other than vibrationally excited ozone, because of its simple first-order decay kinetics.[72] The kinetics of vibrationally excited ozone cascading downward through its vibrational levels was expected to be more complex than the simple process observed at these wavelengths.[62] Bevan and Johnson observed two transient species absorbing with maxima near 285 and 310 nm and assumed that they were due to vibrationally excited ozone states, kinetically distinguishable from the ground state.[73] Von Rosenberg and Trainor observed vibrational excitation in two vibrational modes of ozone formed from Reaction I-3.[74,75] Using flash photolysis and time-resolved IR detection they were able to determine energy partitioning in IR-active products, vibrational relaxation rates, and recombination rates. They suggested that the species previously observed near 310 nm[72,73] was vibrationally excited ozone and/or electronically excited ozone, which was far enough below the dissociation limit to make cascading more probable than dissociation. They further suggested that the absorption maximum near 310 nm could be the ozone $^3B_2$ bound electronic state.[74]

Recent determinations which used oxygen as the third body and monitored oxygen atom disappearance concluded that the overall rate constant for Reaction I-3 lies between 5.7-6.9 x 10^{-34} $cm^6/molec^2$ s [58,59] in agreement with earlier studies.[65] In studies where ground vibrational state ozone formation was monitored, the apparent rate of formation was consistently slower than the rate of oxygen atom disappearance. This anomaly has been attributed to vibrationally and/or electronically excited ozone which was not being directly monitored.[77] It was suggested that the proper measurement of ozone should be the integrated absorbance over the entire Hartley band which would include all ozone species.[76,77] Kleindienst et al. modeled ozone formation in the flash photolysis of oxygen-ozone mixtures by assuming that the $^3B_2$ state of ozone acted as the unobserved intermediate and needed to account for the anomaly in the observed rate of recombination.[77] Using the same assumption the data for ground vibrational state ozone formation monitored at 253.7 nm in the pulsed electron radiolysis of pure oxygen have been modeled.

II. EXPERIMENTAL APPARATUS AND PROCEDURES

A. Monochromators and Light Transport Apparatus

In the early stages of this work Baird Atomic Interference filters were used for wavelength isolation. These were broadband filters and only total light changes in a 20-40 nm region around the central wavelength could be detected. Also, they did not provide useful throughput of light for our purposes. Only exploratory work was carried out under these conditions. Subsequently, two types of monochromators were used: a Jarrell-Ash Model 82-415SP 0.25 meter monochromator and a McPherson 218 0.3 meter monochromator.

0.25 meter monochromator

The Jarrell-Ash monochromator was used during the major part of the development of the pulse radiolysis system. It was also used for the preliminary work on the excited atomic iodine state at 206.2 nm.[23] The size of the monochromator, 17.7 x 22.1 x 21.4 cm, along with its specifications (Jarrell-Ash Division, Fisher Scientific Co.) made it attractive for use with the close geometry dictated by our laboratory space. The grating used has 1180 G/mm with 3.3 nm/mm linear dispersion and effective aperture of f/3.5. A wavelength motor drive of 100 nm/minute was coupled to the wavelength drive knob to aid gathering spectra on a Photovolt Corporation Model 43 chart recorder.

Three modifications had to be made on the original design of the monochromator to adapt it to the resonance lamp, reaction cell, optics, and photomultiplier housing.

First, the slit arrangement provided with the monochromator could not be directly adapted to our purposes so a new arrangement was designed, Figure 1. The flange fits into the hole where the original slit flange fit into the body of the monochromator, and is bolted to the monochromator body making an o-ring seal. The slit bodies were designed to be screwed into the flange using a tool which fits into the two small holes in the slit body (front view of the slit body). The slits and the flange were threaded with forty threads per inch to allow small changes in position per half revolution of the slit body so the best possible focus could be achieved. In order to preserve the integrity of the threads, the slit bodies were made of brass and the flange was made of aluminum. A Helium-Neon laser was used to help determine the best possible optical focusing arrangement. The entrance slit flange could be aligned and secured to the reaction cell body by its four through holes and four bolts on the cell body.

Next, in order to conveniently look at the emission spectrum from the resonance lamp while directly coupled to the monochromator, an adapter flange was designed, Figure 2. The flange had a hole (not pictured) threaded into the flange cavity which, when combined with a screw whose threads has been ground down on one side and an o-ring for a washer, served as a flushing outlet port. The flushing system will be described later.

Finally, another adapter flange was built to allow direct coupling of the Pacific Photometric Instruments Model 3262 photomultiplier tube

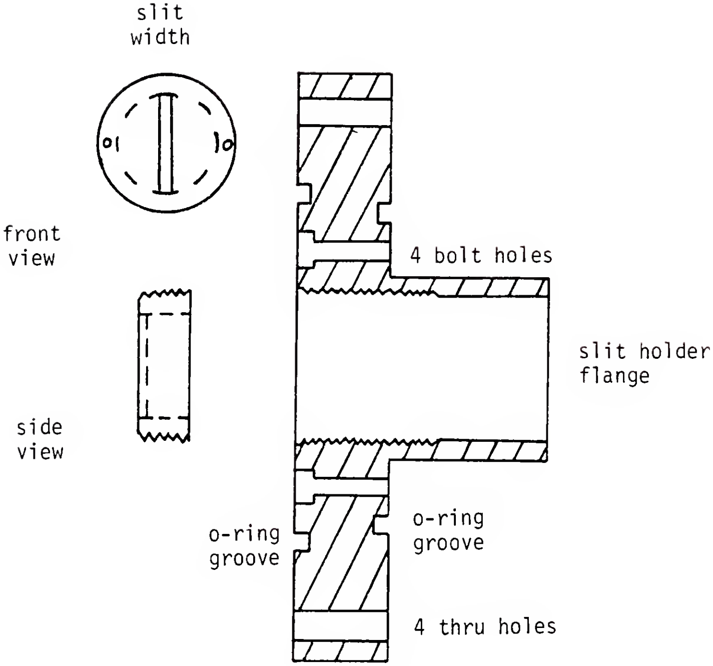

Fig. 1 Entrance and exit slit system flange adaptation to the Jarrell-Ash monochromator. Slit widths of 0.36, 0.56, 0.71, and 1.6 mm x 17 mm high were used.

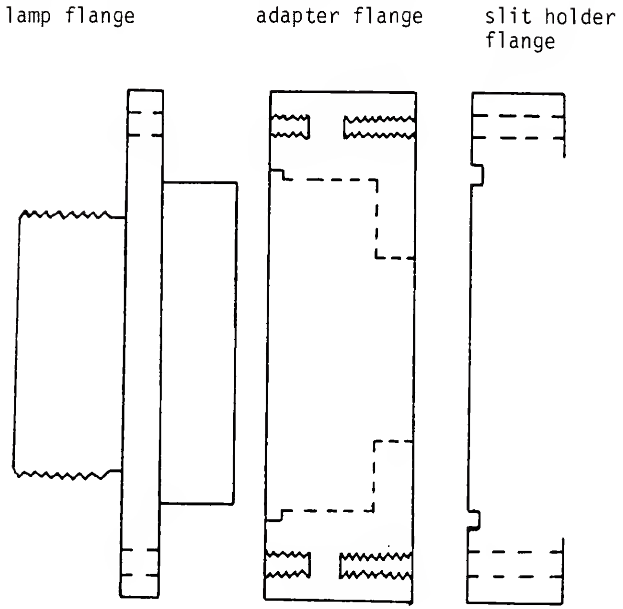

Fig. 2 Coupling arrangement from the lamp flange to the entrance slit flange (Fig. 1).

(PMT) housing to the exit slit flange, Figure 3. The PMT housing screwed onto the outside threads of the flange. For proper alignment the adapter flange through holes matched those of the exit slit flange. Initially, the flange also served as a window holder. A sodium salicylate coated window could be used for detection in the VUV; however, this was never used successfully since the monochromator could not be flushed sufficiently for transmission of VUV radiation through the monochromator to the window.

Light pipe system

After initial operation of the system with the PMT directly coupled to the monochromator, it was quickly realized that the X-ray (X-radiation) and the radio frequency (RF) noise associated with the electron pulse and the irradiation induced fluorescent burst from the optics was not attenuated enough to keep the PMT photocathode from saturating and overloading the preamplifier (preamp) and the dual operational amplifiers resulting in a dead-time[8,81] (recovery time) of tens of microseconds. Removal of the preamp from the signal circuit did not prevent the subsequent overload of the op-amps. The use of a window with or without a sodium salicylate coating in the PMT adapter flange did not aid with radiation protection of the PMT photocathode.

It was known from the literature that displacement of the PMT away from the reaction cell and electron source area,[8,62,81] along with extensive lead shielding,[82,83] would greatly aid in reducing the pulsed radiation interference and subsequent saturation of the photocathode. However, due to the small laboratory space it was decided to keep the PMT and the monochromator in the same room as the Febetron 706. There was enough

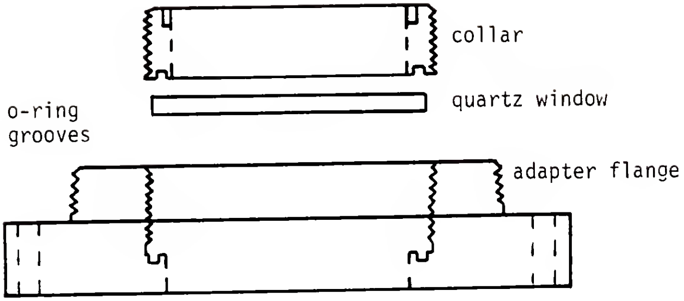

Fig. 3 Exit slit flange adapter flange and widow mechanism for connecting the exit slit flange to the PMT housing, Model 3262, for end-on PMTs. The window, when used, is sandwiched between o-rings. The collar is tightened down with a special tool to make the o-ring seals.

space in the room, though, to displace the PMT about one meter from the monochromator, which would remain bolted to the reaction cell.

The idea of a light pipe was first tested using Pyrex glass rods. For work in the UV region, though, quartz rods were necessary. The throughput was found to be favorable, but the quartz rods produced an unfavorable flourescent pulse upon irradiation by the X-ray pulse. Standard 8 x 4 x 2 inch lead blocks were used to make a lead cave for the rods and the PMT housing.[82,83] This reduced the amount of flourescence, but it was not reduced to a satisfactory level. The X-rays which came through the unprotected areas and the backscatter were enough to make ordinary optical grade quartz fluoresce.

Heraeus-Amersil Suprasil 2 radiation grade quartz rods, 3 mm diameter and 3 feet long, were then acquired to serve as a relatively fluorescence free light pipe. An apparatus was designed for coupling onto the exit slit flange, aligning and housing the fragile rods, and for maximizing the light level at the PMT window, Figure 4. With this arrangement the dead-time of the detection system was reduced to less than 1.5 microseconds and thus allowed useful initial microsecond time resolution. The first definitive work on the excited atomic iodine state, at 206 nm, was carried out using this geometry.[23]

Figure 4 depicts the quartz rod light pipe, housing, and guides. Nylon guides A, B, and F are detailed in Figure 5. In operation, B type guides were bolted onto A and D in order to center the stainless steel (SS) oval housing, C. The housing provided both protection for the rods as well as added rigidity to the apparatus over its 27 inch length. This arrangement also allowed sheets of plumber's lead to be wrapped

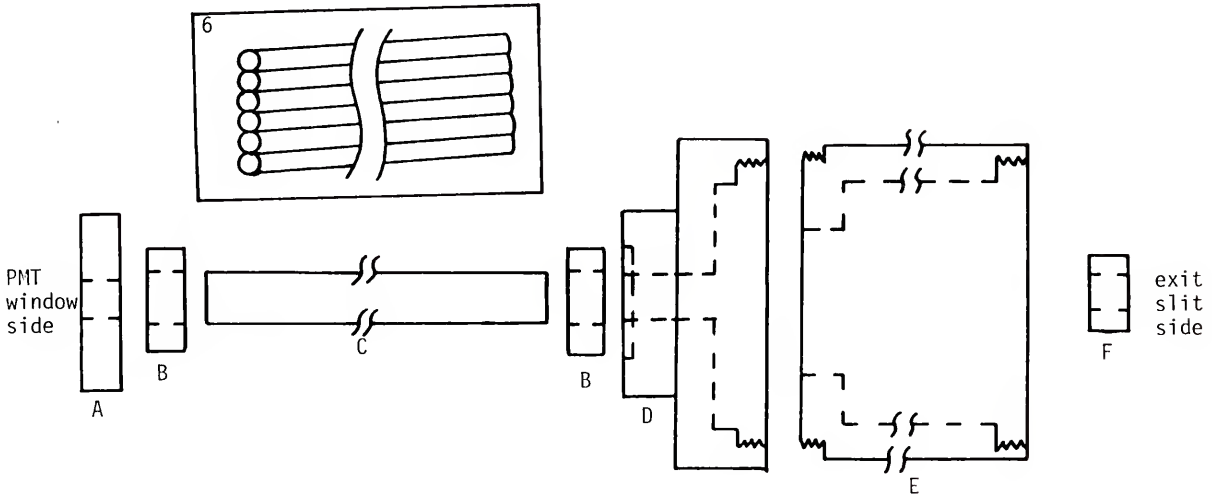

Fig. 4 Quartz rod light pipe guides and hosuing. A, nylon guide, which fits into the PMT housing Model 3262; B, nylon guide for SS oval housing; C, 27 inch SS oval housing; D, aluminum adapter flange; E, 6 inch aluminum extender; F, nylon guide, which fits into the exit flange; G, quartz rod bundle, 3 mm x 18 mm 36 inches long.

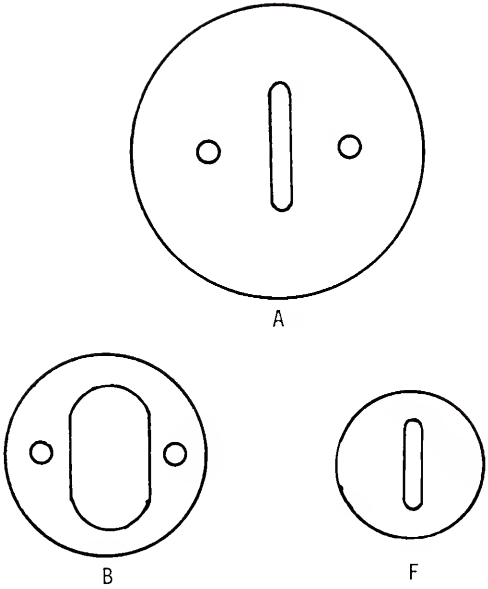

Fig. 5 Nylon guides. A, nylon light pipe guide, with threaded holes for centering the quartz rods in the PMT housing; B, nylon guide, with thru holes, for centering the 27 inch SS oval housing; F, nylon light pipe guide, for centering the quartz rods in the exit slit flange.

around the housing to aid with radiation protection without putting any mechanical strain on the rods themselves. Nylon guide A aligned the rods at the PMT end and centered the light pipe onto the PMT window due to its designed snug fit into the PMT housing.

Flange D was designed to adapt extender E to a B type guide. The 6 inch extender E had been previously designed to extend the PMT housing from the exit slit window flange adapter (Figure 3). The purpose of the extender had been to allow better shielding of the photocathode, but this, by itself, had proved inadequate. It was therefore integrated into the apparatus because of its strength and convenient threaded coupling mechanism. Plumber's lead could also be wrapped around the extender for additional radiation shielding. The exit slit flange adapter flange (Figure 3) was used without the window and collar mechanism. As before, it coupled E to the exit slit flange. Nylon guide F aligned the rods and centered them onto the exit slit.

The total geometry was designed to allow the rod bundle to make contact with the exit slit and have up to one inch variability from the PMT window. In general, the rods were kept about 2 mm from the PMT window and made contact with the exit slit.

Finally, a lead slug, Figure 6a, was added to the PMT window side of guide A. The addition of this X-radiation shield halved the previous radiation burst intensity at the photocathode and brought the detection system to a net dead-time of less than 1.5 microseconds. This is the best that could be achieved with this type of geometry using only lead shielding. Further reduction of the noise interference characteristic to pulse radiolysis systems would necessitate RF shielding of the e-beam, signal lines, and all the related electronics. Optimum noise reduction

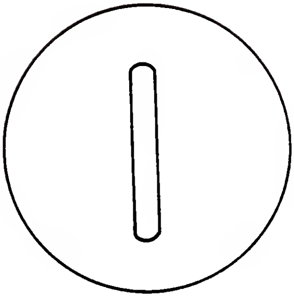

a) 2 1/16 inch diameter x 1/2 inch thick lead shield for end-on PMT housing, Model 3262.

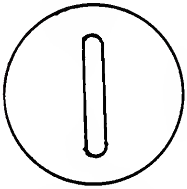

b) 1 1/4 inch diameter x 1/2 inch thick lead shield for side window PMT housing, Model 3150.

Fig. 6 Lead shields for PMT photocathodes in the Pacific Precision Instruments PMT housings.

could be best achieved by removing all the related electronics, except the analyzing light source, from the room which houses the e-beam source.[8,62,81-83] Either or all of these methods would have to be employed for submicrosecond resolution.

0.3 meter monochromator

Studies in the VUV could not be carried out until a McPherson 218 vacuum monochromator was substituted for the Jarrell-Ash. This monochromator has an f/5.3, a 2400 G/mm grating and a 1.33 nm/mm linear dispersion. It also had to be adapted to the reaction cell and optical system.

Figure 7 shows the single-pass reaction cell arrangement for studies in the VUV. The single-pass cell and the lamp system were the same as used with the Jarrell-Ash monochromator. The extension flange, EF, was designed for three purposes. First, it had to provide enough space for the lead cave, PB, to be built around the exit slit and photomultiplier, P, area. It also had to contain a sliding lens holder used for mounting a condensing lens. Focusing onto the monochromator entrance slit was achieved by sliding the holder along the inner walls, Figure 8.

A coupling flange, CF, was designed for dual purpose. A two inch diameter by one eighth-inch thick Suprasil 2 window was epoxied to the reaction cell side of the flange. The window separates the reaction cell from the entire monochromator vacuum system. The flange was bolted between the reaction cell and the vacuum extension flange, Figure 7. This linear geometry aligned the lamp axis, through the reaction cell, with the entrance slit of the monochromator. Fine alignment and focusing was carried out with a He-Ne laser.

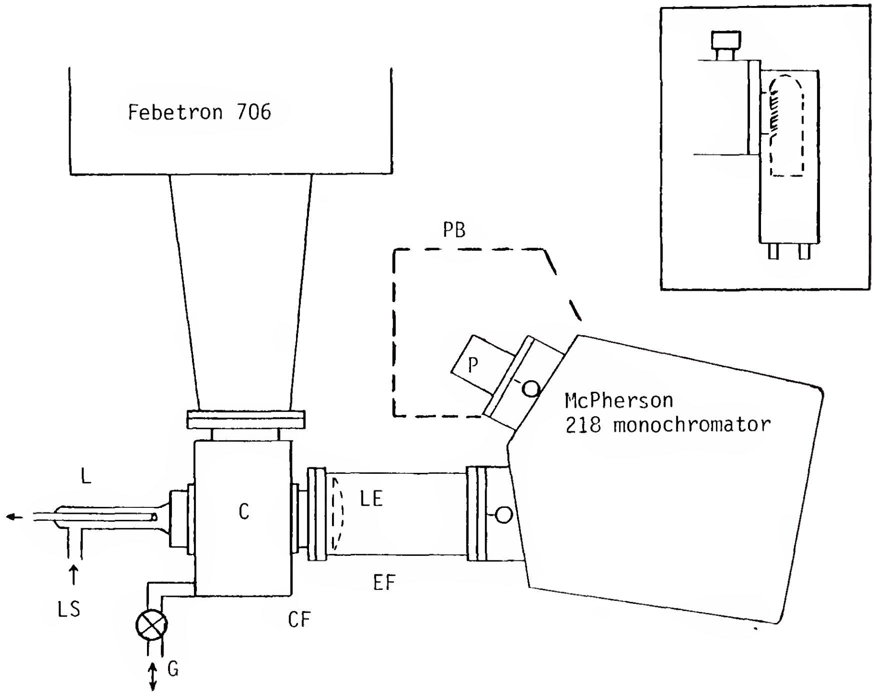

Fig. 7 Single-pass cell arrangement for VUV work. Inset: Photomultiplier tube housing (Model 3150) and monochromator exit window geometry.

C - Reaction chamber
CF - Coupling flange
EF - Vacuum extension flange
G - Sample handling system
L - Iodine lamp

LE - Condensing lens
LS - Lamp flow system
P - Photomultiplier
PB - Lead cave

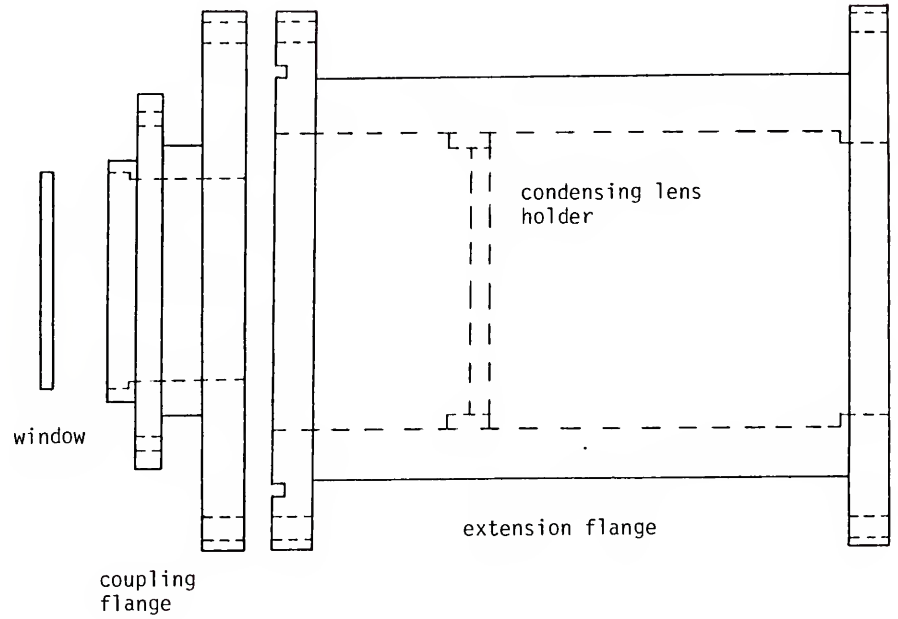

Fig. 8 Vacuum extension flange and lens focusing arrangement.

Next, an exit window flange was designed which would align the Pacific Precision Instruments side window PMT housing Model 3150, used with this geometry, onto it and also bring the exit window to near contact with the PMT window. This close geometry minimized the atomspheric absorption path length between the exit window and the PMT window. Figure 9 shows the exit window flange. The inset in Figure 7 shows how the alignment was made. The one inch diameter by one eight-inch thick Suprasil 2 window was epoxied into the flange and extended 1/32 inch out from the flange. The PMT housing (Model 3150) butts against the main flange window. This geometry ensured reproducibility of the geometry and proper alignment, and also kept both windows from contacting and damaging each other.

The monochromator vacuum pumping system design, Figure 10, was copied from the pumping system of another McPherson 218 monochromator in this laboratory. A useful modification which was made was to enlarge the liquid nitrogen well. This extended the time between necessary refilling of the well, for proper operation, from twenty minutes to one hour.

With the main and backing valves closed and the roughing valve open, the Kinney KC-5 vacuum compound pump will rough pump the monochromator directly. Once the pressure is below 1 torr, the roughing valve is closed and the backing valve is opened to rough pump up to the main valve. With the pressure below 1 torr the liquid nitrogen well is filled. After about ten minutes the main valve is opened. When the monochromator pressure is about 0.1 torr the oil (Dow corning 704) diffusion pump is turned on. The diffusion pump body was cooled by flowing water filled coils. An automatic safety thermostat switch, in series with the diffusion pump power cord, monitors possible overheating of the diffusion pump in

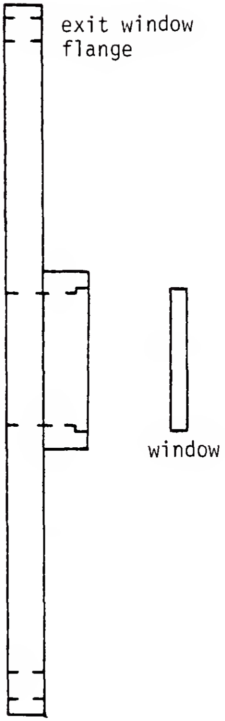

Fig. 9 McPherson 218 exit window flange and window.

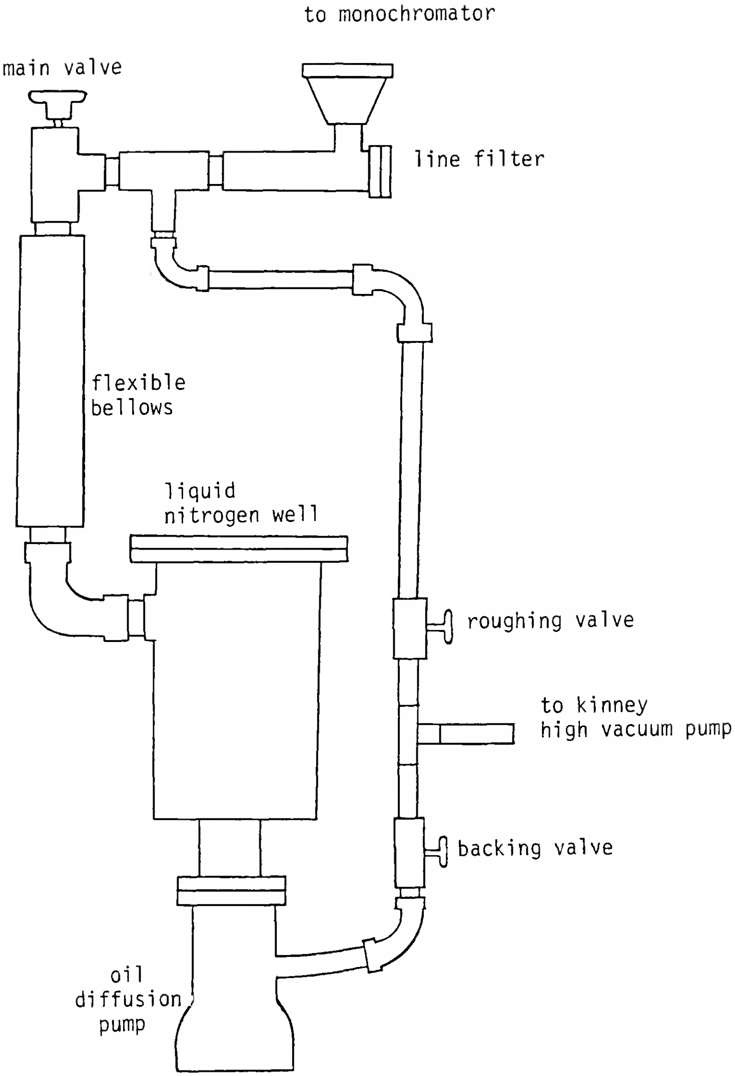

Fig. 10 High vacuum pumping system for the McPherson 218 monochromator.

a loss of coolant accident. The pumping system provided adequate vacuum for work down to the 160 nm cut off of the windows, lens, and PMT window. The vacuum extension flange was evacuated directly through the entrance slit of the monochromator. In order to speed up its evacuation time, the slit was opened to near its maximum width of 2 mm and closed down as needed after a useful vacuum had been attained. Active pumping was always maintained during an entire experimental session.

B. Optical Efficiencies

0.25 meter monochromator and flushing system

Figure 11 shows the linear geometry used with the Jarrell-Ash monochromator and quartz light pipe system. Basically, the light from the lamp, L, traverses the single-pass reaction cell, C, and the monochromator, M, in an overall linear geometry. At the exit slit the quartz rod light pipe bundle, Q, carries the light to the photomultiplier window.

Although a simpler optical train could have been used for studies above 200 nm, Figure 12, this tight geometry had desirable qualities for studies down to 180 nm. For studies of the ground state iodine atom useful throughput of the 178.3 nm light would have to be attained. In order to achieve a useful throughput below 190 nm, without a vacuum, the monochromator and PMT system would have to be purged with nitrogen or helium.

Nitrogen purging was first attempted. The light pipe and the reaction cell were omitted for initial testing of the purging system. The lamp was coupled to the monochromator via the flanging mechanism shown in Figure 2 and the PMT housing was coupled to the exit slit flange shown in Figure 3. The PMT housing adapter flange was first used

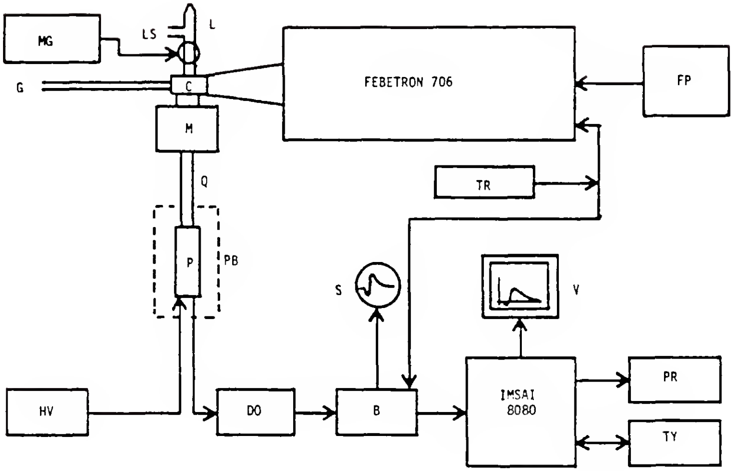

Fig. 11 University of Florida Pulse Radiolysis System

B - Biomation 610B
C - Reaction chamber
DO - Dual op amp
FP - Febetron power supply
G - Sample handling system
HV - PMT power supply
L - Iodine lamp
LS - Lamp flow system
M - Monochromator
MG - Microwave generator
P - Photomultiplier
PB - Lead cave
PR - Printer
Q - Quartz rod light pipe
S - Oscilloscope
TR - Trigger source
TY - Teletype
V - Video

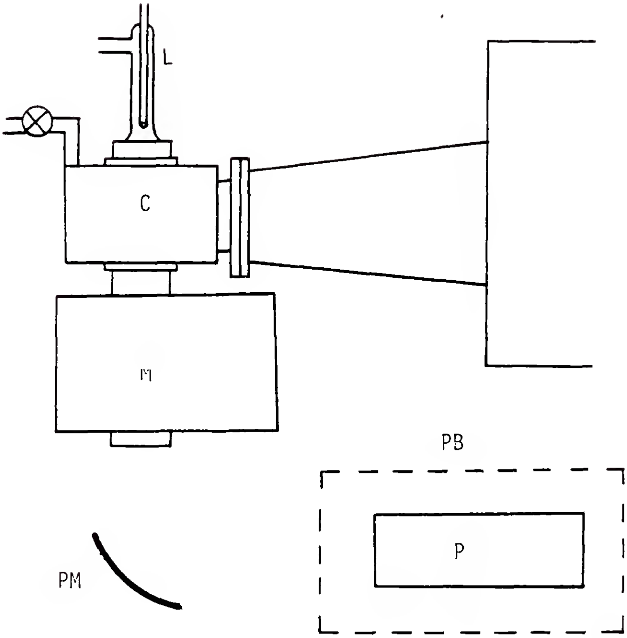

Fig. 12 90^0 optical configuration using a 10 or 7.5 cm focal length parabolic mirror. This configuration focuses the light onto the PMT window while keeping the PMT window from facing the X-ray pulse directly.

L - Light source
M - Monochromator
P - Photomultiplier tube
PB - Lead cave
PM - Parabolic mirror
C - Reaction cell

without a window. A SWAGELOK eighth-inch pipe to quarter-inch tubing fitting (SS-400-12) was put into the side of the monochromator to serve as an inlet port for the purging gas. The monochromator cover and potential areas for leaks were sealed with Apiezon Q sealing compound. The slits served as flushing outlet ports for the monochromator. Since the lamp adapter was being used, the half-threaded screw served as one outlet port on the entrance slit side. The exit slit flushed nitrogen into the PMT housing where it leaked to the outside. Generally, fast flushing was first done followed by several hours or days of slow flushing while the lamp spectra were periodically taken. No useful gain in light throughput was achieved nor useful wavelength extension below 190 nm. Unfortunately, at one point nitrogen purging of the PMT area caused high voltage breakdown of some of the components of the PMT base. The resistors had to be replaced due to the damage incurred from arcing.

A sodium salicylate coated window was then used in the exit slit adapter flange (Figure 3) as a fluorescent screen for detection of VUV radiation. Various methods of deposition and thicknesses of the sodium salicylate were tested. Access to wavelengths below 190 nm was not achieved, and a lowering of throughput was observed since the isotropic nature of the induced fluorescence greatly reduced the intensity at the photocathode.

Extensive helium purging was then attempted. The helium was first passed through a sodium hydroxide trap, followed by a large molecular sieve-silica gel trap, and finally passed through a smaller molecular sieve trap which was immersed in a liquid nitrogen filled dewar. The sodium hydroxide was eventually removed from the system as its presence did not show any useful effect. Various flushing rates were tested. The system was purged for days and sometimes for weeks while the lamp spectrum was taken at various times. Although some gain in transmission of lower wavelengths was observed, as well as an overall gain in intensity in other wavelengths, no net benefit for the experimental requirements was achieved. Figure 13 shows the lamp spectrum with nitrogen purging, Figure 14 shows the spectrum with helium purging.

It was apparent that the volume being purged was too large to achieve optical efficiency below 190 nm. Because satisfactory throughput could not be achieved with this close geometry, and because of the expected parent compound absorption in the wavelength region of interest, and since it was apparent that the linear dispersion associated with this monochromator would not suffice for adequate line isolation at useful slit widths, it was futile to pursue studies below 200 nm with the Jarrell-Ash monochromator.

0.3 meter monochromator

For studies of the ground state iodine atom at 178.3 nm a McPherson 218 monochromator and vacuum system were borrowed from a UV-VUV spectrometer system in this laboratory. Subsequently, after it was determined that it provided the experimental requirements, a McPherson 218 was purchased for the pulse radiolysis system and was adapated as discussed previously.

The geometry used with this type of monochromator is shown in Figure 7. Light from the lamp traversed the reaction cell and was condensed onto the entrance slit. After being dispersed the light of the selected wavelength was detected by the photomultiplier. This

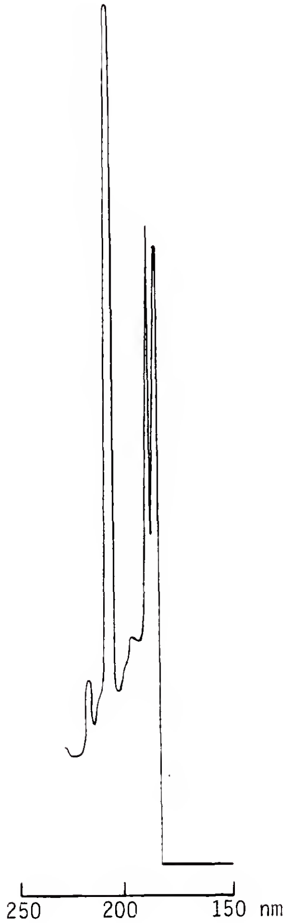

Fig. 13 Iodine discharge lamp spectrum with nitrogen flushing of the optical path. Jarrell-Ash monochromator, 0.356 mm slits, and 50 watts microwave power.

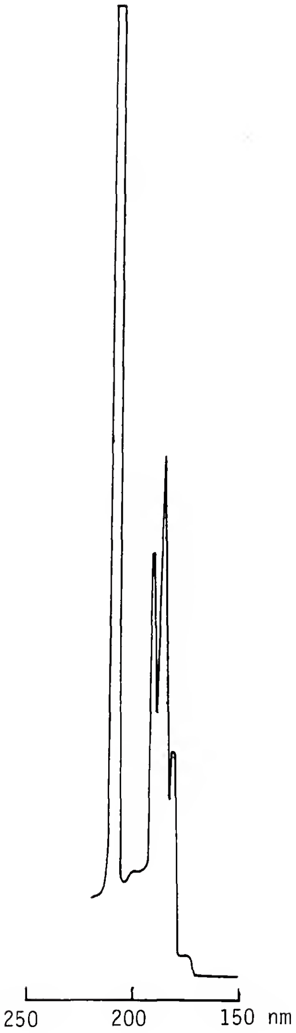

Fig. 14 Iodine discharge lamp spectrum with helium flushing through NaOH, grade 42 silica gel, 10x molecular sieve, and a molecular sieve-liquid nitrogen trap. Jarrell-Ash monochromator, 0.356 mm slits, and 50 watts microwave power. The vertical scale is twice that used in Fig. 13.

geometry could potentially be used for absorption spectrophotometry in the visible, ultraviolet, and vacuum ultraviolet regions.

A 2 inch diameter plano-convex lens, LE, with a 5 inch focal length was used as the condensing lens. The throughput from the discharge lamp, L, provided adequate light intensity for good signal-to-noise conditions for useful observations. Final studies of the excited state and ground state iodine atom were carried out with this geometry.

The observable signal was also dependent on the strong absorption by the 206 and 178 nm atomic iodine states. For work with species with lower absorption coefficients a multiple-pass reaction cell system with a useful net optical throughput was needed in order to achieve an observable signal.

C. Reaction Cells

Two types of aluminum reaction cells were used: a versatile single-pass cell and a multiple-pass cell. The single-pass cell was used for the atomic iodine studies. The multiple-pass cell was used for the ozone studies and the attempts to look for molecular iodine absorption following pulse radiolysis of alkyl halides.

Single-pass reaction cell

The single-pass cell, Figure 15, had been previously designed in another laboratory. The convenient multiport system made it very useful for our purposes. The cell has six 2.25 inch flange ports and a body cavity of ca. 800 cm^3. Two of the ports were on the two large cover plates. The cover plates made o-ring seals with the cell body. All attachment flanges were designed with a short barrel in order to fit the

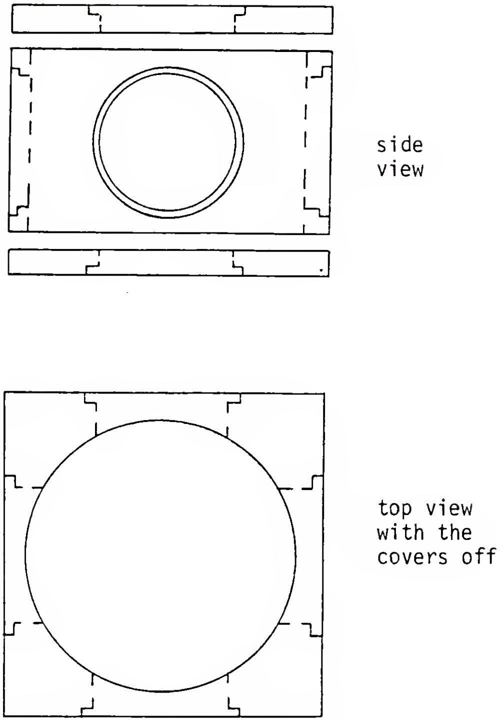

Fig. 15 Single-pass cell with six equal flange ports. O-ring seals are made at each port lip and between the two cover plates and the reaction cell body.

ports and make o-ring seals with the port's lip. Viton o-rings were used because of their resistivity to chemical attack.

The effective interaction volume was defined by the intersection of the e-beam with the analyzing light beam. The primary e-beam has a diameter of 2.5-3 cm, spreading only slightly, but there is also an outer region due to secondary electrons which adds considerably to the effective cross section. (The range of 100 keV electrons in air at STP is 6 inches.)[84] The light beam enters the cell with a maximum diameter of 2.5 cm, but ca. 90% of the intensity is within a diameter of about 1.5 cm diverging only slightly, due to the ca. 1 cm ID and collinear cylindrical shape of the discharge lamp body.

The many detection methods which could be used with the single-pass cell makes it a versatile apparatus for future studies. The analyzing light may be used perpendicular to the e-beam and linear with the condensing lens, as used in these absorption studies. The light traversed the cell in a region where the energy deposition per unit volume was very nearly homogeneous. Relatively uniform irradiation was insured since the range of the electrons was substantially greater than the thickness of the light beam and e-beam interaction region.[14,85] For pressures used in these experiments the interaction length is about 2-3 cm, while the range of the electrons was about one meter.

Emission studies could also be carried out using this cell. Light could be gathered from four different ports, all perpendicular to the e-beam. Finally, the resonance fluorescence detection technique could be used with this cell.[86,87] In this very sensitive technique the light source, e-beam, and the light gathering lens would need to be perpendicular to each other. The multiport system would allow several geometric variations of this principle.

Multiple-pass reaction cell

The multiple-pass cell was designed to help observe species with relatively low absorption coefficients by providing a longer absorption path length. For wavelengths above 300 nm, multiple-pass cells greatly increase the signal-to-noise ratio (S/N).[14] Below 300 nm the wavelength dependency of mirror reflectivity plays an increasing role with decreasing wavelength. Therefore, in designing a multiple-pass system the expected increase in absorption must outweigh the reflective light losses. A simple, 39.1 cm, six-reflection multiple-pass cell was designed for studies in the visible and ultraviolet regions down to 200 nm.

A White cell is typically used to obtain a long path length in a confined volume.[13,14,62,88] Because of the damaging effects on mirrors by the chemicals in the reaction cell and the expense of UV-VUV grade White cell type mirrors and coatings, a plane mirror multiple-pass system was used.

Figure 16 shows the multiple-pass cell optical arrangement. This geometry was successfully used for studies of the oxygen-ozone system at 253.7 nm. For work in the VUV with this cell, vacuum window flange adapters would have to be designed in order to couple the light source and the monochromator to the cell. The monochromator and the PMT arrangement was the same as that in Figure 7. The multiple-pass cell was attached to the Febetron using the same flange that was used for the single-pass cell.

Figure 17 shows the multiple-pass mirror configuration. The incoming light beam traversed the cell and was reflected off the entrance mirror which initially directed the light along the plane mirrors. The exit mirror redirects the light beam through the exit window. The cell

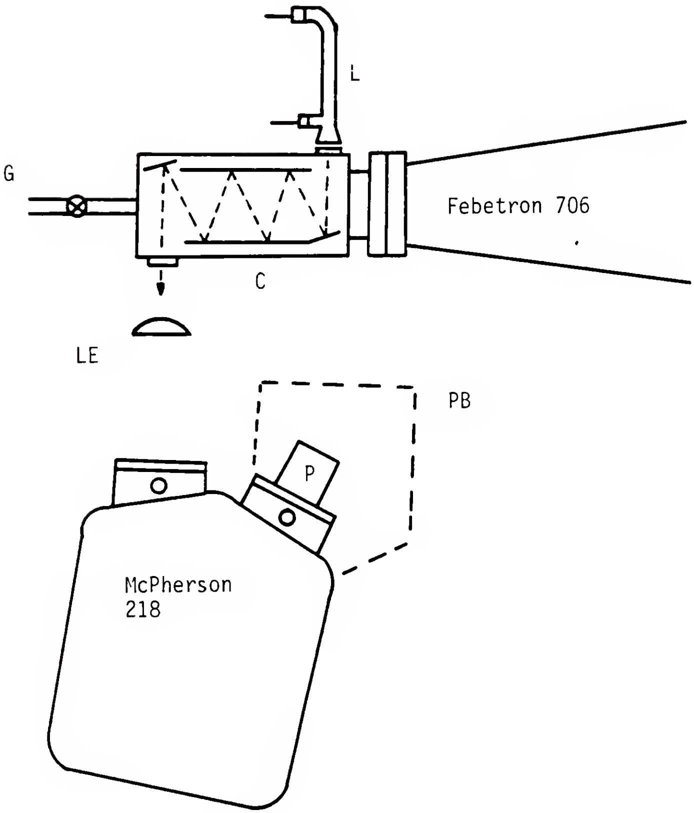

Fig. 16 Multiple-pass reaction cell arrangement for visible and UV studies.

C - Multiple-pass reaction cell
G - Sample handling system
L - Mercury lamp
LE - Condensing lens
P - Photomultiplier
PB - Lead cave

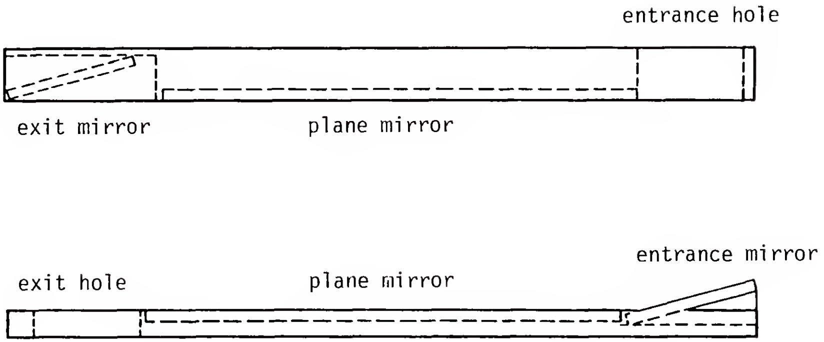

Fig. 17 Multiple-pass reaction cell mirror system with MgF_2 coated first surface aluminum mirrors.

windows were 1 inch diameter by one eight-inch thick Suprasil 2. The first surface mirrors were MgF_2 coated aluminum (coating for UV #7992, Oriel Corporation). The system pressure determined the e-beam divergence, which in turn determined the actual interaction path length.

Reaction cell-Febetron 706 coupling flange

Both reaction cells were attached to the field emission tube window face plate by a simple rotating flange mechanism, Figure 18. The reaction cell flange fit through the attaching flange and was free to rotate. Tension was provided by tightening the nuts on the Febetron face plate bolts, Figure 19. As the attaching flange was tightened toward the Febetron face plate it pressed the cell flange forward. The cell flange was thus firmly pressed onto the o-ring on the face plate and was no longer free to rotate. Four nuts and bolts were used to secure the attaching flange in order to provide uniform tension. The pitch of the cell could be changed slightly by differential tightening of the nuts, i.e., when the upper nuts are tightened the back of the cell is raised. Thus, with this simple flanging mechanism the cell could be rotated and leveled for proper optical alignment with the rest of the optical system.

The cell flange also served as the cell e-beam window holder, Figure 18. A 1.25 inch diameter by 0.075 mm thick titanium window was sealed to an aluminum disk with Varian Associates "Torr Seal." The window disk rested on an o-ring which made a vacuum seal. Pressure was applied to the disk by tightening the threaded ring. The ring was made of brass and the flange of aluminum in order to preserve the integrity

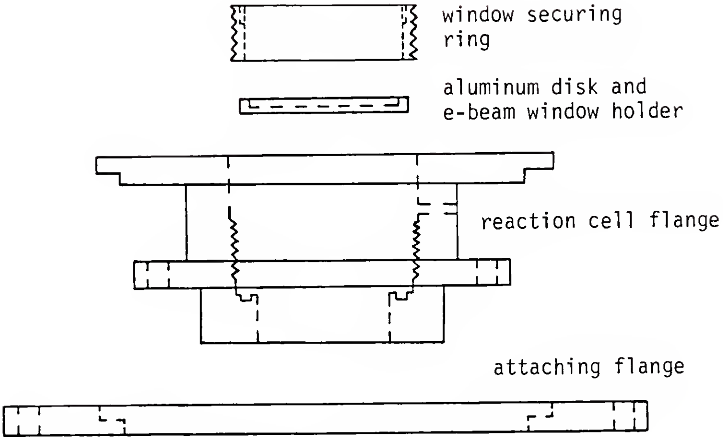

Fig. 18 Reaction cell-Febetron 706 face plate coupling mechanism. The cell flange contains the e-beam window and mechanism.

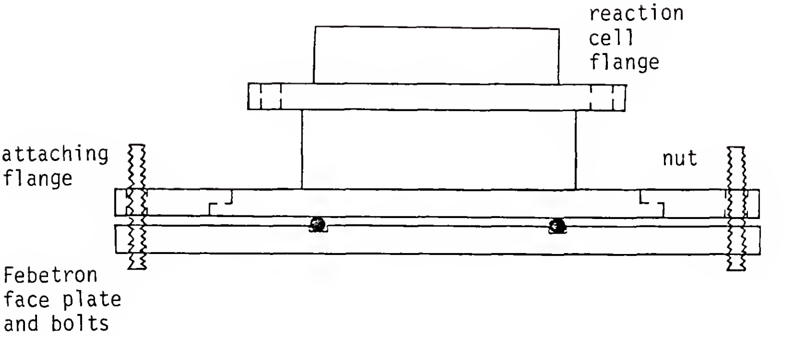

Fig. 19 Complete assembly of the reaction cell flange onto the Febetron face plate. The reaction cells were attached to the reaction cell flange.

of the threads. Care was taken to make sure that the window was not deformed while the epoxy cured, so as to minimize any possible defocusing effects by the window on the e-beam. The window was removed from the field emission tube window enough to prevent possible damage to the tube window from spallation which could occur from the electron impact on titanium.

D. Spectrophotometry

Light source

The technique of absorption spectrophotometry requires a light source, an absorption path, a monochromator, and a photomultiplier. All other related equipment support these and aid in achieving an observable signal.

The light source used could be a standard commercial lamp suited to the spectral region of interest or it could be of novel design. Since the signal-to-noise ratio is directly proportional to the square root of the light intensity, it is important that the source be relatively intense. High power spectral lamps that emit a continuum distribute their over-all power over a spectral region. Their intensities per wavelength interval may not be great enough to carry out studies of discreet line absorption. High power light sources, unless filtered, could also photolyze the chemical system under study and complicate the observed signal. Less expensive low-power line sources may often be more intense over a narrow spectral band of interest than high power continuum lamps. Usually in order to produce radiation at discreet wavelengths an appropriate atomic or ionic state must be produced. Low power (less than 125 watts) electrodeless discharges have been shown to produce intense radiation primarily from neutral atoms.[89]

There are various methods of coupling microwave power to sustain a discharge, but the most effective method is through a tuned cavity.[90] A tuned cavity microwave discharge light source was therefore chosen for the kinetic spectrophotometry system. The lamp system will be detailed later.

Absorption path and monochromators

The reaction cells described previously, coupled with the Febetron 706 high pulse-current irradiation system, produced concentrations of transient species in the cells which were high enough to allow direct observation by absorption spectrophotometry.

Of the two monochromators used, the McPherson 218 best exemplified the versatility needed for spectrophotometry over a varying wavelength region. A major factor in assessing a monochromator is its light throughput. The light gathering power, LGP, best assesses this quality.[17] LGP is defined by

$$\mathrm{LGP} = (h/f^2)\ m, \qquad \text{II-1}$$

where h is the slit height (mm), f the effective aperature (f#), and m the linear dispersion (nm/mm). An LGP of about 0.3 or greater has been recommended for fast kinetic spectrophotometry.[17] For this monochromator $f = 5.3$, $m = 1.33$ nm/mm, and $h = 6$ or 8 mm. Thus, the LGP for this monochromator, as used, was either 0.28 or 0.38 nm.

Photomultipliers

Photodetectors used in fast absorption spectrophotometry must be sensitive enough to measure small changes of light intensity in the spectral region of interest, and they must have a fast frequency response relative to the half-life of the transient of interest. Two types of photomultipliers were used under different conditions with the two different monochromators. Two EMI end-on 50 mm window PMTs Models 9750QB and 9856B were used with a Pacific Precision Instruments Model 3262 housing, Figure 11. Because of its lower noise sensitivity, an EMI Model 3150B 39 mm side window PMT in a Pacific Precision Instruments Model 3150 housing was eventually used for the spectrophotometry system, Figure 7.

Initial studies in the UV employed the Model 9750QB PMT. The window was Spectrosil quartz with an optical range of 165-650 nm. The 2 mm thick window had 90% transmission down to 190 nm but dropped to 50% by 170 nm. The bialkali photocathode had a quantum efficiency of 22% at 200 nm. The 9856B PMT was used for tests in the visible region. It had a soda-lime window with a spectral range of 320-650 nm. The 2 mm thick window had 88% transmission down to 350 nm and fell off to 38% at 320 nm. The maximum quantum efficiency of 20-28% was between 470 to 400 nm.

Standard photomultiplier tube base electronics have been customized in order to achieve desired rise times, gains, and linearities in their respective systems.[17,91,92] Figure 20 shows the diagram of the base components used with the end-on PMTs. Although this circuit provides linearity under usual spectroscopic conditions, it deviated from linearity after exposure to the large electromagnetic radiation pulse. In order to maintain dynode voltages when high currents were drawn, capacitors in the range of tenths to several microfarads were needed.[17] It can be seen in Figure 20 that the capacitors were relatively small in value and also, that they were not on all the dynodes. Also, when high currents

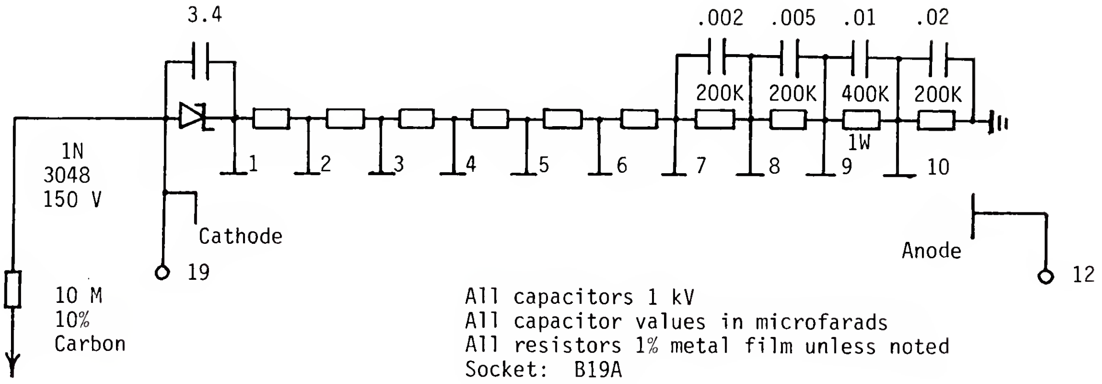

All capacitors 1 kV
All capacitor values in microfarads
All resistors 1% metal film unless noted
Socket: B19A

Fig. 20 Photomultiplier tube base schematic used with EMI 9750 QB and 9856B PMTs and Model 3262 housing.

were drawn the voltage drops could be substantial across the large resistors. Both of these factors combined to produce nonlinearity in the signal, especially during the first few microseconds after the radiation pulse.

The 9783B side window PMT was acquired to help alleviate some of these and other problems. The side window PMT was used in all the spectrophotometry geometries, after its initial tests, because of its more favorable properties under the harsh electromagnetic interference pulse conditions. The PMT window was 2 mm Spectrosil quartz. The quantum efficiency reached a maximum of 22% at 300 nm and fell off to 18% at 200 nm. Figure 21 shows the diagram of the base components. The value of the capacitors on the last stages was increased and the resistor values were decreased relative to Figure 20. This combination greatly helped reduce, but not eliminate,, nonlinearity after the radiation pulse. Further improvement could be achieved by using capacitors to stabilize the voltage on each dynode.[17,91] Also, since each dynode contributed to the nonlinearity, the minimum number of dynodes necessary for a useful signal should be used.[92] This PMT used one less dynode in the circuit than the other two PMTs.

High beam-current machines, such as the Febetron 706, produce large electromagnetic disturbances which interfere with the PMT circuitry.[14] Although the interference is initiated during the e-beam pulse, the overload and subsequent recovery could last several microseconds. Several procedures were used to reduce noise which affected the PMT and its circuitry. The electrons were always absorbed in and by the reaction cell and returned to ground. The RF interference was reduced equally

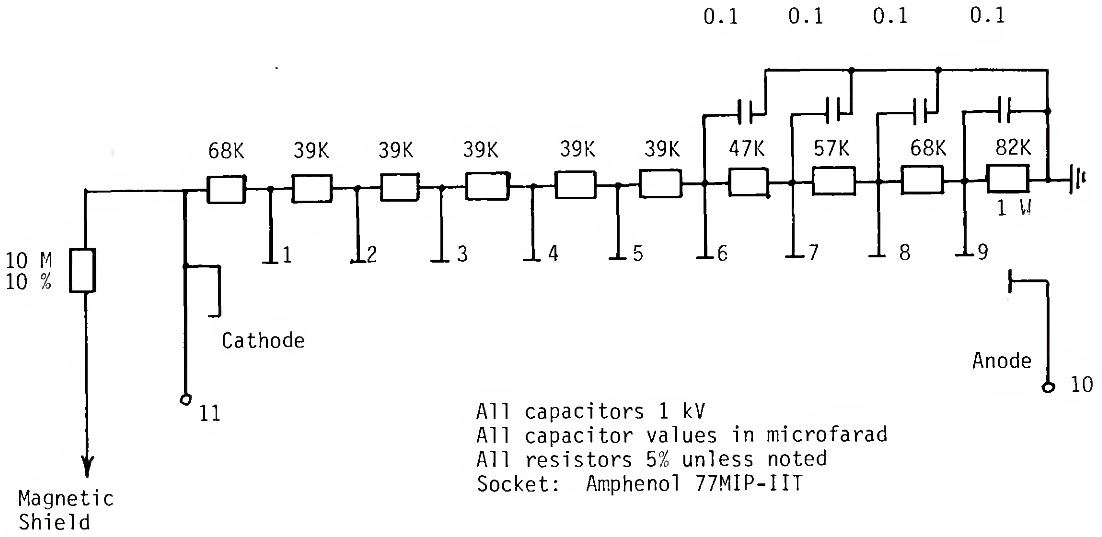

All capacitors 1 kV
All capacitor values in microfarad
All resistors 5% unless noted
Socket: Amphenol 77MIP-IIT

Fig. 21 Photomultiplier tube base schematic used with EMI 9783B side window PMT and Model 3150 housing.

whether the reaction cell was directly grounded or grounded through the Febetron.

Cerenkov radiation is not a problem with either reaction cell since the light paths in both cells are transverse to the e-beam. The Cerenkov light angle is very small and thus travels in nearly the same direction as the e-beam. Collinear optical systems suffer more from Cerenkov light interference than transverse optical systems.

The X-ray pulse is by far the largest contributor to interference and subsequent PMT overload. Shielding of the X-rays with lead greatly attenuated the pulse intensity at the PMT photocathode. Unless the exposed photocathode is removed several meters from the Febetron area behind proper shielding, gross overloading of the PMT will occur. While using typical experimental geometries, tests showed that encasing either PMT in lead bricks and masking the photocathode with a half-inch lead slug produced a low intensity noise pulse of approximately 80 ns duration and 30 ns FWHM. In typical operation, though, where the photocathode was exposed, microseconds noise pulse durations were observed due to the higher intensity of the X-ray pulse at the photocathode. The McPherson 218 monochromator offered some advantage toward reducing the X-ray problem since the photocathode did not face the reaction cell area directly as did the PMT geometry with the Jarrell-Ash monochromator. Backscatter interference, though, was still evident and substantial.

E. Lamp Systems

Because the signal-to-noise ratio is proportional to $(I/bw)^{\frac{1}{2}}$, where I is the light intensity at the photocathode and bw is the amplifier and circuitry bandwidth and since the bandwidth is usually large and fixed by the electronics, S/N may be increased through increasing light intensity, as long as PMT linearity is maintained.

The basic factors involved in designing the lamp system were size, power, intensity, emission spectrum, and stability. These factors were carefully considered to ensure applicability for the chemistry being studied.

Iodine lamp

In order to observe a signal for low concentrations of transient species by fast absorption spectrophotometry, a stable intense light source[17] rich in the wavelengths of interest was needed. Hartek et al. first developed an electric discharge iodine lamp.[93] An argon carrier flow system was used, as it was found to reduce buildup of impurities in the lamp. Strong emission from OH radical bands showed that water vapor, when present, was the most troublesome impurity in their system. Since the vapor pressure of iodine was high, but less than 1 torr at room temperature, it was ideal for use in a discharge lamp. Similar intense atomic line sources using microwave excitation of flowing mixtures[89] including iodine-argon mixtures[36-38] were eventually developed.

For our purposes an iodine lamp system was developed and powered by a Raytheon Model PGM-10X1 microwave generator, Figure 22. The continuous-wave microwave energy at 2450 MHz was generated by a magneton oscillator. A Microwave Devices Incorporated Model 752.3 bi-directional RF power and standing wave ratio (SWR) meter was attached to the output coupler on the front panel of the Raytheon. The front panel also had a relative

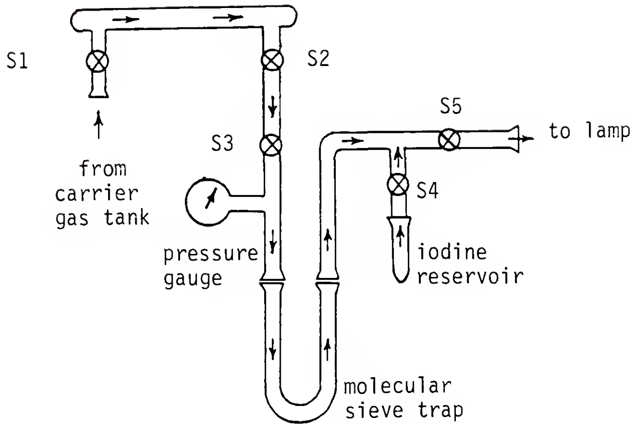

a) Iodine lamp flow system.

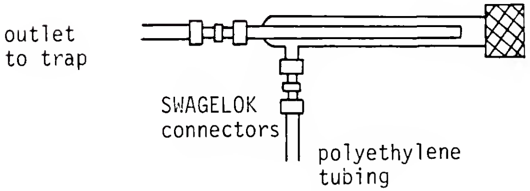

b) Iodine lamp. SWAGELOK connections couple 1/4 inch quartz tubing to 1/4 inch polyethylene tubing. The knurled brass coupler attaches the lamp to the lamp flange (Fig. 2).

Fig. 22 Lamp system.

power meter which indicated a percent-of-power output. Maximum power output was about 85 watts, with less than 1% ripple. In typical operation only 50 watts was used. An RG 214/U flexible coaxial cable carried the microwave energy from the meter to an Evenson cavity.[90]

As previously mentioned, tuned cavities are the most efficient method of delivering microwave power to sustain a discharge.[90] Figure 23 shows the Opthos Instruments Company Evenson-type cavity used in these studies. The cavity was mounted onto the lamp by sandwiching the lamp body between its main body and the bottom plate. When the standing wave ratio was maximized the most efficient power coupling to the plasma was achieved. The bi-directional power meter was used to ascertain a properly tuned cavity.

With the lamp system assembled and with a stable gas flow the power was turned to about 50-60 watts. The discharge was initiated by a Tesla coil, which provides initial ionization of the gas mixture. When the pressure in the flow system was below 5 mm Hg, a discharge was sustained.

The screw adjustment was turned, as required, to minimize the reflected power (maximize the delivered power) indicated by the power meter. The sliding tuner was also adjusted to further reduce the reflected power. In general, intense and narrow atomic emission lines were best produced when the pressure in the flow system was kept around 1 torr.[36,93,94] Once the cavity was tuned it remained in good adjustment for several days if left undisturbed. Once tuned, the SWR could be maximized daily in a few seconds.

Under these conditions, and with proper caution, the microwave equipment posed no hazards to laboratory workers. It should be noted,

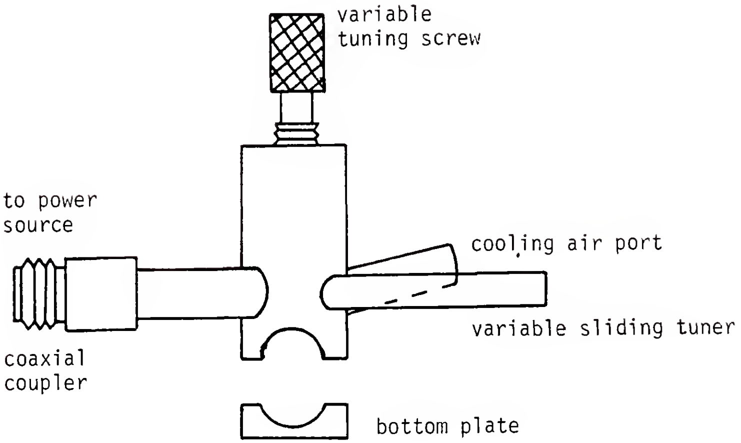

Fig. 23 Evenson cavity. The lamp body was designed to fit between the cavity body and the bottom plate. Proper tuning of the cavity is achieved with both variable tuners.

however, that these types of discharges are rich in UV and VUV radiation and thus proper eye protection should be worn.

The lamp flow system was constructed of Pyrex and polyethylene tubing, Figure 22. Fisher and Porter teflon stopcocks and Ace Glass Incorporated teflon stopcocks with Ace Glass Incorporated brand "FEFTE" o-rings were used. Pyrex joints #15 were used in order to facilitate coupling of different segments of the system, as well as to facilitate disassembly and cleaning. One quarter-inch OD, polyethylene tubing, was used to allow the greatest mobility when coupling the lamp to the reaction cell from the nearby vacuum rack.

The gas flow system consisted of a three stage pressure reduction area between the argon carrier gas tank and the molecular sieve trap. By adjusting stopcocks S1-S3 (Figure 22), the pressure was reduced from just above atmospheric to about 1 torr by a constant pumping rate with a Welch Duo-Seal mechanical pump. On the high pressure side of the molecular sieve trap, the approximate pressure of the gas flowing through the lamp was indicated by a Kollsman Instrument Corporation absolute pressure gauge. The 10X-molecular sieve prevented fast back diffusion of molecular iodine into the guage. In operation, six inches of the molecular sieve, in 10 mm OD thin wall Pyrex tubing, would become saturated in one month. The trap contained about fifteen inches of the sieve. When one third of the trap was contaminated, that third was removed and the trap was refilled from the opposite end. The contaminated sieve was not regenerated, but instead was properly disposed.

At room temperature the vapor pressure of iodine was less than 1 torr. With stopcock S4 open, a constant and stable source of molecular iodine was provided from the reservoir to the lamp area. The length of the glass and polyethylene tubing from the iodine reservoir to the inlet of the lamp was about one meter. Proper mixing occurred over this length. Quarter inch stainless steel SWAGELOK fittings were used to make all the glass to polyethylene tubing connections.

The outlet of the lamp went to a Pyrex 29/42 trap in series with the mechanical pump. A carbon dioxide-isopropanol bath was used to efficiently sublime and trap the iodine. The argon carrier gas passed through the trap and was pumped away. The pump was exhausted directly to the outside of the laboratory building.

The lamp body eventually used in the majority of the alkyl halide studies was made of a #22 glass o-ring joint, a two inch Vycor graded seal, and a quartz main body, Figure 24b. The inner tubulation is also quartz. The geometry was designed such that the Evenson cavity mounted over the quartz-rich side of the graded seal. Quartz was needed because the local heating near the cavity could deform regular glass. Local cavity cooling was achieved by rushing filtered air through the Evenson cavity cooling port, Figure 23.

Figure 24a shows the type of microwave lamp which previously had been used for photochemical work in this laboratory. The lamp body was made the same as previously described. The front tubulation, though, was made of glass. This lamp was first used for this work, but several disadvantages were quickly realized.

A teflon collar, TC, was fitted over the neck of the o-ring joint. A brass coupler, BC, screwed down onto a flange, which was bolted onto the reaction cell, Figure 25. At the same time the coupler pressed on

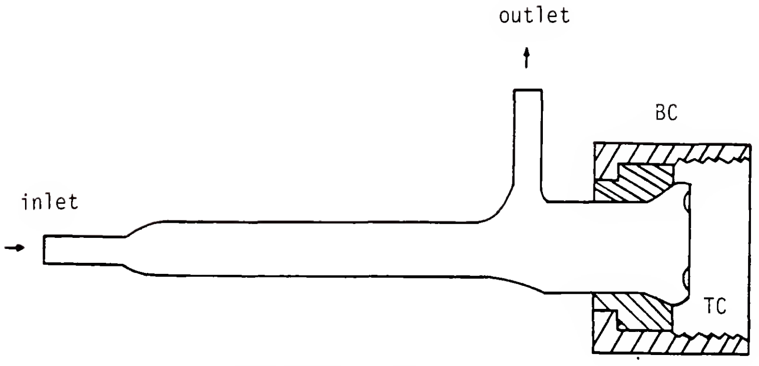

a) Original lamp body
TC, teflon collar
BC, brass coupler

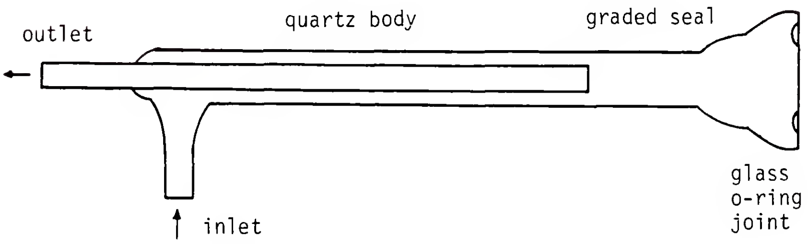

b) Improved lamp body.

Fig. 24 Microwave discharge lamp bodies.

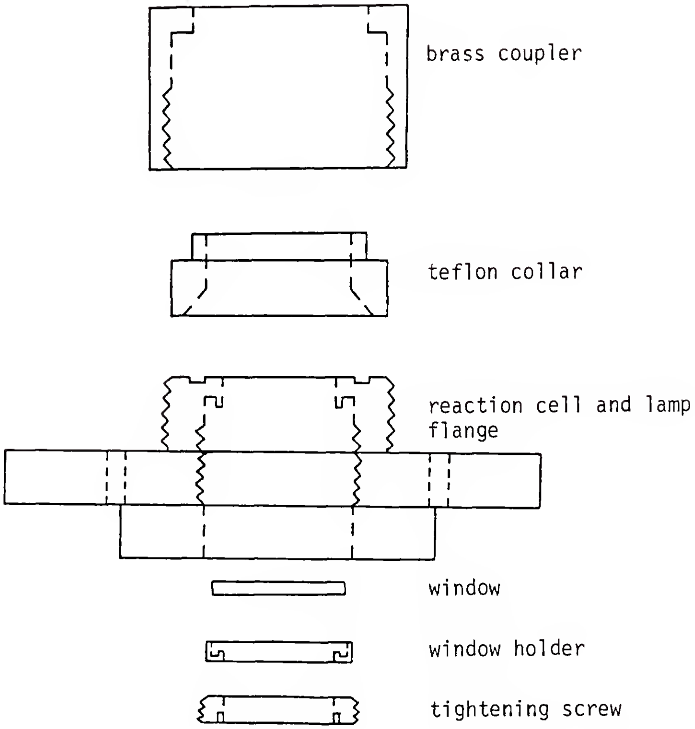

Fig. 25 Lamp window and coupling flange. The lamp body is coupled to the flange by the brass coupler and the teflon collar. The lamp window is sandwiched between o-rings and kept snugly in place by the pressure provided on the window holder by the tightening screw.

the teflon collar which centered and tightened the o-ring joint and made the vacuum seal. A Heraeus-Amersil Suprasil 2 window, which was sealed by o-rings inside of the flange, separated the lamp system from the reaction cell cavity. This window system was preferred to the sealed type where the window is epoxied directly to the lamp,[89] since window material could easily be varied for different spectral ranges and conditions without manufacturing another lamp body. It also facilitated cleaning and annealing of the windows for optimum performance.[95]

The problems encountered with this first lamp were twofold. First, it may be seen from Figure 24a that the Evenson cavity could not be placed closer to the window than the region directly behind the front tubulation, about 10 cm. In the 0.5-1 torr pressure range, the discharge plasma varied from about 5-2 cm, respectively, in total length. Second, two layers (volumes) develop in the lamp which are important. The principles involved with these types of lamps have been extensively discussed elsewhere.[96] An emitting layer, powered by the microwave cavity, contains radiating and absorbing atoms. Absorbing atoms are removed by diffusion to the walls or possible chemical reactions. A reversing layer, which contains absorbing atoms, develops in the volume between the discharge and the lamp window (the volume in the o-ring joint area). The larger the reversing layer, the more self-absorption and subsequent reduction in transmitted intensity. The diffusion rate, deactivation rate, and the efficiency of recombination at the walls determine the concentration gradient of the absorber atoms. Recombination efficiencies on glass and silica surfaces for ground state iodine atoms are high,[97] and thus are helpful in reducing the ground state absorber atom concentration. Ground state iodine atom recombination with argon as a third body is slow.[98] Therefore, a substantial amount of ground state iodine atoms capable of absorbing light emitted from the discharge can be expected near the axis of the lamp rather than near the walls. A much higher concentration of ground state atoms is expected than any other state. Minimizing the reversing layer would therefore be advantageous. The steady state concentration of the excited state atom, I*, was expected to be very small due to its rapid deactivation by molecular iodine.[38]

Clear synthetic fused silica windows, Suprasil 2, were used in the lamp flange because of their high discoloration and degradation resistance to VUV, X-ray, and electron radiation. Suprasil 2 is specified to have 90% transmission at 200 nm, 85% at 170 nm, and 20% at 160 nm, for a 1/8 inch thick window. Suprasil 2 is practically free of fluorescence. As previously discussed photomultiplier tube saturation and overload from window fluorescence after electron and X-ray bombardment had been a gross problem in the early stages of development of the pulse radiolysis system.

Even with the high radiation resistance of the window, it was impractical to run the discharge against the window in order to minimize the absorbing layer. The o-ring on the lamp side of the window could become a source of contamination upon exposure to the discharge. With sealed lamp systems the epoxy becomes a source of contamination when exposed to the discharge.[89] Thus, there is no practical way of eliminating the reversing layer, but it was possible to reduce it from the size that it was with the lamp in Figure 24a.

The long reversing layer, the efficient atomic recombination on glass and silica, and the temperature differential between layers may have been the causes for substantial deposition of thin films of iodine and iodine oxides on the walls and window in front of the discharge region. This region was much cooler than the region near the plasma, and once condensed, iodine (and its oxides) would remain for long periods during regular operation. Overnight pumping of the lamp system reduced the amount deposited on the walls, but this cleansing process was not practical for normal operation. This posed a serious problem since the transmission of the window was markedly reduced after several minutes to a few hours of routine operation. Switching the direction of the flow so that the outlet was in front, Figure 24a, helped increase the time before substantial window contamination occurred by providing direct pumping between the window and the plasma, but this did not solve the problem.

Figure 24b shows the lamp which was designed to eliminate several of the disadvantages of the first lamp. An annular tubulation was used for the outlet port. This provided active pumping on the lamp axis to help remove substances from the front of the discharge. The Vycor graded seal was blown as close to the o-ring joint as possible. Since there was no front tubulation, the Evenson cavity could then be butted against the brass collar. The center of the cavity was then about 4 cm from the window. With this setup the discharge extended to within 1.5 cm of the window. The path length of the reversing layer was greatly reduced and the window region remained warm during operation and thus prevented gross deposition of iodine. This helped solve the physical, and some of the chemical, problems.

With the new lamp the spectral line intensities were increased and contamination of the window was noticeable only after several days of routine operation. As with the previous lamp, the entire lamp system had to remain relatively oxygen free. Iodine oxides (possibly IO_2 or I_2O_4 and I_2O_5) readily formed in the discharge area and were sources of window contamination. Water vapor was a constant contamination in the lamp system, although its emission around 310 nm was not a problem in the spectral region of interest. The water vapor did not cause any instability in the operation of our lamp.[93] A relatively constant light intensity was reached within seconds of the plasma formation and would remain stable for at least ten minutes. In practical operation the lamp was rarely operated for more than one minute during one pulse experiment.

This lamp provided very stable, intense line emissions. It had several advantages not found in other lamps used heretofore. First, it reduced the length of the absorbing layer in the lamp. This led to higher intensities. Also, the iodine reservoir stopcock, S4, did not have to be open very much to provide sufficient molecular iodine for useful intensities. Thus, it allowed use of the lower parent to carrier gas ratios, which helped minimize possible parent contamination of the lamp window. The flow system pressure was kept at ca. 1 torr to provide an intense and stable discharge. Finally, it allowed the quick exchange and cleaning of the windows and the lamp body.

Figure 26 shows the spectral region of interest scanned on the McPherson 218 0.3-meter monochromator with 0.15 mm slit widths. Line reversal could not be determined at this slit width.[96] In operation the optical system was always optimized for maximum throughput.

The excited atomic iodine state, $5^2P_{\frac{1}{2}}$, was easily studied using the intense 206.2 nm line. Efficient absorption of this line along with its intensity made it the most useful for studying the excited state atom.

a. $6^2P_{3/2} - 5^2P_{1/2}$ 206.2 nm
b. $6^4P_{1/2} - 5^2P_{1/2}$ 187.7 nm
c. $6^4P_{3/2} - 5^2P_{1/2}$ 184.4 nm
d. $6^4P_{5/2} - 5^2P_{3/2}$ 183.0 nm
e. $6^2P_{1/2} - 5^2P_{1/2}$ 179.9 nm
f. $6^2P_{3/2} - 5^2P_{3/2}$ 178.3 nm

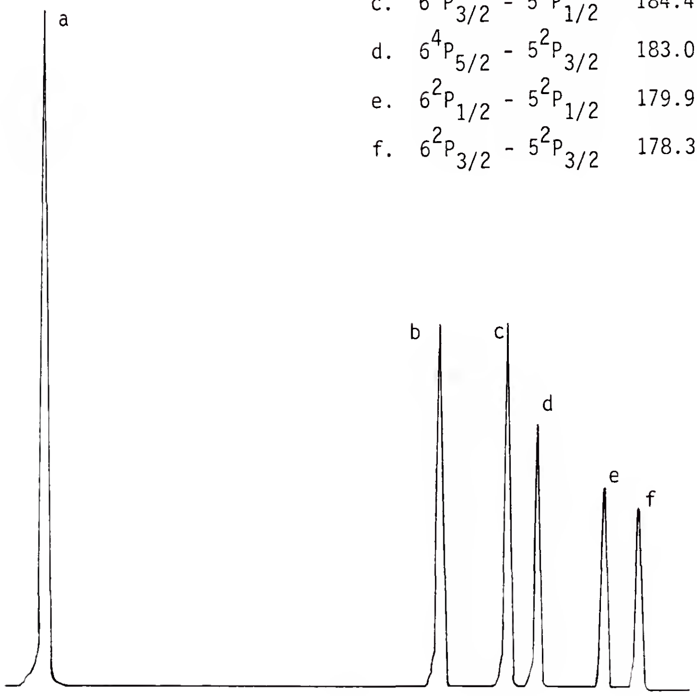

Fig. 26 Iodine emission spectrum from the microwave discharge lamp using a sodium salicylate fluorescent screen to cut off stray visible light from other orders.

Efficient absorption of the 178.3 nm line made it the most desirable for studying the ground state iodine atom.[37,38] It was for this reason that efficient VUV spectrophotometry was necessary. Useful absorption signals were not detected for the other lines with either monochromator or optical system.

Although the lamp emitted light in the VUV, several lines below 200 nm could not be detected until a vacuum monochromator was used. The importance of the vacuum monochromator can be seen in Figures 27 and 28. The spectrum is the same as Figure 26, but with different resolution and scanning speed and with no fluorescent screen. It can be seen that after ten minutes of active pumping good optical transmission was achieved at wavelengths below 180 nm. In operation, the monochromator was pumped for one hour prior to a set of experiments, at which point useful transmitted light at 178.3 nm could be observed. In Figures 26-28 the reaction cell was evacuated.

A major reason an intense light source was needed was due to the expected parent alkyl iodide absorption in the spectral region of interest. Figure 29a shows the lines b-f under high vacuum in the reaction cell. When 2.5 torr of methyl iodide was introduced into the reaction cell, Figure 29b, immediate loss of intensity for lines d-f was observed. Figure 29c and 29d show the line intensities returning for lines d and e after thirty seconds and five minutes, respectively, of active pumping of the reaction cell. The full intensity of line f did not return until after about ten minutes of active pumping. Figure 30 shows the absorption bands for 2.5 torr methyl iodide. The lamp system, though, as designed and optimized was able to transmit useful light intensity for work with the 206.2 nm line using 10 torr or less of alkyl iodide parent compound

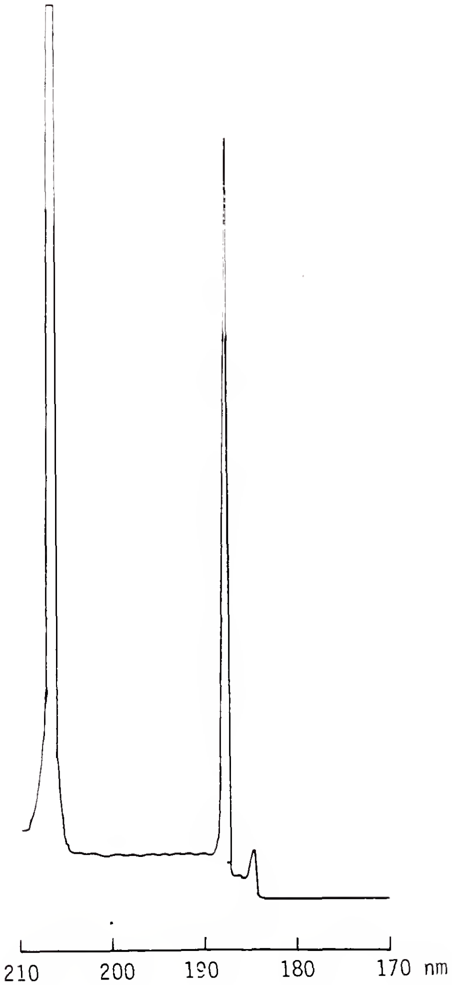

Fig. 27 Iodine discharge lamp spectrum after 5 minutes of active pumping on the McPherson 218. 50 watts microwave power and 0.4 mm slits.

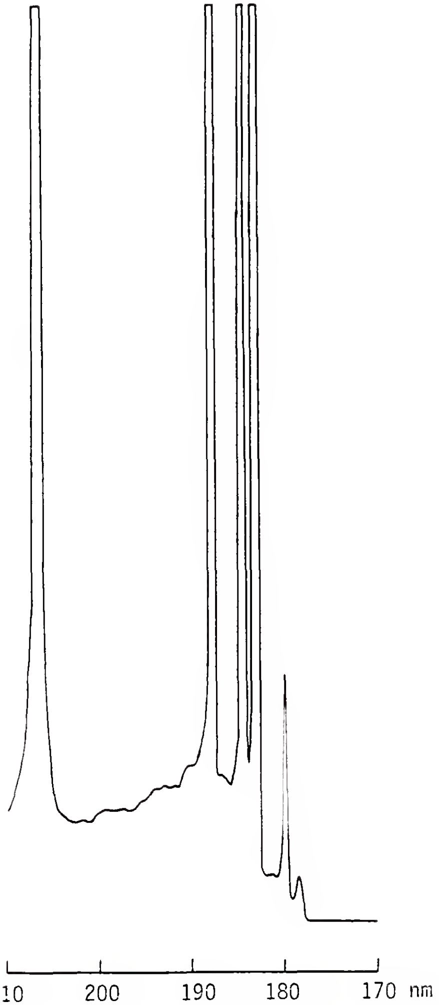

Fig. 28 Iodine discharge lamp spectrum after 10 minutes of active pumpimg on the McPherson 218. 50 watts microwave power and 0.4 mm slits.

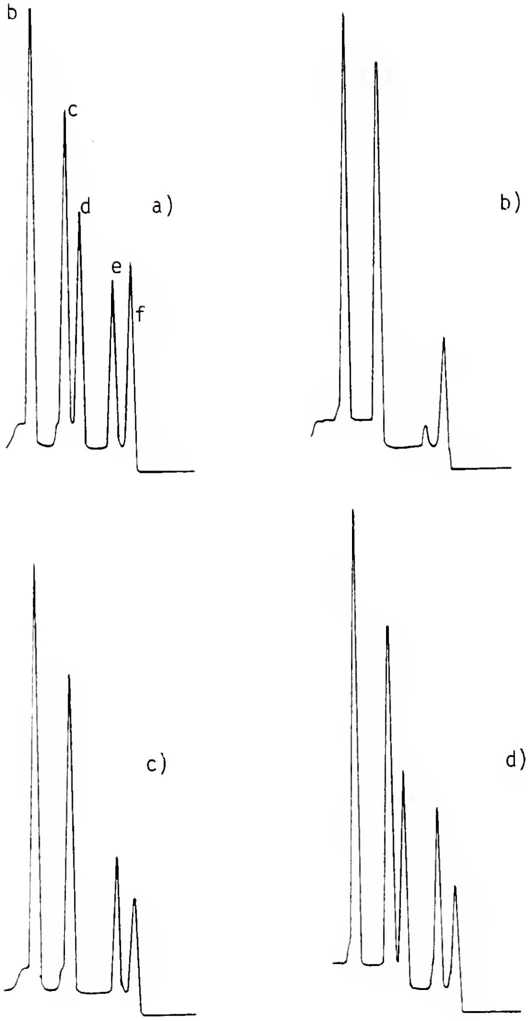

Fig. 29 Chemical compound absorption interference in the spectral range 170 to 190 nm (Fig. 26).

a) Evacuated reaction cell.
b) 2.5 torr methyl iodide in the reaction cell.
c) ca. 30 seconds of active pumping on the reaction cell.
d) ca. 5 minutes of active pumping on the reaction cell.

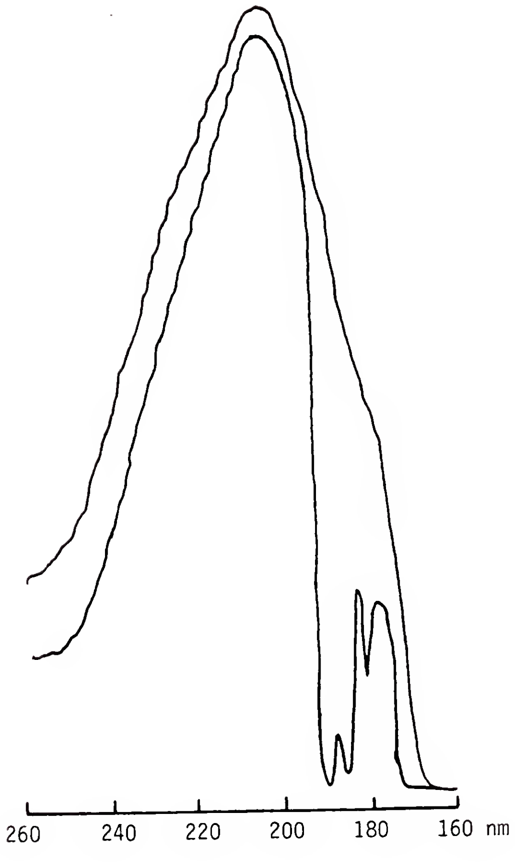

Fig. 30 Absorption band for 2.5 torr methyl iodide in the 200 nm region. Upper line is maximum light intensity through an evacuated reaction cell from a 60 watt deuterium light source.

or 3 torr or less for the 178.3 nm line. The perfluoroalkyl iodides did not absorb as much in this region as the alkyl iodides.

In general, the lamp was found to be very versatile in operation. After overnight pumping and change of the molecular sieve and parent compound, various emission spectra could be observed. Among these, Figure 31 shows the OH radical emission, with argon carrier gas, from the microwave lamp.[99]

The microwave lamp system used in these studies has several other advantages. Since no internal electrodes were used, the lamp body is simpler in design and construction. The use of an efficient resonant cavity also produces a high degree of molecular dissociation,[90] and therefore produces an intense emission spectrum. An added advantage of the electrodeless lamps was that no high voltage points existed outside of the power source. Only microwave radiation shielding must be used. Finally, the flow system had the greatest advantage of being able to handle various carrier gases and parent compounds, enabling the whole system to be a versatile light source.

Mercury lamp

The monitoring light source used for the oxygen-ozone studies was an intense low pressure electric discharge mercury lamp, Figure 32. The lamp system, already available in our laboratory, had been originally designed for AC operation. The lamp was converted to DC by rectifying the AC and stabilizing its steady-state operation with a large, high voltage capacitor. DC operation was necessary since sixty-cycle fluctuation was readily detected in the time scales used in the experiment, and the

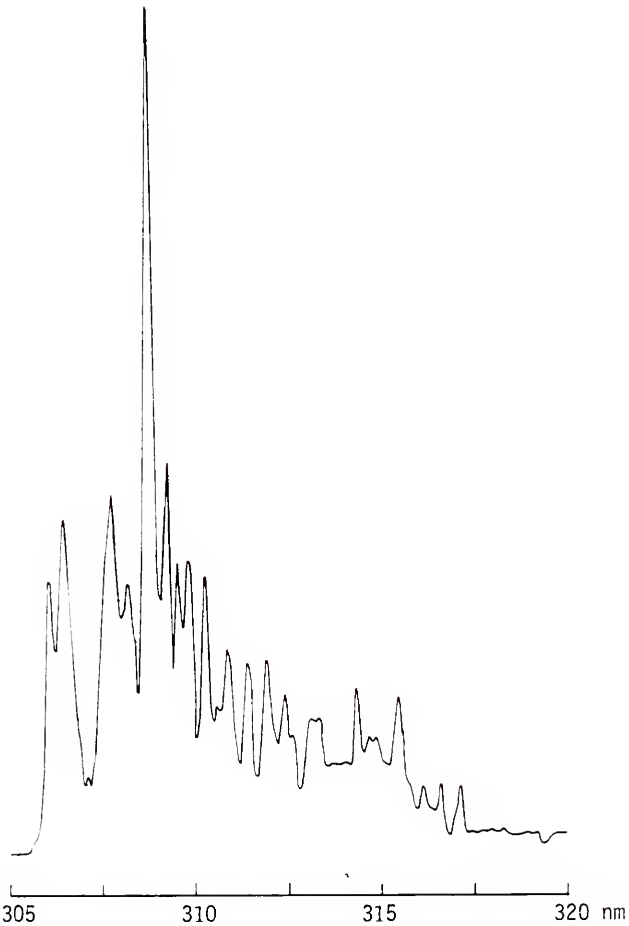

Fig. 31 Emission spectrum of OH ($A^2\Sigma^+ - X^2\Pi$) from the microwave discharge lamp. Lamp pressure ca. 1 mm argon and water vapor.

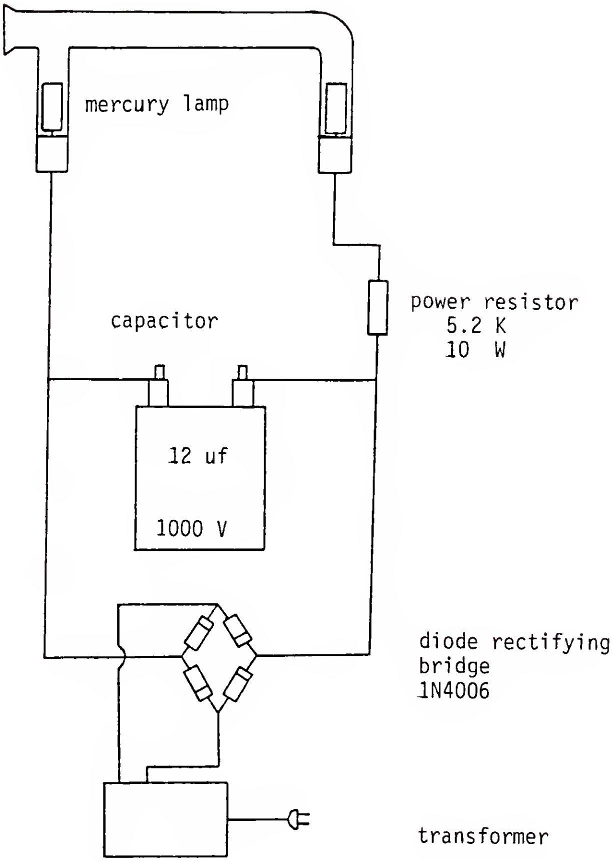

Fig. 32 Mercury lamp system in DC operation mode.

DC provided a constant baseline for the experimental measurements. A power resistor was used in series with the lamp to serve as the current limiter when the lamp was in operation. The lamp was always started with a Tesla coil in order to provide initial ionization. The lamp was used with the experimental configuration shown in Figure 16.

The lamp did not have the stability observed with the microwave discharge lamp. The light intensity versus time changed over the course of its warm-up which took about 90 seconds. After this time the light intensity would gradually decrease mainly due to buildup of ozone near the lamp window and around the optical path outside of the reaction cell (Figure 16) as well as in the reaction cell. The ozone was formed from the photolysis of oxygen by the 184.9 nm mercury line. In order to minimize the ozone buildup by photolysis of the oxygen in the reaction cell, the pulsed experiment was always carried out 35 seconds after the lamp was started. This time was chosen because between 30 and 60 seconds after the lamp was started it showed consistent and reproducible light intensities, and it was early enough so that internal and external ozone buildup was a negligible factor.

Graphs were made of the buildup of the lamp intensity so that maximum intensities at the time of the electron pulse would be known. Since the experiment measured intensities, the initial intensity was needed for the calculation of optical densities. Figure 33 shows the lamp intensity, in relative units, versus time, with the reaction cell evacuated. Figure 34 shows the lamp intensity versus time at various oxygen pressures in the reaction cell. The use of these curves to compute the optical densities for the experimental conditions will be described later.

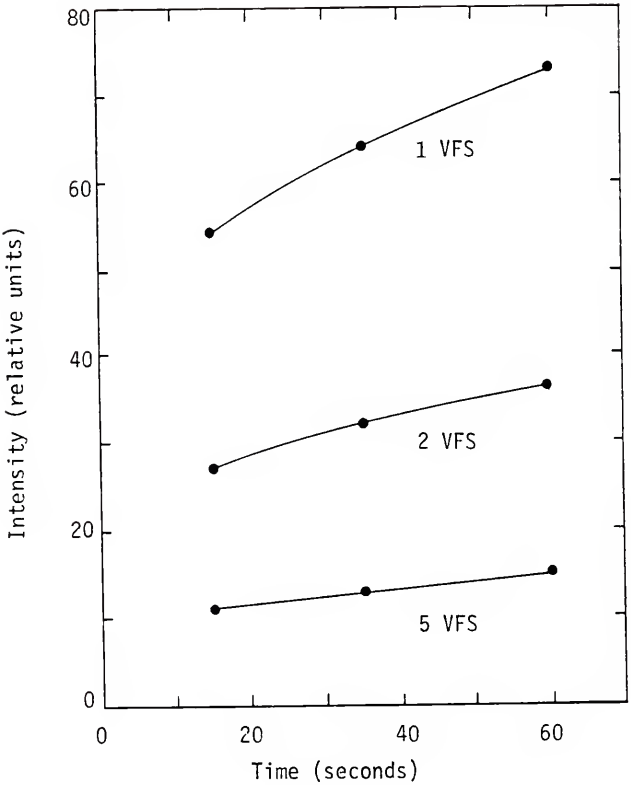

Fig. 33 Hg lamp intensity versus time for various input sensitivities of the transient recorder (volts full scale) with the reaction cell evacuated. The slit widths were 0.8 mm.

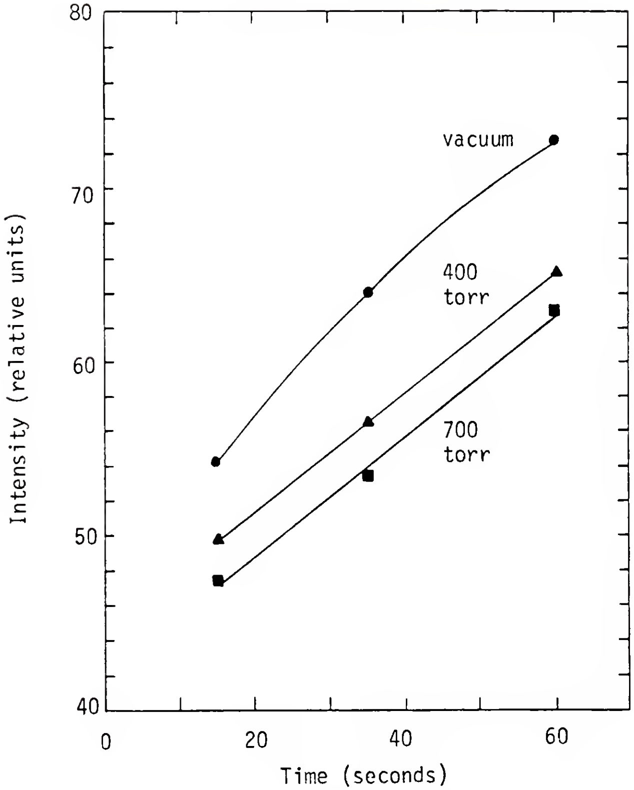

Fig. 34 Hg lamp intensity versus time for two initial oxygen pressures and vacuum in the reaction cell at 1 VFS transient recorder input sensitivity. The slit widths were 0.8 mm.

F. Febetron 706 System

The electron beam source is the apparatus around which the pulse radiolysis system was designed. In principle the electron beam could be used as a direct sample irradiation beam or it could be used to generate an X-ray irradiation beam. The efficiency of conversion is low and the deposition of X-ray energy in a sample is usually low also. For example, a 2 MeV electron may convert about 2% of its energy into X-radiation. A small percentage of this X-radiation would be absorbed by the sample. Thus, the dose per pulse from direct electron beam irradiation of the sample would be about 10^4 times larger than from converted X-rays.[85] Conversion efficiencies for electrons below 1 MeV are even less.[100] Therefore, in practical operation for fast kinetic spectrophotometry, where a large concentration of transients was desirable, it was advantageous to use the electron beam directly. The electron beam can deliver 4 Mrads of surface dose in a thick aluminum absorber. With an efficient X-ray target (converter) the electron beam could produce an X-ray dose of 100 R at the target surface. This X-ray dose 30 cm from the target, through air, is 80 mR. Larger Febetrons, like the 705, can deliver a dose, at this distance, of 25 R. For our purposes the e-beam was utilized directly.

As previously discussed, low pressure (atmospheric or less) pulse radiolysis requires a large pulse current for production of observable concentrations of transients. For fast kinetic spectrophotometry the initiating pulse should ideally be shorter than the rate process being observed. The range of lifetimes which can be studied is extended by a short pulse. The Febetron 706 easily met these two basic requirements. Equipped with a Model 5515 high vacuum field emission tube it could deliver a beam energy of 10 Joules, a peak current of about 8 kiloamperes, and a maximum electron energy of 600 KeV in a pulse duration of 3 nanoseconds, FWHM[101]. The pulse-to-pulse repeatability was specified as 5%. This was observed to be fairly consistent, although a 5-10% difference in pulses was observed for about 50% of the pulses during normal operation under equal conditions.

Details of the Febetron 706 system may be found elsewhere.[100,102] Figure 35 shows a diagram of the system. Briefly, 15 modules in the Marx-surge pulser circuit were charged from the high voltage power supply in parallel, with their central spark gaps in open circuit. A triggered voltage breakdown of the spark gaps discharged the modules in series. The high voltage output to the short pulse adapter was thus created by addition of the charging voltages. The high voltage, coaxial, oil-dielectric capacitor in the short pulse adapter received the high surge current pulse. After a predetermined voltage was reached and subsequent breakdown a shorter pulse was discharged into the field emission tube and passed out the tube window.

The e-beam tube incorporated a cold cathode electron source and a thin window of low density material. The high density e-beam was accelerated through the thin window.

Since the energy density of the e-beam was high enough to cause melting, evaporation, or spallation of metals the titanium reaction cell window was designed to be several centimeters from the tube window. This design insured that melted, evaporated, or spalled materials could not condense on or strike the tube window causing subsequent damage.

In our experience the Febetron 706 was found to be a highly reliable low maintenance system. Its various operating requirements are simple. A compressed air tank is used for pressurization of the module chamber,

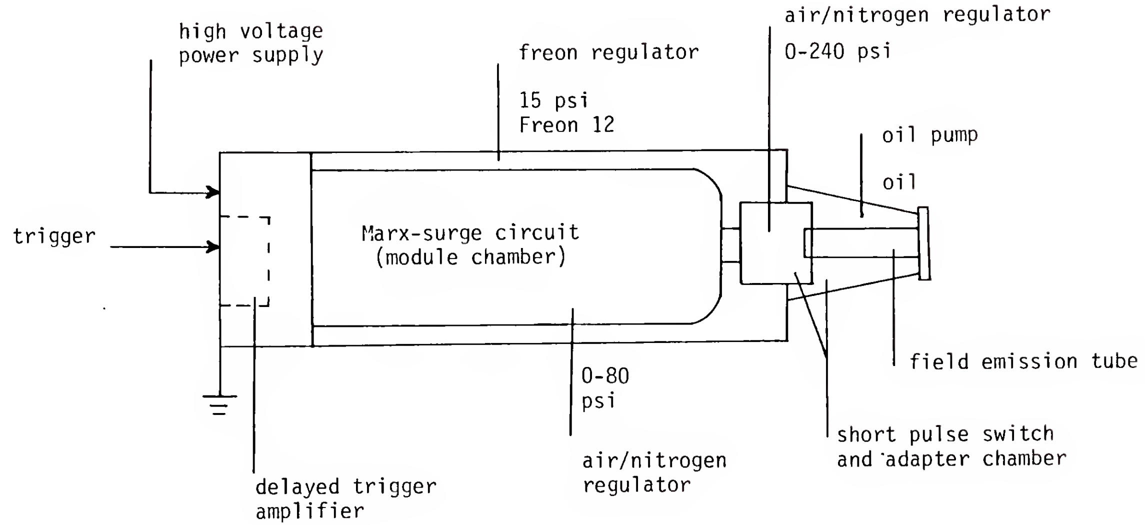

Fig. 35 Febetron 706 System.

at a maximum 80 psi, and the short pulse adapter, at a maximum 240 psi. Each chamber had its own pressure regulator and gauge. Freon 12 was used in the pulser case at a constant 15 psi pressure.

The transformer oil in the short pulse adapater was circulated from a large reservoir by an electric pump. During normal experimental operation the oil was circulated once daily. The lifetime of the Model 5515 field emission tube was extended beyond 3500 pulses by using it below its maximum output potential. In typical use the total output energy used was about 7 Joules, which corresponds to about a 510 keV maximum electron energy.

G. Transient Recorder and Computer System

Early pulse radiolysis studies used the kinetic spectrophotographic method for the detection system.[8,9] Transient signals were either photographed from a spectrophotometer directly or from an oscilloscope. Expensive high speed photographic film was generally used, followed by manual methods of data analysis. Methods for automatic digitization and analysis of the transient signal were quickly developed.[21,22,103] These methods not only facilitated data acquisition, but greatly reduced the time for analysis of large amounts of data. Substantial savings could also be realized by reducing the use of high speed photographic film.

Present methods employ transient recorders to obtain and store a digital record of the transient signal as a function of time. Such recorders can be directly interfaced to a computer, oscilloscope, or graphic recorder for data display and analysis.

The data acquisition and analysis system developed for the pulse radiolysis system has been described previously.[23] A Biomation Model 610B transient recorder (Biomation) was used to digitize the signal which came from the PMT through two amps in series, Figure 11.[104] The amplifier's bandwidth extended from DC to about 5 MHz.

The Biomatation has an input range from 50 mV to 50 V full scale. The analog bandwidth, though, is directly limited by the input sensitivity. The higher sensitivity scales have lower bandwidths. From 50 mV to 5 V the bandwidth changes from 100 kHz to 2.5 MHz. The analog circuitry preceding the digital circuitry may not be fast enough, under certain conditions, to fully utilize the digital circuitry. The digital circuitry could store a new six-bit word into its 256 word memory as slow as every 50 ms or as fast as every 100 ns. Thus, the analog risetimes could only be neglected when the time between sampling was greater. Therefore, to achieve useful microsecond sampling rates the Biomation had to be used in the 0.5 to 2 V input scales. This necessitated the use of high lamp intensities and high PMT gain. Fortunately, the study of the fast decay of the excited state iodine atom associated with the parent compound pressures used was also associated with a high light intensity. No mismatching of the analog and digital circuitry was observed. For the ground state atom studies, lower lamp intensity necessitated the use of a higher input sensitivity. This, though, did not present a problem since longer sampling rates were used due to the longer lived signals. The ozone studies posed no problems either since the light was intense and the signal was long-lived.

If a signal were to require a high sensitivity scale, the transient lifetimes involved could usually be extended by using lower pressures.

This would help insure faithful digitization of the signal.

In operation the Biomation was used in the single-sweep-delayed-sweep mode. This mode allowed a one shot sampling of the pulse experiment at a chosen delay interval after the trigger signal. Once taken the data could not be lost, changed or disturbed by any subsequent trigger signals until the user armed the input for the next signal. In practice, the trigger delay on the Biomation was set at zero and instead the Febetron trigger pulse was delayed. The Febetron trigger amplifier had a ten turn graduated helipot in conjunction with a decade scale from 10 microseconds to 100 ms. This device was far more sensitive and reproducible than the ungraduated one turn trigger delay on the Biomation.

This triggering system would trigger the Biomation to start sampling first and after an appropriate delay-time the Febetron was triggered, all from one initial manual trigger. In one sweep the Biomation could record the initial intensity before the electron pulse (baseline), the pulse, and the subsequent signal. By varying the sampling rate and the trigger delay the entire signal could be analyzed with any resolution desired that was not analog bandwidth limited.

The IMSAI 8080 S-100 bus microcomputer system, which was developed elsewhere in our laboratory,[105] is based on the Intel 8080 microprocessor chip, Processor Technology Company 3P+S parallel and serial input-output (I/O) board, is similar in concept to larger more versatile systems based on the PDP 11 family hardware.[21,22] However, ours was the first full-featured fast pulse data acquisition and analysis system based on an 8-bit microprocessor to be described in the literature.[23,106]

Operation of the IMSAI 8080 microcomputer required several levels of supporting software. Programs were loaded via an Innovex brand 8 inch floppy disk system controlled by a Peripheral Vision Company interface system and disk operating software. Interaction with the console keyboard and video display was supported by a ROM firmware package associated with the "Merlin" video controller board. This unit, which plugged into the S-100 bus of the computer, also provided hardware and software for good quality graphical display of the experimental results. However, an additional program written in assembly code was necessary to provide the specific graphic features required for the display of pulse radiolysis data. Additional programs written in assembly code provided for transfer of data from the Biomation transient digitizer to the computer, and for transfer and display of the video screen image to the Integral Data Systems Model 225 printer. The interface between all of the computer facilities and the user was provided by a program in BASIC language, running under a considerably modified Processor Technology Company "5K BASIC" interperter. Modifications to the latter included provision to work with a North Star Company floating point mathematics board, to speed up computation; provision of additional built in functions including LOG (natural logarithim), EXP (exponentiation), and others; and the ability to transfer 8-bit bytes and 16-bit words from main memory into BASIC's work space using PEEK and POKE functions. Work on all of the systems programs was done by Mr. Scott Crumpton and Mr. Mark Adler of this laboratory.

H. Computer Programs

The BASIC programs allowed full interaction between the operator and the complete computer system. Program listings are provided in Appendix I. Both programs have similar commands and executions with two exceptions. Only the experimental program (EXP), used during the pulse experiment, had a command (11) which made a hard copy of the data on paper tape, for subsequent data reduction. Only the analytical program (ANA), used solely to reduce data, had a command (8) which was used to print experimental data on the teletype as well as an option for interpolation or extrapolation of the linear least squares (LLS) calculated curve. For EXP the data from the Biomation was transferred directly to the computer. For ANA the data were transferred to the computer through the teletype from paper tape.

In typical operation an EXP program was used to acquire data from a set of pulse experiments and store the data on paper tape. Its data reduction capabilities, Commands 1-7, were rarely used for on-the-spot data analysis due to the time consuming attention required by the operation of the entire pulse radiolysis system by a single operator. Some data were analyzed on-the-spot but only to observe general trends in a set of experiments. Instead, at a more convenient time, the analytical program was used to thoroughly analyze the data.

The programs could input data into memory via command 0 for subsequent manipulation. Commands 1-3 transfer information to a buffer. Command 1 clears the buffer and stores a new signal into memory. Command 2 sums and averages a signal into the buffer for signal averaging, thus achieving better S/N. Command 3 could subtract a signal from the buffer. This was used when a compound noise and physical signal was observed during a pulse experiment. The noise signal, which could usually be observed with the analyzing light turned off, could then be subtracted to yield the signal of the phenomenon under study. For the systems studied this was only necessary when the sampling rate was less than or equal to 2 microseconds per word or the volts full scale the Biomation was 1 VFS or less with a 50 Ohm terminator and 700 volts on the PMT. These sampling rates and conditions would always contain the overload noise pulse within the experimental signal.

Commands 4 and 5 allowed linear least squares fit of a single-experiment signal and the data in the buffer, respectively. Left and right hand cursors could be adjusted to define the time interval over which LLS fit would be carried out. Print-outs of the curve fit and pertinent LLS fits were taken and plotted over the data curve in order to achieve a visual, as well as a numerical, best fit format.

Commands 6 and 7 were used to print raw data values of a single-experiment and the buffer, respectively, on the video. In conjunction with a command to print the data being displayed on the video, a printout of the raw data could also be attained.

Commands 9 and 10 input information which was used for the graphic hard-copy and simplification of the video display, respectively. The graphic output will be detailed later.

I. Reagents and Their Purification

Methyl iodide

Eastman and Mallinckrodt Analytical Reagent grade methyl iodide were initially purified by removing I_2 with Fisher Certified Reagent grade sodium thiosulfate.[107] The liquid was then degassed in the vacuum line for three freeze-pump-thaw cycles. It was then distilled at room temperature into a vessel in a carbon dioxide-isopropanol bath through a Mallinckrodt Analytical Reagent grade phosphorus pentoxide drying tube. The sample was again degassed in a freeze-pump-thaw cycle. Finally, the sample was again distilled in vacuo, without the drying tube, into a storage vessel immersed in a carbon dioxide-isopropanol bath. The first 20 percent and the last 20 percent of the volume were discarded. The storage vessel, which was fitted with a Teflon stopcock, was stored in the dark and the sample was always degassed before use.

Ethyl iodide

Reagent grade ethyl iodide obtained from Baker Chemical was purified and stored using the same method as described above for methyl iodide.

CF_3I and C_2F_5I

Perfluoroalkyl iodides obtained from PCR, Incorporated were used without further purification.

C_4F_9I and i-C_3F_7I

Perfluoroalkyl iodides obtained from PCR, Incorporated were degassed and used without further purification.

Hexafluoroethane

Hexafluoroethane obtained from PCR, Incorporated was used without further purification.

Iodine

Fisher Certified Reagent grade iodine was degassed at 0^{o} C. It was then distilled in vacuo into a small storage tube in a carbon dioxide-isopropanol bath. The tube, fitted with a Teflon stopcock, was on the lamp system vacuum line and was used at room temperature (see Figure 22).

Oxygen

Airco, Incorporated oxygen was used without further purification.

Carrier and flushing gases

Airco, Incorporated argon, helium, and nitrogen, were used without further purification. Sporlan Valve Company Catch-All line filters were used on all the gas lines. The Catch-All filters could be reactivated by heating at 150° C while purging with nitrogen.

J. Sample Preparation

Vacuum system

All samples were prepared in a vacuum line, Figure 36. The pumping system consisted of a Welch Duo-Seal mechanical pump connected through a liquid nitrogen trap to a stainless steel oil diffusion pump. The pumping system was connected to the main manifold through a second liquid nitrogen trap and a 10 mm Teflon stopcock with "FETFE" o-ring seals.

A three-way Eck & Krebs stopcock was used to bypass the diffusion pump, for rough pumping, or direct the flow through it for high speed pumping.

The main manifold was designed with four stopcock ports. Two 3 mm stopcocks were used as buffer gas inlets. Pyrex o-ring joints (#9) connected the stopcocks to the tank gas lines. One 3 mm stopcock was used to isolate the main manifold thermocouple (TC) tube. A 10 mm stopcock separated the main manifold from the submanifold and the Wallace & Tiernan differential pressure gauge.

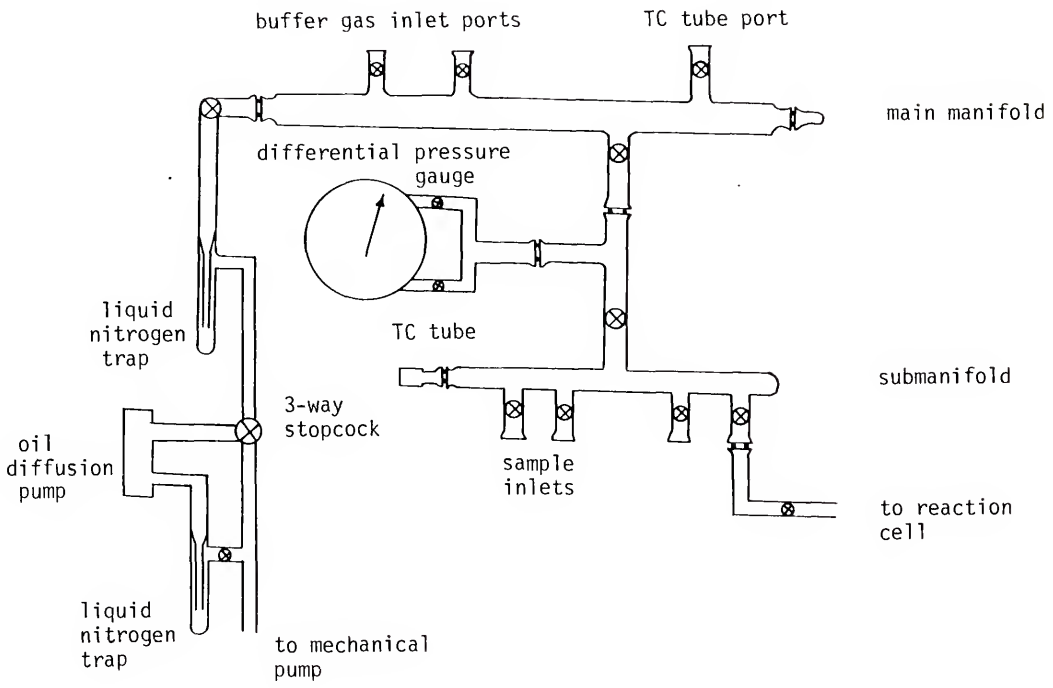

Fig. 36 Vacuum line and pumping system. Schematic.

The submanifold was designed with five stopcock ports. Three 3 mm stopcocks served as sample inlet ports as well as a convenient arrangement for in-vacuo distillation. One 3 mm metering stopcock was used as a sample filling port to the reaction chamber. A 10 mm stopcock was used to isolate the submanifold from the main manifold and the Wallace & Tiernan differential pressure gauge.

A glass tube was used to connect the submanifold with the reaction cell. A 3 mm stopcock at the reaction cell was used to isolate the cell from the rest of the vacuum system as well as serve as the inlet and outlet port for the cell.

All major connections were made with #9 Pyrex o-ring joints. The total design of the vacuum system allowed the system to be taken apart at the o-ring joints when major work had to be carried out on a section.

Metering and filling of the reaction cell

High vacuum was monitored with CVC thermocouple tubes, GTC-004, and a thermocouple gauge. Sample pressures were measured with a Wallace & Tiernan Model 62B-4D-0800 differential pressure gauge (range: 0-800 mm Hg). The case of the gauge was always pumped to a high vacuum and isolated with a 3 mm stopcock. The gauge sample capsule was opened to the chemical sample or isolated through a 3 mm stopcock. The gauge could be used to monitor either glass manifold as well as the entire vacuum system.

All alkyl iodides were expanded into the submanifold, the differential pressure gauge, and the reaction cell. Once the desired pressure was reached the reaction cell was then isolated from the rest of the system. The rest of the vacuum system was pumped down and the buffer gas was introduced through the main manifold into the submanifold and the pressure gauge. To promote mixing of the gases the buffer gas was metered into the reaction cell by three or four expansions.

Low alkyl iodide pressures were attained by volume ratioing between the cell and the submanifold.

For the oxygen-ozone studies, oxygen was expanded into the reaction cell from the main manifold through the submanifold. No mixing technique was required.

When used, the hexafluorethane buffer gas was metered into the submanifold and expanded into the reaction cell.

K. Sample Irradiation

Radiation source and reaction cell

The Febetron 706 e-beam accelerator and the two reaction cells have been described.

The electron beam exiting the field emission tube traverses about 2.5 cm of air before entering the reaction cell through a 2 mil titanium window. The reaction cells were designed so that relatively uniform irradiation was ensured in the region that was sampled by the analyzing light beam. The reaction cell coupling collar to the Febetron allowed reproducible positioning of either reaction cell.

Typically, the parent compound of interest was introduced into the reaction cell at the desired pressure or reduced to a useful pressure by volume ratioing. The buffer gas was metered into the cell so as to promote mixing of gases through turbulence. With the pulse radiolysis and microcomputer system ready, the Febetron was energized and triggered. Due to the build-up of products in the reaction cell, each chemical sample was rarely used for more than two pulses.

III. THE GAS PHASE PULSE RADIOLYSIS OF ALKYL IODIDES

A. Experimental Results

I* deactivation by RI

The pulse radiolysis of the alkyl iodides was carried out at room temperature. The excited state atom was monitored at 206.2 nm using the iodine discharge lamp and atomic absorption spectrophotometry. The pulse radiolysis was carried out over the parent pressure range of 0.5-30 torr, depending upon the extent of the parent compound absorption and its effect upon signal quality. For example, above 9 torr methyl and ethyl iodide absorption interference hindered achieving satisfactory S/N ratios. The argon buffer gas pressures ranged from about 150-600 torr; at these pressures isothermal conditions in the reaction cell following e-beam irradiation were ensured.[36] The buffer gas absorbed energy from the e-beam and transferred energy to the parent compound which subsequently dissociated.

All the computer fits were carried out on the buffer with at least two averaged pulse signals.[23] Since Febetrons are low pulse repetition rate accelerators and due to the complexity of changing reaction samples, rarely were more than four pulses averaged in the buffer for identical experimental conditions. Good signal averaging was achieved with at least three pulses. Figure 37 shows the absorption signal at 206.2 nm for a single pulse experiment. Figure 38 shows the averaged optical signal of three pulses. Significant curve smoothing may be observed.

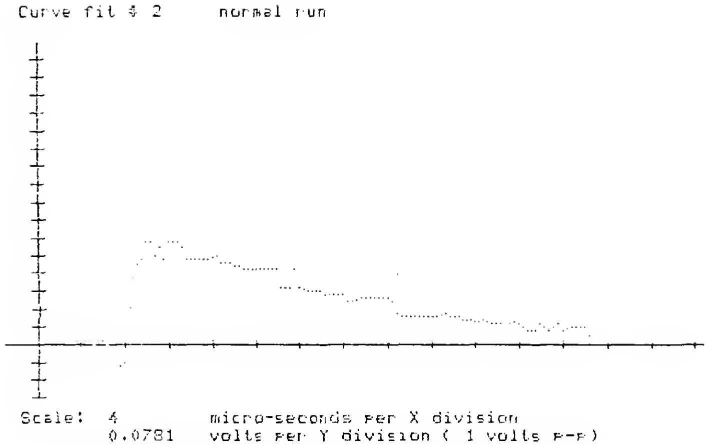

Fig. 37 Graphical display of optical signal versus time for a single Febetron pulse. Conditions: 3.2 torr methyl iodide and 180 torr Ar.

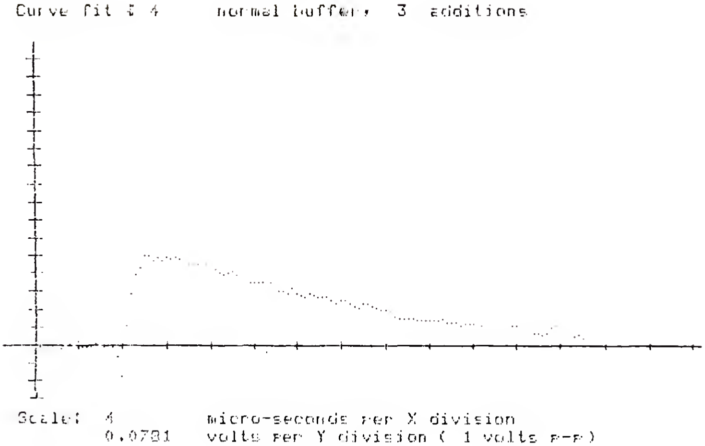

Fig. 38 Graphical display of optical signal versus time for three Febetron pulses summed into the buffer. Conditions as in Fig. 37.

This signal quality is comparable to typical 8-32 runs carried out in flash photolysis experiments.[36,37]

Figure 39 shows a typical curve fit for an apparent first-order experimental signal. Curve fitting was typically carried out over as much of the signal as possible. Signal resolution was achieved by varying the sample interval time scale on the Biomation as needed during data gathering. The best fit was dictated by the goodness-of-fit parameter, the correlation coefficient, along with visual inspection. In general, the first 2-4 microseconds were not fitted due to possible noise interference effects. Even so, these studies allowed observation of the deactivation of I* at much faster time scales and resolution than other recent studies,[35-39] albeit the use of higher parent and buffer gas pressures increased the apparent deactivation rate and thus necessitated faster detection times.

Statistical values relevant to the linear least squares calculated curve were automatically provided below the curve fit plot, Figure 39. The calculated rate constant was divided by the experimental sample interval to yield the apparent rate constant.

Optical densities were calculated from the measured initial light intensity under the experimental conditions prior to irradiation, I_o, and from the digitized optical signal, I_s, from the equation

$$\mathrm{OD} = \log \frac{I_o}{I_t} = \log \frac{I_o}{I_o - I_s} , \qquad \text{III-1}$$

where I_t is the transmitted light intensity at any time after the pulse. Given the input parameter I_o, optical densities were calculated by the computer from the observed optical signal.

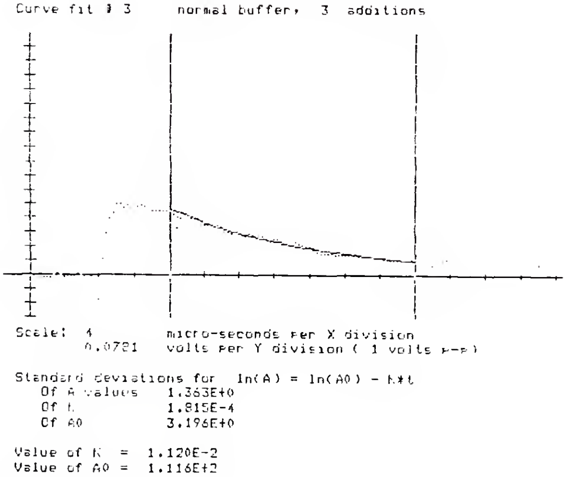

```
Curve fit # 3      normal buffer,  3  additions
```

```
Scale:  4         micro-seconds per X division
        0.0721    volts per Y division ( 1 volts p-p )

Standard deviations for  ln(A) = ln(A0) - k*t
   Of A values    1.363E+0
   Of k           1.815E-4
   Of A0          3.196E+0

Value of K  =  1.120E-2
Value of A0 =  1.116E+2
```

Fig. 39 Curve fit of data from Fig. 38.

The observed apparent deactivation rate constants were plotted as a function of the parent compound pressure in order to calculate k_{RI}, the deactivation rate constant due to the parent compound. The overall rate of deactivation of I* is given by $k_{RI}[RI] + \Sigma k_i[G_i]$. The first term is the deactivation rate due to the parent compound and the second term is the sum of all other gas phase deactivation rates. The slopes of the linear fits yielded k_{RI}. The intercept of each plot was taken to be the sum of all the first-order deactivation processes not attributable to the parent compound. The concentration of buffer gas as well as other species in the system (i.e. impurities or reaction intermediates) are included in $[G_i]$. For the total pressures used and the time scales of observation, diffusion was a negligible contributor to the first-order processes.[43] Table 1 lists the calculated deactivation rate constants. Figures 40 and 41 show representative plots of the apparent rate versus parent compound pressure.

I* deactivation rates by the buffer gas

Table 2 lists the first-order rate constants attributed to the buffer medium, $\Sigma k_i[G_i]$. The specified impurities of AIRCO, Inc. argon are 10.5 ppm, water; 5 ppm, oxygen; 20 ppm, nitrogen; and 3 ppm, hydrocarbons. The respective rate constants for deactivation of I* are (in cm^3/molec s) water,[53] 2.3×10^{-12}; oxygen,[53] 2.5×10^{-11}; nitrogen,[108] 1.5×10^{-16}; and hydrogen,[37] 1.2×10^{-13}; hydrocarbons such as methane have rate constants comparable to hydrogen.[27] Since substantial air leaks into the reaction cell were suspected in the methyl iodide experiments and since the reaction cell subsequently had at least a five times slower leak rate under high vacuum, only the perfluoroalkyl iodide intercepts were used to obtain an average of 9.87×10^3 s^{-1} for the apparent first-order buffer gas quenching rate. The individual contributions from the listed impurities in decreasing order are (in

Table 1

I^* Quenching Rates by RI

RI	I^* quenching by RI k, cm^3/molec s	Reference	
CH_3I	$2.0 \pm 0.1 \times 10^{-13}$	This work	
	2.0	Palmer and Padrick	Ref. 39
	2.5	Baughcum and Leone	Ref. 40
	2.6	Donovan and Fotakis	Ref. 44
	5.7	Donohue and Wiesenfeld	Ref. 38
	17	Donovan, Hathorn, and Husain	Ref. 28
C_2H_5I	$5.0 \pm 0.3 \times 10^{-13}$	This work	
	1.9	Donovan, Hathorn, and Husain	Ref. 28
	6.1	Donohue and Wiesenfeld	Ref. 38
CF_3I	$8.8 \pm 1.5 \times 10^{-16}$	This work	
	3.5	Husain and Wiesenfeld	Ref. 108
C_2F_5I	$9.7 \pm 1.0 \times 10^{-15}$	This work	
i-C_3F_7I	$1.7 \pm 0.1 \times 10^{-15}$	This work	
	0.28	Beverly and Wong	Ref. 54
	0.80	Wilson and Lee	Ref. 55
C_4F_9I	$1.8 \pm 0.1 \times 10^{-14}$	This work	

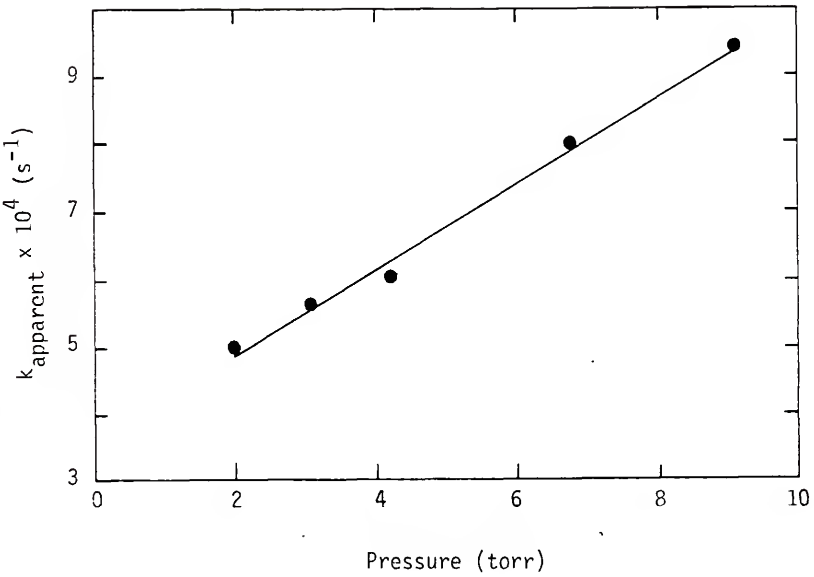

Fig. 40 Pulse radiolysis of methyl iodide with 180 torr argon. Deactivation of I* measured at 206.2 nm.

$k_{RI} = 2.0 \times 10^{-13}$ cm^3/molec s

$k_{buffer} = 6.2 \times 10^{-15}$ cm^3/molec s

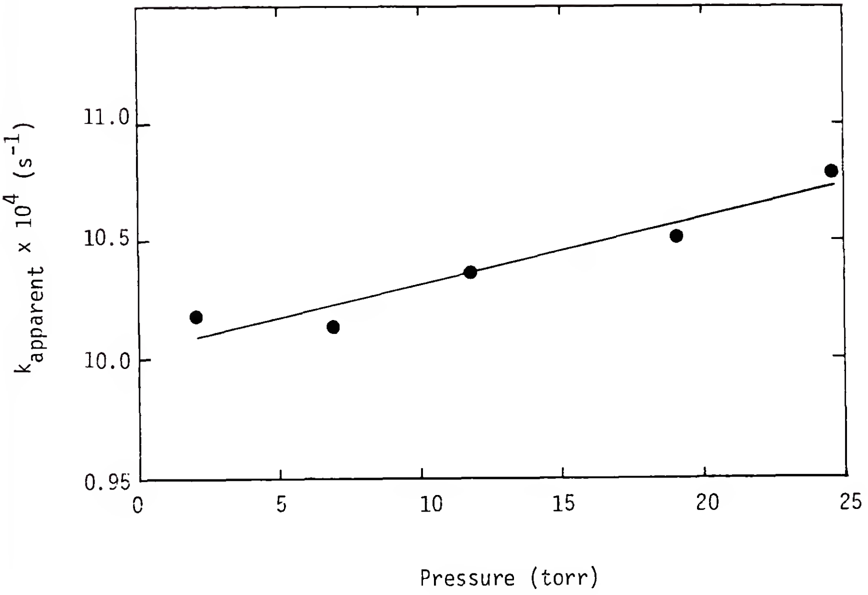

Fig. 41 Pulse radiolysis of trifluoromethyl iodide with 575 torr argon. Deactivation of I* measured at 206.2 nm.

k_{RI} = 8.8×10^{-16} cm^3/molec s

k_{buffer} = 5.4×10^{-16} cm^3/molec s

Table 2

I^* Quenching Rates by the Medium

RI	Pressure from argon tank (torr)	I^* quenching by the medium k, cm^3/molec s	
CH_3I	183	$(6.2 \times 10^{-15})^a$	
CF_3I	575	5.4×10^{-16}	
C_2F_5I	575	5.8×10^{-16}	
i-C_3F_7I	575	4.5×10^{-16}	
C_4F_9I	575	5.4×10^{-16}	
	(Argon)	9.9×10^{-17}	Ref. 109
	(Argon)	$\leq 3.8 \pm 0.4 \times 10^{-16}$	This work

a) Note: Probably high due to an air leak.

s^{-1}) oxygen, 2.33 x 10^3; water, 450; hydrogen and hydrocarbons, 10; and nitrogen was even more negligible than hydrogen and the hydrocarbons. Because of the magnitude of the deactivation rate constant of oxygen, even small impurities of it in the buffer gas cause major effects. The remaining deactivation rate was attributed to argon and was calculated to be 3.8 ± 0.4 x 10^{-16} cm^3/molec s. Since larger concentrations than specified have been found in similar compressed gas tanks[61] this value should be set as an upper limit as an I* deactivation rate constant for argon.

Branching ratios

In order to measure branching ratios I was observed at 178.3 nm and I* at 206.2 nm; the oscillator strengths of these two transitions are almost equal[110] and their optical densities may be directly compared.[111] Initially and at short times a population inversion was evident. Table 3 lists the initial I* fractions and the branching ratios along with determinations by photoinitiation. The parent compound pressures used ranged from 0.5-4 torr with 575 torr argon buffer gas. These low pressures were used to avoid parent compound absorption interference with achieving good signal quality at 178.3 nm. The parent pressures also had to be representative of a potential laser system, since lasing threshold by photoinitiation for these gases occurs around 0.5 torr.[46]

Computer simulation

The computer simulation program was originally written in FORTRAN II[112] and converted to FORTRAN IV[113] and used on an S-100 bus CP/M-

Table 3

I^* Fraction and Branching Ratios

RI	I^* fraction $\frac{[I^*]_0}{[I^*]_0+[I]_0}$	Branching ratio $\Phi = \frac{[I^*]_0}{[I]_0}$	Method	Reference	
CH_3I	0.73	2.7	Pulse radiolysis	This work	
	0.76		Flash photolysis	Palmer and Padrick	Ref. 39
	0.78	3-4	Laser photolysis	Riley and Wilson	Ref. 32
	0.81		Laser photolysis	Baughcum and Leone	Ref. 40
	0.92	11.5	Flash photolysis	Donohue and Wiesenfeld	Ref. 37
CF_3I	0.79	3.8	Pulse radiolysis	This work	
	0.90		Flash photolysis	Husain and Wiesenfeld	Ref. 108
	0.91	10	Flash photolysis	Donohue and Wiesenfeld	Ref. 37
C_2F_5I	0.73	2.7	Pulse radiolysis	This work	
	0.98	50	Flash photolysis	Donohue and Wiesenfeld	Ref. 37
$i\text{-}C_3F_7I$	0.76	3.2	Pulse radiolysis	This work	
	0.90	8.8	Flash photolysis	Donohue and Wiesenfeld	Ref. 37
C_4F_9I	0.65	1.8	Pulse radiolysis	This work	

based Z80 microcomputer. The program was modified to create a disk file of the output concentration versus time data, as well as printing it on the console video display or line printer. The output data file was picked up from the disk by a BASIC program which normalized the concentration data and displayed the data in graphical form on the video screen using a Vector Graphics high-resolution bit-mapped graphics board and on an Integral Data Systems Model 225 dot-matrix printer, using special assembly language subroutines. The graphical programs were written by F. Kelley St. Charles and R.J. Hanrahan.

The input parameters to the program are the mechanistic steps, their rate constants, the identification of reactants and products, their initial concentrations, and information which controls the computation intervals.

B. Discussion

In less than ten years after its discovery[25] the atomic iodine laser was shown to be a high-powered photochemical laser.[48] Initial kinetic studies on potential laser systems were carried out on the alkyl iodides.[27] After it was determined that perfluoroalkyl iodides provided better laser peak power as a function of parent pressure than alkyl iodides,[46] major laser development was based on the perfluoroalkyl iodides.[48] The reason for their use is their slower I* quenching rates compared to the alkyl iodides. Table 1 shows that the order of quenching rates are $C_2H_5I > CH_3I > C_4F_9I > C_2F_5I > i\text{-}C_3F_7I > CF_3I$, in agreement with laser output studies.[46] A slow quenching rate is favorable for maintaining a population inversion since collisional and chemical reactions are the only competing relaxation processes with emission. There has been only one study which yielded evidence of significant I* reactivity with methyl iodide,[34] otherwise chemical reactivity has been found to be negligible relative to collisional quenching.[39]

To check the dependency of a kinetic model upon the post-irradiation species in the reaction cell, computer curves were calculated[112] using the information from the signal in Figure 39. Figure 42 shows calculated curves for I* deactivation, intermediates, and products for

	k, cm^3/molec s	
$I^* + CH_3I \rightarrow I + CH_3I$	2.0×10^{-13}	III-2
$I^* + CH_3I \rightarrow I_2 + CH_3$	5.0×10^{-15}	III-3
$I^* + CH_3 \rightarrow I + CH_3$	6.4×10^{-12}	III-4
$I^* + I_2 \rightarrow I + I_2$	3.6×10^{-11}	III-5
$CH_3 + CH_3 \rightarrow C_2H_6$	4.9×10^{-11}	III-6
$I + I \xrightarrow{Ar} I_2$	3.9×10^{-14}	III-7
$I + I \xrightarrow{CH_3I} I_2$	4.1×10^{-14}	III-8
$I^* + C_2H_6 \rightarrow I + C_2H_6$	2.4×10^{-14}	III-9
$I + CH_3 \rightarrow CH_3I$	2.0×10^{-13}	III-10
$CH_3 + I_2 \rightarrow CH_3I + I$	1.7×10^{-13}	III-11
$I^* \xrightarrow{buffer} I$	$3.6 \times 10^{4}\ s^{-1}$	III-12

It was found that I* deactivation was not very sensitive to Reaction III-3 since it has such a slow rate constant. A twofold change in the rate constant had negligible effect upon the overall I* decay half-life. Reaction III-5 was also negligible because of the low concentrations of I_2 at early times. This was also confirmed by the inability to detect I_2 formation in the time scales prior to diffusion loss under the most favorable conditions for its formation from the CF_3I irradiated system.[114]

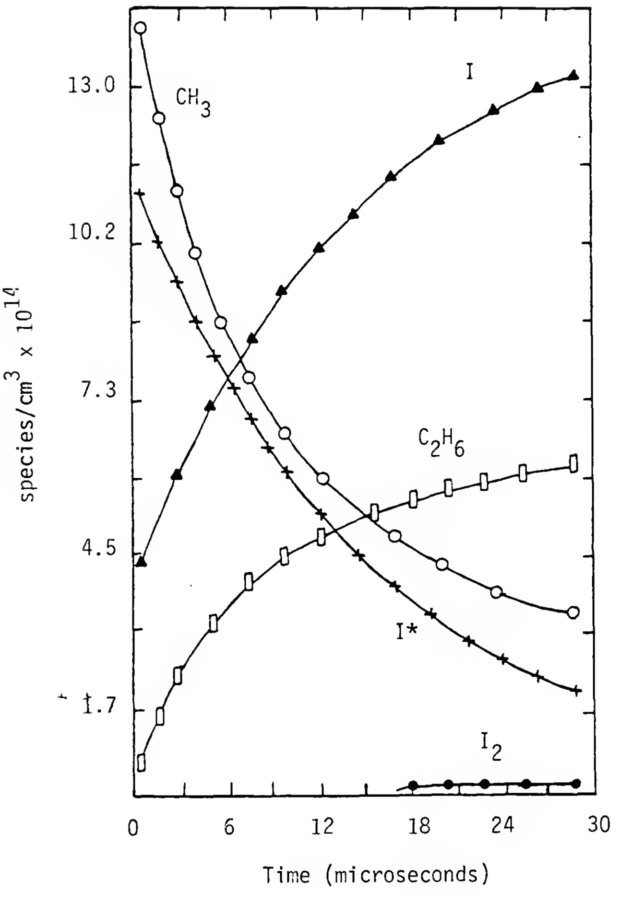

Fig. 42 Computer calculation for I* deactivation, intermediates, and products. The I* curve models the decay curve in Fig. 38.

Similarly, Reaction III-9 is not important during the first half-life of I* deactivation. Reaction III-4 is significant to I* quenching at very early times but Reaction III-6 quickly depletes the initial CH_3 concentration. The role of vibrationally hot methyl radicals in this system is still not completely understood though recent studies[32,40] conclude that only a small amount of hot radicals are formed following UV irradiation of methyl iodide. Analysis for reaction products from hot methyl radical reactions[1] would greatly help ellucidate their role in each lasant system. The major contributions to I* deactivation are due to the large deactivation rate constant and high parent compound concentrations for Reaction III-2 and the large buffer gas concentration for Reaction III-12.

Also important to the output of the laser is the extent of the population inversion, which is measured by the branching ratio. Table 3 shows that the branching ratios for CF_3I and i-C_3F_7I are the largest for these pulse radiolysis studies. In conjunction with their lower deactivation rate constants they would be the most favorable candidates for a linear e-beam initiated laser.

In these experiments about one joule was deposited in the reaction cell. Electron accelerators which can deliver kilojoule pulses and laser cells with magnetic fields which guide the e-beam through the laser cell are available.[115] Various techniques may be used for efficient deposition of energy.[115,116] In light of the low energy deposition in these experiments and the observed branching ratios which are comparable to photoinitiation by high energy flashes created from discharges of hundreds of joules[34,37,39,46] an e-beam initiated atomic iodine laser shows good promise for total system energy efficiency as has been found with e-beam initiated lasers in other chemical systems.[115]

IV. FORMATION OF GROUND STATE OZONE IN THE PULSE RADIOLYSIS OF OXYGEN

A. Experimental Results

Dosimetry

Figure 43 shows a typical absorption versus time curve for the formation of ground state ozone at room temperature following e-beam irradiation of pure oxygen at 750 torr pressure. The absorption versus time curves were measured at 253.7 nm near the absorption maximum for ground state ozone, $^1A_1$.[74] Dosimetry of the system using the maximum ozone yield at 253.7 nm and taking a G value for O_3 formation of 13.8 molecules/100 eV[63] gave an average dose absorbed by oxygen of 7.3×10^{18} eV/g at 750 torr, in agreement with previous studies which used similar electron accelerators, Figure 44.[63,73]

The energy absorbed by argon in the alkyl iodide experiments was calculated to be 1.174 times that of the oxygen dosimeter at equal pressures above 500 torr by using the relationship $E_{sample}/E_{dosimeter} = S_{sample}/S_{dosimeter}$, where E is the energy absorbed and S is the electron stopping power.[117]

Oxygen-ozone kinetics

The pseudo-first order rate constants at each pressure were determined by a least-squares fit of log $(OD_f - OD_t)$ versus time.[61,62,73] Figure 45 is an example of the linear plots which result. The optical density after the ozone concentration reached a plateau is OD_f, as

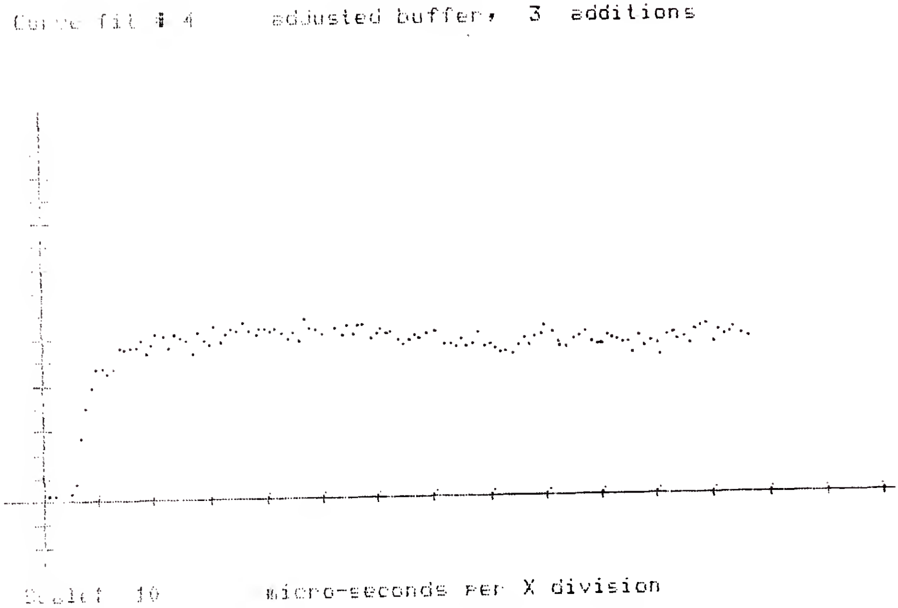

Fig. 43 Ozone absorption growth monitored at 253.7 nm following the pulse radiolysis of 750 torr O_2.

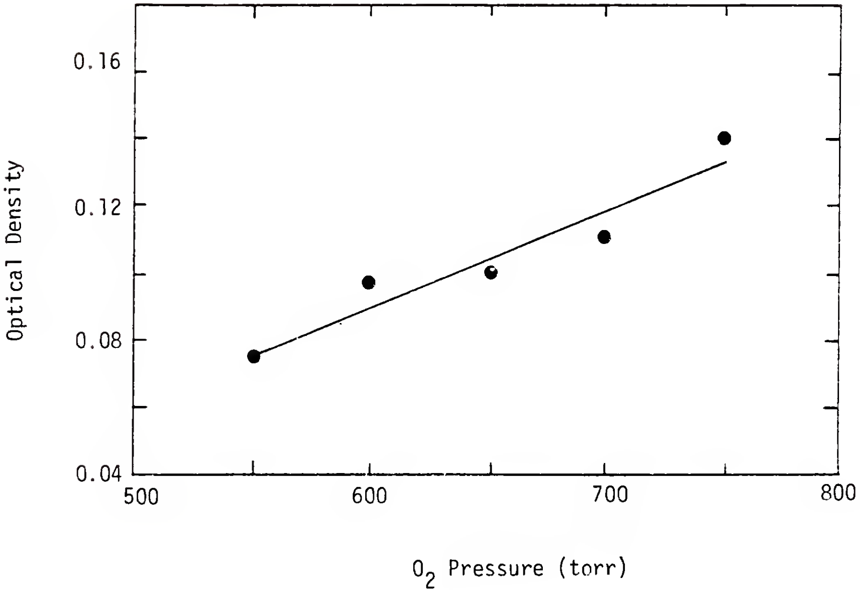

Fig. 44 Dosimetry: Ozone yield in the pulse radiolysis of oxygen measured at 253.7 nm. The linear relationship of ozone formed versus oxygen pressure is due to the linear relationship of energy deposited versus oxygen pressure.

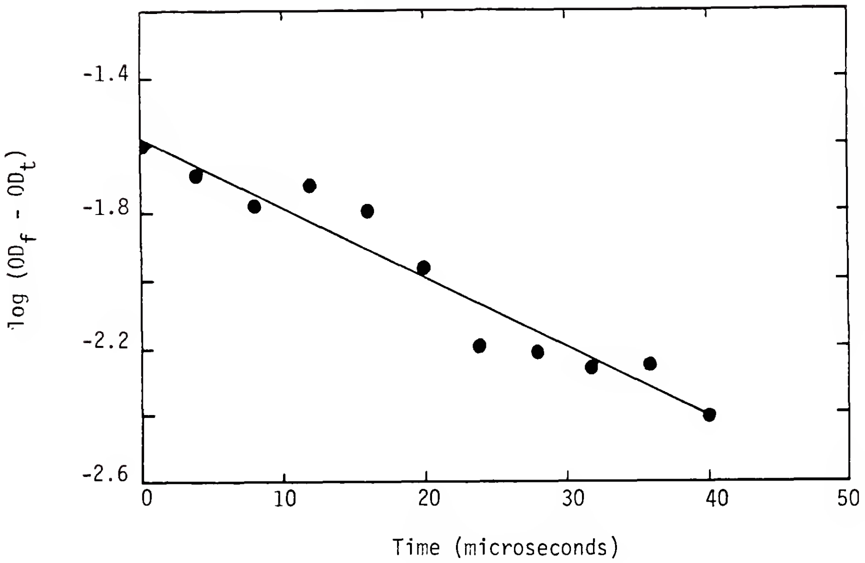

Fig. 45 First-order plot of ozone absorption growth (Fig. 43) following the pulse radiolysis of 750 torr O_2.

observed in Figure 43, and OD_t is the optical density at any time after the pulse. The data were compressed for convenience in making Figure 45 by combining groups of two experimental points and displaying every other group as a plotted point. Optical densities were automatically calculated using the appropriate mode of the data analysis computer program.[23] Usually, two to four pulses were averaged into a memory buffer to enhance the signal/noise ratio before calculations were carried out.[23] A linear least squares fit program was used to obtain the slope of each plot. No obvious deviations from linearity nor any induction period was observed in the plots as had been observed in previous pulse radiolysis work on pure oxygen.[71,73]

If Reaction I-3 correctly describes the process being observed then the pseudo first-order rate constant (obtained directly from the slope of the experimental graphs) can be converted to a true termolecular rate constant by dividing by the square of the oxygen concentration. (See for example the work of Sauer and Dorfman[61] and Hochanadel et al.[62]) If this calculation is made, the rate constant for Reaction I-3 with oxygen as the third body at 750 torr was $3.9 \pm 0.6 \times 10^{-34}$ $cm^6/molec^2$ s, in apparent agreement with previous studies.[61,62,64,71]

An attempt was made to examine the validity of a third-order fit to the rate constant data by varying the O_2 gas pressure. The range of variation possible was quite limited, however. Pressures much above 1 atm were ruled out by glass components, epoxy-sealed optical windows, and the thin foil used to admit the e-beam to the cell. Pressures much lower than 0.5 atm were impractical because of the decreased amount of energy deposited in the cell, and the consequent decrease in the light absorption signal. Over this limited range of pressures, the pseudo first-order rate constants appeared to be proportional to the first power of the oxygen gas concentration. Figure 46 shows a plot of k(apparent) versus oxygen pressure; the slope of the line shown corresponds to a rate constant of 4.1 x 10^{-15} cm^3/molec s. This value is based on the two higher pressure points, which agree with a first-order dependence on oxygen. The deviation of the lowest pressure point (500 torr) is in the direction of an oxygen dependence even lower than first-order. The 2nd-order rate constant was calculated from the two higher pressure points, but the value increases by only 10% if all three data points are used. This rate constant gives a half-life for vibrational ground state ozone formation of 6.9 microseconds at 750 torr total pressure, in good agreement with the 5 microsecond half-life reported for pulse radiolysis of oxygen at atmospheric pressure.[72]

B. Discussion

A simple sequence of simultaneous reactions was formulated to model the data for ozone formation.

$$O\,(^3P) + O_2\,(^3\Sigma_g^-) + O_2 \xrightarrow{ak_0} O_3\,(^1A_1) + O_2 \qquad \text{IV-1}$$

$$O\,(^3P) + O_2\,(^3\Sigma_g^-) + O_2 \xrightarrow{bk_0} O_3\,(^3B_2) + O_2 \qquad \text{IV-2}$$

$$O\,(^3P) + O_2\,(^3\Sigma_g^-) + O_2 \xrightarrow{ck_0} O_3^*\,(^1A_1) + O_2 \qquad \text{IV-3}$$

$$O_3\,(^3B_2) + O_2 \xrightarrow{k_4} O_3\,(^1A_1) + O_2 \qquad \text{IV-4}$$

$$O_3^*\,(^1A_1) + O_2 \xrightarrow{k_5} O_3\,(^1A_1) + O_2 \qquad \text{IV-5}$$

Recent measurements place the total rate constant k_0 for oxygen atom disappearance in the range 5.7-6.9 x 10^{-34} cm^6/$molec^2$ s.[58,59] This value corresponds to the sum of the three Reactions IV-1, 2, and 3.

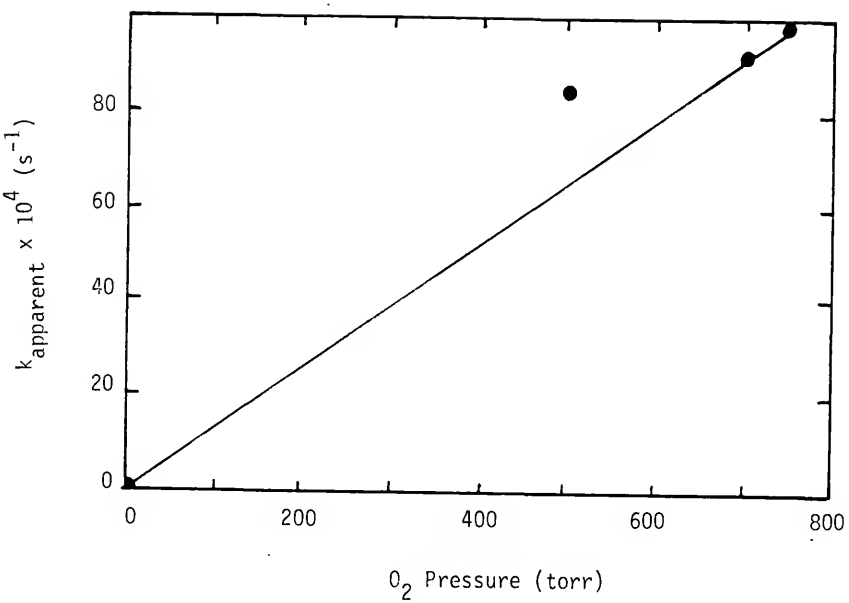

Fig. 46 Ground vibrational state ozone formation rate versus O_2 pressure. Zero points were added to the plot. The point at 500 torr was not used in the calculation of the rate constant.

The quantities a,b, and c represent the branching ratios for Reactions IV-1, 2, and 3 so that a+b+c=1. Von Rosenberg and Trainor measured a minimum branching ratio of 0.6 for Reaction IV-3 following flash photolysis of pure oxygen.[74] Kleindienst et al. calculated a branching ratio of 0.6 for Reaction IV-2 compared to other possible pathways in the flash photolysis of oxygen-ozone mixtures.[77] They stated that vibrationally excited ozone did not play a significant role in their modeling scheme. These reported branching ratios are clearly in conflict, exceeding unity without any contribution from Reaction IV-1.

Since the reported half-life of the ozone precursor decay is about 5 microseconds,[62,72] in good agreement with the half-life which was observed for the ground state ozone formation, the kinetic model was based on the assumption that the same precursor accounts for these observations. The value of k_4 was varied to match the calculated curve for formation of ground vibrational state ozone with the experimental, consistent with assignment of reasonable values to the branching ratios and the known value of k_0. Vibrationally excited ozone in the ground electronic state is O_3^*. The rate constant k_5 was taken from infrared studies of vibrationally excited ozone emission and ranged from $1.0\text{-}2.3 \times 10^{-14}$ cm^3/molec s.[73,74,76]

Taking the net rate constant of oxygen atom disappearance as 6.4×10^{-34} cm^6/molec^2 s, various branching ratios were used to model the observed data. Figure 47 shows calculated curves for ozone formation and for the intermediates. The $^1A_1$ curve matches the observed signal in Figure 43. The branching ratios used are a=b=0.2 and c=0.6. In general k_4 could only be increased to about 5.7×10^{-15} cm^3/molec s, which corresponds to $t_{\frac{1}{2}} = 5$ microseconds at this pressure, if Reaction IV-2 had a greater branching ratio than Reaction IV-1 and greater than or equal to Reaction IV-3. The best fits used b+c= 0.7 ± 0.1.

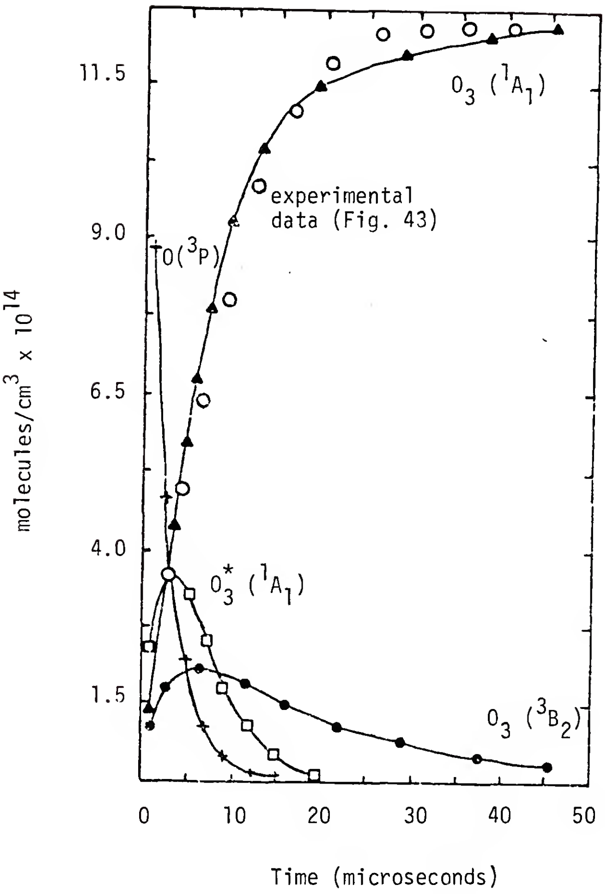

Fig. 47 Computer calculation for a=b=0.2 and c=0.6. The O_3 ($^1A_1$) curve models the formation curve in Fig. 43. The O_3 ($^3B_2$) curve has a decay half-life of 14 microseconds.

The calculated curves agree with previous observations that a large fraction of ozone formed from Reaction I-3 with oxygen as a third body is formed in excited states.[62,73-77] Since the deactivation of the vibrational states has been observed to be relatively fast[73,74,76] and would not account for a half-life for ground vibrational state ozone formation greater than 3 microseconds then a substantial fraction of ozone must be formed in a metastable state with a slower deactivation rate than vibrational relaxation with oxygen. In the absence of independently measured branching ratio data in the pulse radiolysis of oxygen only a lower limit of 2×10^{-15} cm^3/molec s can be established for Reaction IV-4. This is about 10 times that suggested by Kleindienst et al.[77] Although there is reasonable fit of the observed data with this modeling scheme, there is no reasonable agreement with the observed half-life of the $^3B_2$ state decay.

If the reaction

$$O_3\,(^3B_2) + O_2 \xrightarrow{k_{4b}} O_3^*\,(^1A_1) + O_2 \qquad \text{IV-4b}$$

was considered as an efficient channel for deactivation of O_3 ($^3B_2$), with a rate constant greater than k_4 and less than k_5, it had the net effect of decreasing k_4 toward the stated lower limit and increasing the branching ratio for Reaction IV-2 for fitting of the experimental data. Figure 48 shows a calculated curve for ozone formation and for the intermediates. The branching ratios are a=0.1, b=0.6, and c=0.3. The half-life for the $^3B_2$ decay is 4.6 microseconds and k_{4b} is 6.0×10^{-15} cm^3/molec s. The best fits used b+c=0.8 ±0.1. Thus it is suggested that in order for the $^3B_2$ state of ozone to have a half-life decay of about 5 microseconds a second deactivation channel such as Reaction IV-4b must be present.

Two major conditions which must be considered with this modeling scheme are (1) that the production of oxygen atoms by back reactions is negligible during the time of observation and (2) that all the ozone

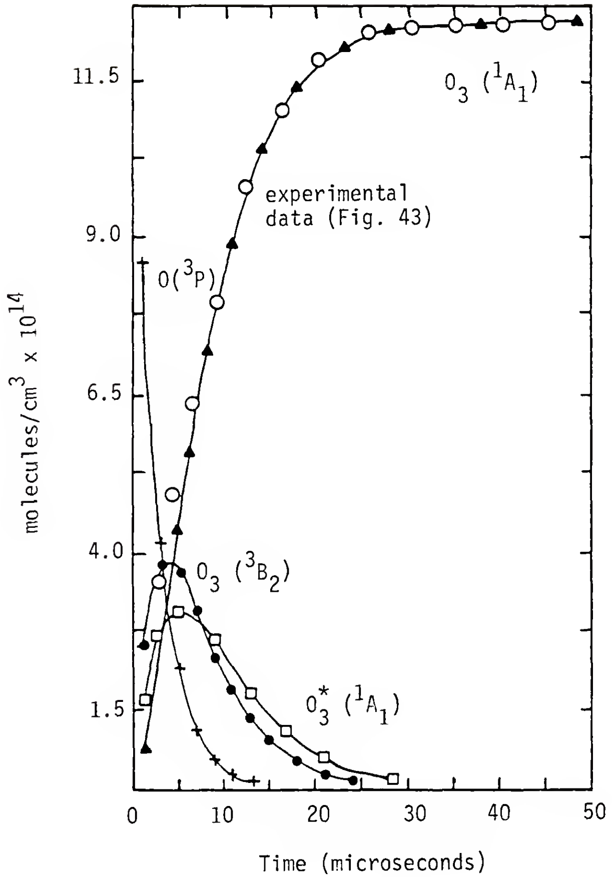

Fig. 48 Computer calculation for a=0.1, b=0.6, and c=0.3. The O_3 ($^1A_1$) curve models the formation curve in Fig. 43. The O_3 ($^3B_2$) curve has a decay half-life of 4.6 microseconds.

formation is from a single oxygen atom precursor. Using the value 6.4×10^{-34} cm^6/molec^2 s for the rate of oxygen atom disappearance, the oxygen atom half-life is about 1.8 microseconds under the experimental conditions. The first condition is ensured since the observation of ozone formation was carried out over tens of microseconds. Also, the total disappearance of ozone from the optical path occurred over a time scale of 0.2 to 0.5 seconds. This process was due mostly to diffusion out of the optical path, though slow collisional decomposition following ozone absorption of the monitoring light also occurred. The latter process was negligible during the time scale of ozone formation. All other possible channels of oxygen atom formation following pulse radiolysis are expected to have been completed prior to initial observations.[61,62] Since sufficient energy is readily available under conditions of pulse radiolysis it is expected that both ground state O (^{3}P) and excited state O (^{1}D) were formed. De-excitation of O (^{1}D) by oxygen is very rapid with a rate constant greater than 9.9×10^{-12} cm^3/molec s.[118] At 750 torr of oxygen this would correspond to a half-life of about 3 ns. Thus it was assumed that the reactive oxygen atom species was O (^{3}P). Both the ozone $^1A_1$ ground state and the $^3B_2$ excited state form from ground state oxygen atom and ground state oxygen molecule.[119]

The agreement between the calculated and experimental data suggest than an electronically excited ozone precursor is a plausible explanation for the discrepancy in earlier investigations between the directly measured rate of oxygen atom disappearance and the independently measured rate of formation of vibrational ground state ozone. Although the disappearance of oxygen atoms is a third-order process[58,59] the formation of the majority of ground vibrational state ozone at 253.7 nm is nearly second-order with a rate constant of 4.1×10^{-15} cm^3/molec s.

APPENDIX

APPENDIX I

PULSE RADIOLYSIS COMPUTER PROGRAMS

Data Analysis Program

```
0 REM -- ANA47.BAS, FROM ANA46.BAS
1 GOTO 5000
2 POKW 40961,257
3 POKW 53262,17
4 Z9=CALL( 49418 )
5 GOTO 5260
6 REM
7 REM
8 REM -- CURVE FIT DATA IN K
1000 PRINT "Equation number ? ",;INPUT ,H9
1020 IF H9<0 THEN 9180
1040 H9=H9+1
1060 IF H9<=5 THEN 1340
1080 PRINT
1100 PRINT "Choose from:"
1120 FOR I=1 TO 5
1140 PRINT %%,"    ",I-1,"    ",
1160 ON I GOSUB 1240,1260,1280,1300,1320
1180 NEXT I
1200 PRINT
1220 GOTO 1000
1240 PRINT " A = A0 - K*t";RETURN
1260 PRINT " ln( A ) = ln( A0 ) - K*t";RETURN
1280 PRINT " ( 1/A ) = ( 1/A0 ) + K*t";RETURN
1300 PRINT " ln( A ) = ln( A0 ) - K*( 1/t )";RETURN
1320 PRINT " ln( A ) = ln( A0 ) - K*ln( t )";RETURN
1340 PRINT "Curve fit #",F1,"      Equation: ",
1360 ON H9 GOSUB 1240,1260,1280,1300,1320
1380 REM -- TURN MERLIN OFF HERE
1400 POKE 53262,65
1420 Z9=CALL( 49418 )
1440 S=0;S1=0;S2=0;S3=0;S5=0;S8=0;T3=0;T4=0;T5=0
1460 FOR I=N2 TO N3
1480 ON H9 GOTO 1500,1520,1540,1560,1580
1500 X( I )=I*2;Y( I )=K( I );GOTO1600
1520 X( I )=I*2;Y( I )=LOG( ABS( K( I ) ) );GOTO1600
1540 X( I )=I*2;Y( I )=1/K( I );GOTO1600
1560 X( I )=0.5/I;Y( I )=LOG( ABS( K( I ) ) );GOTO1600
1580 X( I )=LOG( I*2 );Y( I )=LOG( ABS( K( I ) ) )
1600 S1=S1+X( I );S2=S2+Y( I )
1620 S3=S3+X( I )*X( I )
1640 S5=S5+X( I )*Y( I )
1660 NEXT I
1680 T1=S1/N1;T2=S2/N1
1700 D1=N1*S3-S1*S1
```

```
1720 D2=(N1-2)*D1
1740 M=(N1*S5-S1*S2)/D1
1760 B=(S2-M*S1)/N1
1780 FOR I=N2 TO N3
1800 ON H9 GOTO 1820,1840,1860,1880,1900
1820 R(I)=M*I*2+B;GOTO1920
1840 R(I)=EXP(M*I*2+B);GOTO1920
1860 R(I)=1/(M*I*2+B);GOTO1920
1880 R(I)=EXP(0.5*M/I+B);GOTO1920
1900 R(I)=EXP(B)*(I*2)↑M
1920 S=S+(K(I)-R(I))↑2
1940 S8=S8+(Y(I)-M*X(I)-B)↑2
1960 T3=T3+(X(I)-T1)*(Y(I)-T2)
1980 T4=T4+(X(I)-T1)↑2;T5=T5+(Y(I)-T2)↑2
2000 NEXT I
2020 Q1=SQR(ABS(S8*S3/D2))
2040 ON H9 GOTO 2060,2080,2100,2080,2080
2060 M=-M;GOTO 2140
2080 M=-M;B=EXP(B);Q1=B*(EXP(Q1)-1);GOTO 2140
2100 Q1=1/(B-Q1)-1/B;B=1/B
2120 REM --- PLOT FITTED DATA
2140 I1=0;I2=0
2160 FOR I=N2 TO N3
2180 Y5=R(I)*Y7+Z1
2200 IF Y5<0 THEN 2260
2220 POKW I1+Y1,I*2+Z2;POKW I1+Y2,Y5+0.5
2240 I1=I1+2;I2=I2+1
2260 NEXT I
2280 POKW V+4,Y1;POKW V+6,Y2;POKW V+8,I2
2300 POKE V+12,255;POKE V+13,255
2320 Z9=CALL(P+9)
2360 REM -- TURN MERLIN BACK ON NOW
2380 POKE 53262,17
2400 Z9=CALL(49418)
2420 REM -- PRINT GRAPH AND RESULTS
2440 PRINT "Print it ? ",;INPUT ,C
2460 IF C=0 THEN RETURN
2480 IF C<>1 THEN 2440
2500 POKE 40962,2
2520 PRINT %%,"
```

```
2540 PRINT TAB(10),"Curve fit #",F1,"     ",
2541 ON A9 GOTO 2542,2544
2542 PRINT "normal ",;GOTO 2546
2544 PRINT "adjusted ",
2546 ON ABS(W) GOTO 2548,2550
2548 PRINT "run";GOTO 2560
2550 PRINT "buffer, ",A7," additions"
2555 PRINT "S=",ABS(J)
2556 ON A9 GOTO 2560,2557
2557 PRINT %3%,"Exp=",L2
2560 Z9=CALL(P1)
2580 PRINT %4%,TAB(10),"Scale:",
2600 PRINT TAB(17),X9*20,
2620 PRINT TAB(27),"micro-seconds per X division"
2630 ON A9 GOTO 2640,2660
2640 PRINT TAB(17),Y9*10/128,
2645 PRINT TAB(27),"volts per Y division (",
2650 PRINT Y9,"volts p-p)"
2655 GOTO 2700
2660 PRINT TAB(17),Y7,
2665 PRINT TAB(27),"Y multiplication factor"
2670 PRINT
2675 PRINT TAB(10),"Initial intensity = ",Y8
2700 PRINT %EZ3%
2720 PRINT TAB(10),"Standard deviations for ",
2740 ON H9 GOSUB 1240,1260,1280,1300,1320
2760 PRINT TAB(13),"Of A values  ",SQR(S/(N1-1))
2780 PRINT TAB(13),"Of K           ",SQR(ABS(N1*S8/D2))
2800 PRINT TAB(13),"Of A0          ",Q1
2820 PRINT
2840 PRINT TAB(10),"Value of K  = ",M
2860 PRINT TAB(10),"Value of A0 = ",B
2880 PRINT %5%
2900 PRINT TAB(10),"Correlation coefficient = ",ABS(T3/SQR(T4*T5))
2920 PRINT
2940 POKE 40962,1
2960 RETURN
2980 REM
3000 REM
3020 REM -- MAIN PROGRAM
3040 REM
5000 POKW 40961,257
5020 P=28672;V=P+2476;M5=P+2560
5040 P1=27392
5060 R5=24576+3584
5080 N=127
```

```
5100 Z1=30;Z2=15
5120 L0=(N+1)*2+20
5140 X1=M5+4;Y1=X1+L0+4;Y2=Y1+L0+4
5160 DIM F(N),G(N),R(N),H(N),K(N),X(N),Y(N)
5180 PRINT
5200 PRINT "Initialize ? ",;INPUT ,C
5220 IF C=1 THEN GOSUB 8980
5240 B7=CALL(B5)
5250 REM -- PROCESS COMMANDS
5260 PRINT
5280 PRINT "Command ? ",;INPUT ,C
5300 IF C<0 THEN 9180
5320 IF C<12 THEN 5380
5340 PRINT "*** Invalid command ***"
5360 GOTO 5260
5380 IF C>6 THEN 5440
5400 ON C+1 GOSUB 5540,5760,5920,6040,6220,6380,6940
5420 GOTO 5260
5440 ON C-6 GOSUB 7080,7490,7580,7660,7950
5480 GOTO 5260
5500 REM
5520 REM -- 0 = GET BIOMATION DATA
5540 PRINT %%,"Start reader now"
5550 Z9=CALL(B5+9)
5560 PRINT "Stop reader"
5570 IF Z9<>0 THEN PRINT "*** CRC error ***"
5580 I1=Y1
5600 FOR I=0 TO N
5610 Z9=PEEK(B7+I)+Z0;F(I)=Z9
5620 ON A9 GOTO 5640,5630
5630 Z9=LOG(Y8/(Y8-Z9))
5632 IF Z9<0 THEN Z9=0
5634 Z9=Z9↑L
5640 K(I)=Z9
5643 IF F(I)<0 THEN F(I)=0
5645 Z9=Z9*Y7+Z1+0.5
5646 IF Z9<0 THEN Z9=0
5650 POKW I1,Z9
5660 I1=I1+2
5680 NEXT I
5700 W=1
5720 GOTO 7240
5740 REM -- 1 = NEW BUFFER
5760 FOR I=0 TO N
5780 G(I)=F(I)
5800 NEXT I
5820 A7=1
5830 J=0
5840 IF W<>1 THEN GOSUB 6940
5860 W=3
5880 RETURN
5900 REM -- 2 = ADD TO BUFFER
```

```
5920 FOR I=0 TO N
5940 G(I)=G(I)+F(I)
5960 NEXT I
5980 A7=A7+1
6000 GOTO 7080
6020 REM -- 3 = SUBTRACT FROM BUFFER

6040 IF A7>0 THEN 6100
6060 PRINT "*** Too many subtracts ***"
6080 RETURN
6100 FOR I=0 TO N
6120 G(I)=G(I)-F(I)
6140 NEXT I
6150 J=J-1
6160 A7=A7
6165 IF A7=0 THEN A7=1
6180 GOTO 7080
6200 REM -- 4 = CURVE FIT RUN
6220 IF ABS(W-2)<>1 THEN GOSUB 6940
6240 GOSUB 6580
6260 IF N1<10 THEN RETURN
6270 W=-1
6340 GOTO 1000
6360 REM -- 5 = CURVE FIT BUFFER
6380 IF A7>0 THEN 6420
6400 PRINT "*** Buffer is empty ***";RETURN
6420 IF FIX(W/2)<>1 THEN GOSUB 7080
6440 GOSUB 6580
6450 W=-2
6460 IF N1<10 THEN RETURN
6540 GOTO 1000
6560 REM -- GET CURVE FIT RANGES
6580 N1=0;W=0
6600 PRINT %%,"Low T limit ",
6620 Z9=CALL(P+15);N2=FIX((PEKW(V+10)-Z2+1)/2)
6640 PRINT "Set at ",N2
6660 IF N2=>N THEN 6860
6680 PRINT "High T limit ",
6700 Z9=CALL(P+15);N3=FIX((PEKW(V+10)-Z2)/2)
6720 PRINT "Set at ",N3
6740 IF N3=>N THEN 6860
6760 IF N2>N3 THEN 6880
6780 N1=N3-N2+1
6800 IF N1<10 THEN 6900
6820 F1=F1+1
6840 RETURN
6860 PRINT "*** Out of range ***";RETURN
6880 PRINT "*** Invalid limits ***";RETURN
6900 PRINT "*** Not enough data points ***";RETURN
6920 REM -- 6 = PLOT RUN
6940 I1=Y1
```

```
6960 FOR I=0 TO N
6965 ON A9 GOTO 6970,6975
6970 POKW I1,Z9;I1=I1+2;Z9=F(I);GOTO 6980
6975 Z9=LOG(Y8/(Y8-F(I)));Z9=Z9↑L
6980 K(I)=Z9
6985 Z9=Z9*Y7+Z1+0.5
6986 IF Z9<0 THEN Z9=0
7000 NEXT I
7020 W=1
7040 GOTO 7240
7060 REM -- 7 = PLOT BUFFER
7080 IF A7<1 THEN 6400
7100 I1=Y1
7120 FOR I=0 TO N
7130 ON A9 GOTO 7135,7138
7135 Z9=G(I)/A7;GOTO7145
7138 IF G(I)<0 THEN G(I)=0
7140 Z9=LOG(Y8/(Y8-G(I)/A7));Z9=Z9↑L
7145 K(I)=Z9
7150 Z9=Z9*Y7+Z1+0.5
7151 IF Z9<0 THEN Z9=0
7155 POKW I1,Z9;I1=I1+2
7160 NEXT I
7180 W=2
7200 GOTO 7240
7220 REM -- DRAW AXIS AND PLOT DATA IN MEMORY
7240 Z9=CALL(P+3);REM - CLEAR SCREEN
7260 POKW X1-4,Z2;POKW X1-2,20
7280 POKW Y1-4,Z1;POKW Y1-2,10
7300 POKW V+4,X1-4;POKW V+6,Y1-4
7320 Z9=CALL(P+6);REM - DRAW AXIS
7340 POKW X1-4,1000;POKW Y1-4,1000
7360 POKW V+4,X1-4;POKW V+6,Y1-4
7380 Z9=CALL(P+6);REM - RESET ORIGIN
7400 POKW V+4,X1;POKW V+6,Y1
7420 POKW V+8,N;POKE V+12,0;POKE V+13,0
7440 Z9=CALL(P+9);REM - GRAPH DATA
7460 RETURN
7480 REM -- 8 = USE CALCULATED SLOPE
7490 ON A9 GOTO 7493,7495
7493 J2=1;GOTO 7500
7495 J2=2.303
7500 PRINT TAB(3),"F=",TAB(15),"K=",TAB(30 ),"R=",TAB(42 ),"I"
7505 PRINT %E3%
7507 FOR I=N2 TO N3 STEP 5
7510 PRINT F(I),TAB(12),K(I)/J2,TAB(27 ),R(I)/J2,TAB(40),I
7512 NEXT
7515 FOR I=0 TO N2 STEP 2
7517 PRINT F(I),TAB(12),K(I)/J2,TAB(40),I
7518 NEXT
7519 PRINT "INPUT X",;INPUT X
7520 IF X>N3 THEN GOTO 7531
7521 ON H9 GOTO 7522,7523,7524
```

```
7522 Y=2*M*X+B; GOTO 7529
7523 Y=B*EXP(-M*2*X);GOTO 7529
7524 Y=(1/B)+(2*M*X); Y=1/Y
7529 PRINT "Y=";Y/J2
7530 IF X<=N3 THEN GOTO 7519
7531 ON A9 GOTO 7540,7535
7535 PRINT "The R(I),K(I), and Y values are OD's"
7540 RETURN
7560 REM -- 9 = SET MODE AND SCALE FACTORS
7580 PRINT "Mode (1=normal,2=adjusted,3=switch) ? ";;INPUT ;A8
7581 IF A8<1 THEN 7580
7582 IF A8>3 THEN 7580
7585 IF A8<>3 THEN 7590
7586 ON A9 GOTO 7587,7588
7587 A9=2;Y7=Y6;GOTO 7620
7588 A9=1;Y7=1;GOTO 7620
7590 PRINT "Sample interval (micro-seconds) ? ";;INPUT ;X9
7593 A9=A8
7595 ON A9 GOTO 7600,7610
7600 PRINT "Full scale amplitude (volts) ? ";;INPUT ;Y9
7602 Y7=1
7609 GOTO 7620
7610 PRINT "Initial intensity ? ";;INPUT ;Y8
7612 PRINT "Graph height multiplier ?";;INPUT;Y6;Y7=Y6
7615 PRINT "Spectral line exponent ?";;INPUT;L;L2=1/L
7620 W=0
7625 RETURN
7640 REM -- 10 = CALIBRATE ZERO BASE LINE
7660 PRINT "Zero base offset ? ";;INPUT ;Z0
7670 RETURN
7930 REM -- 11 = PRINT DATA ON SCREEN
7950 GOTO 2440
7980 RETURN
8920 REM
8940 REM
8960 REM -- INITIALIZATION
8980 POKW V,57344;POKW V+2,65535
9000 Z9=CALL(P);Z9=CALL(P+12)
9020 I1=0
9040 FOR I=0 TO N
9060 POKW I1+X1,I1+Z2;I1=I1+2
9080 NEXT I
9100 RETURN
9120 REM
9140 REM
9160 REM -- EXIT
9180 Z9=CALL(P+12)
9200 POKW 40961,0
9220 PRINT "Run terminated"
9240 END
```

The Data Acquisition Program has different execution and comment lines from the Data Analysis Program in the following:

Data Acquisition Program

```
0 REM -- EXP45 , FROM EXP4.BAS

5440 ON C-6 GOSUB 7080,7500,7580,7660,7950,8120

5540 R1=R1+1
5550 PRINT %%,"Waiting-"
5560 Z9=CALL(B5+3)

7480 REM -- 8 = PRINT LAST CURVE FIT
7500 IF W<0 THEN 2500
7520 PRINT "*** No curve fit to print ***"
```

Note: these are all the lines between 7480 and 7540 in this program

```
7930 REM -- 11 = PUNCH BIOMATION DATA
7950 PRINT "Run # ",R1
7960 Z9=CALL(B5+6)
7970 INPUT C

8100 REM -- 12 = PRINT DATA ON SCREEN
8120 GOTO 2440
8130 RETURN
```

REFERENCES

1. J.M. Donovan and R.J. Hanrahan, "The Radiation Chemistry of Methyl Iodide in the Gas Phase," Int. J. Radiat. Phys. Chem., 3, 491 (1971).

2. G.A. Kennedy and R.J. Hanrahan, "Effect of Iodine and Other Scavengers on the Gamma Radiolysis of Liquid Perfluorocyclohexene," J. Phys. Chem., 78, 360 (1974).

3. E. Heckel and R.J. Hanrahan, "Ion-Molecule Reactions in the Systems CF_4-CH_4 and CF_4-C_2H_6," J. Chem. Phys., 63, 1027 (1975).

4. A.J. Frank and R.J. Hanrahan, "Gas Phase Radiation Chemistry of Ethyl Bromide," J. Phys. Chem., 80, 1532 (1976).

5. T.Hsieh and R.J. Hanrahan, "Gas Phase Radiation Chemistry of Pentafluoroethyl Iodide," Radiat. Phys. Chem., 12, 51 (1978).

6. M.S. Matheson and L.M. Dorfman, "Detection of Short-Lived Transients in Radiation Chemistry," J. Chem. Phys., 32, 187 (1960).

7. R.L. McCarthy and A. MacLachlan, "Transient Benzyl Radical Reactions Produced by High-Energy Radiation," Trans. Faraday Soc., 56, 1187 (1960).

8. L.M. Dorfman and M.S. Matheson, "Pulse Radiolysis," in Progress in Reaction Kinetics, G. Porter, Ed., Vol. 3, Pergamon Press, NY, 1965.

9. M. Ebert, J.P. Keen, and A.J. Swallow, Pulse Radiolysis, Academic Press, NY, 1965.

10. M.S. Matheson and L.M. Dorfman, Pulse Radiolysis, The MIT Press, Cambridge, Mass., 1969.

11. M.S. Matheson, "Pulse Radiolysis," in Advances in Radiation Research, Physics and Chemistry, J.F. Duplan and A. Chapiro, Eds., Vol. 1, Gordon and Breach Science Publishers, NY, 1973.

12. M.C. Sauer, Jr. and L.M. Dorfman, "Pulse Radiolysis of Gases," J. Am. Chem. Soc., 86, 4218 (1964).

13. R.F. Firestone and L.M. Dorfman, "Pulse Radiolysis of Gases," in Actions Chimiques et Biologiques des Radiations, M. Haissinsky, Ed., Vol. 15, Masson, Paris, 1971.

14. M.C. Sauer, Jr., "Pulse Studies of Gases," in Advances in Radiation Chemistry, M. Burton and J.L. Magee, Eds., Vol. 5, John Wiley & Sons, NY, 1976.

15. J.F. Duplan and A. Chapiro, Eds., Advances in Radiation Research, Physics and Chemistry, Vol. 1, Gordon and Breach Science Publishers, NY, 1973.

16. G.E. Adams, E.M. Fielden, and B.D. Michael, Eds., Fast Processes in Radiation Chemistry and Biology, John Wiley & Sons, NY, 1975.

17. M.A. West, "Flash Photolysis," in Creation and Detection of the Excited State, W.R. Ware, Ed., Vol. 4, Marcel Dekker, Inc., NY, 1975.

18. W.P. Bishop and L.M. Dorfman, "Kinetics of the Reaction of Gaseous Hydrogen Atoms with Molecular Oxygen by Fast Lyman-Alpha Absorption Spectrophotometry," J. Chem. Phys., 52, 3210 (1970.

19. D. Husain and L.J. Kirsch, "Study of Electonically Excited Carbon Atoms by Attenuation of Atomic Emission," Faraday Soc. Trans., 67, 2886 (1971).

20. S.O. Nielsen, P. Pagsberg, H. Christensen, and G. Nilsson, "Special UV Techniques in Pulse Radiolysis," in Advances in Radiation Research, Physics and Chemistry, J.F. Duplan and A. Chapiro, Eds., Vol. 1, Gordon and Breach Science Publishers, NY, 1973.

21. L.K. Patterson and J. Lilie, "A Computer-Controlled Pulse Radiolysis System," Int. J. Radiat. Phys. Chem., 6, 129 (1974).

22. A.T Thornton and G.S. Lawrence, "Computer-Based Systems for the Acquisition and Treatment of Kinetic Data from Flash Photolysis, Laser Photolysis, and Pulse Radiolysis Experiments," Radiat. Phys. Chem., 11, 311 (1978).

23. S.C. Crumpton, M.S. Adler, J.E. Ramirez, and R.J. Hanrahan, "Microcomputer-Based Data Acquisition System for Fast Chemical Kinetics," in Personal Computers in Chemistry, P. Lykos, Ed., John Wiley & Sons, NY, 1981.

24. D.C. Foyt, "A Minicomputer-Based System for Process Control, Data Acquisition, and Data Analysis in a Diverse Fast Kinetics Facility," private communication.

25. J.V.V. Kasper and G.C. Pimentel, "Atomic Iodine Photodissociation Laser," Appl. Phys. Lett., 5, 231 (1964).

26. J.V.V. Kasper and G.C. Pimentel, "Iodine-Atom Laser Emission in Alkyl Iodide Photolysis," J. Chem. Phys., 43, 1827 (1965).

27. R.J. Donovan and D. Husain, "Electronically Excited Halogen Atoms," in Advances in Photochemistry, Vol. 8, J.N. Pitts, G.S. Hammond, W.A. Noyes, Eds., John Wiley & Sons, NY, 1971, and references therein.

28. R.J. Donovan, F.G.M. Hathorn, and D. Husain, "Study of Electronically Excited Iodine Atoms in the Presence of Alkyl Iodides," Trans. Faraday Soc., 64, 3192 (1968).

29. D. Porret and C.F. Goodeve, "Analysis of the Alkyl Iodide Absorption Spectrum," Proc. Roy. Soc., A165, 31 (1938).

30. M. Ito, C. Huang, and E.M. Kowser, "Electronic Absorption Spectra of Iodo- and Bromomethanes," Trans. Faraday Soc., 57, 1662 (1961).

31. G.M. Harris and J.E. Willard, "Photochemical Reactions in the System Methyl Iodide, Iodine-Methane," J. Am. Chem. Soc., 76, 4678 (1954).

32. S.J. Riley and K.R. Wilson, "Excited Fragments from Excited Molecules: Energy Partitioning in the Photodissociation of Alkyl Iodides," Faraday Soc. Discuss., 53, 132 (1972).

33. M.R. Levy and J.P. Simons, "Vacuum Ultraviolet Photodissociation of Alkyl Iodides," J. Chem. Soc., Faraday Trans. 2, 71, 561 (1975).

34. R.T. Meyer, "Flash Photolysis and Time-Resolved Mass Spectrometry," J. Phys. Chem., 72, 1583 (1968).

35. D.H. Burde, R.A. McFarlane, and J.R. Wiesenfeld, "Collisional Quenching of Excited Iodine Atoms," Chem. Phys. Lett., 32, 296 (1975).

36. T. Donohue and J.R. Wiesenfeld, "Relative Yields of Electronically Excited Iodine Atoms in the Photolysis of Alkyl Iodides," Chem. Phys. Lett., 33, 176 (1975).

37. T. Donohue and J.R. Wiesenfeld, "Photodissociation of Alkyl Iodides," J. Chem. Phys., 63, 3130 (1975).

38. T. Donohue and J.R. Wiesenfeld, "Photochemistry of Alkyl Iodides," J. Phys. Chem., 80, 437 (1976).

39. R.E. Palmer and Padrick, "Relative Yield and Rate Constants for Deactivation of Electronically Excited Iodine Atoms Produced by Methyl Iodide Photolysis," J. Chem. Phys., 64, 2051 (1976).

40. S.L Baughcum and S.R. Leone, "Photofragmentation Infrared Emission Studies of Vibrationally Excited Free Radicals," J. Chem. Phys., 72, 6531 (1980).

41. R.J. Donovan and D. Husain, "Spin Orbit Relaxation of Metastable Iodine Atoms," Nature, 206, 171 (1965).

42. R.J. Donovan and D. Husain, "Primary Process in the Photolysis of Alkyl Iodides," Nature, 209, 609 (1966).

43. D. Husain and J.R. Wiesenfeld, "Study of Electronically Excited Iodine Atoms by Time-Resolved Emission," Nature, 213, 1227 (1967).

44. R. Donovan and C. Fotakis, "Isotope Effects in the Quenching of Electronically Excited Atoms," J. Chem. Phys., 61, 2159 (1974).

45. P. Cadman and J.C. Polyani, "Time-Resolved Emission Studies of Electronically Excited Iodine Atoms," J. Phys. Chem., 72, 3715 (1968).

46. M.A. Pollack, "Pressure Dependence of the Iodine Photodissociation Laser Peak Output," Appl. Phys. Lett., 8, 36 (1966).

47. R.N. Schindler and M.H.J. Winjen, "The Gas Phase Radiolysis of Ethyl Iodide," Z. Phys. Chem. Neue Floge, 38, 258 (1963).

48. K. Hohla and K.L. Kompa, "Gigawatt Photochemical Iodine Laser," Appl. Phys. Lett., 22, 77 (1973).

49. G. Breserlow, K. Hohla, and K.J. Witte, 7th European Conference on Plasma Production by High Power Lasers, Garching, 1974.

50. R. Volk, G. Brederlow, R. Brodmann, K. Eidmann, M. Nippus, S. Witkowski, and K.J. Witte, "Performance of the Asterix III High Power Iodine Laser," IEEE J. Quant. Elec., QE-15, 931 (1979).

51. G. Brederlow, R. Brodmann, K. Eidmann, M. Nippus, R. Petsch, S. Witkowski, R. Volk, and K.J. Witte, "Performance of the Asterix III High Power Iodine Laser," IEEE J. Quant. Elec., QE-16, 122 (1980).

52. R.E. Palmer and T.D. Padrick, "Sandia High Power Atomic Iodine Photodissociation Laser," in Electronic Transition Lasers, J.I. Steinfeld, Ed., MIT Press, Cambridge, Mass., 1976.

53. D.H. Burde, C.C. Davis, and R.A. McFarlane, "Collisional Quenching of Excited Iodine Atoms," ibid.

54. R.E. Beverly and M.C. Wong, "Trasverse Discharge Excitation of the Atomic Iodine Laser," Opt. Comm, 20, 19 (1977); 20, 23 (1977).

55. J.W. Wilson and J.H. Lee, "Modeling of a Solar-Pumped Iodine Laser," Va. J. Sci., 31, 34 (1980).

56. J.H. Lee and W.R. Weaver, "A Solar Simulator-Pumped Atomic Iodine Laser," Appl. Phys. Lett., 39, 137 (1981).

57. "Chemical Kinetic and Photochemical Data for Use in Stratospheric Modeling," Jet Propulsion Lab. Publ. 79-27, 1979.

58. I. Arnold and F.C Comes, "Temperature Dependence of the Reactions $O + O_3$ and $O + O_2 + M$," J. Chem. Phys., 42, 231 (1979).

59. O. Klais, P.C. Anderson, and M.J. Kurylo, "A Reinvestigation of the Temperature Dependence of the Rate Constant for the Reaction $O + O_2 + M$ by the Flash Photolysis Resonance Fluorescence Technique," Int. J. Chem. Kinetics, 12, 469 (1980).

60. R.K. Sparks, L.R. Carlson, K. Shobatake, M.L. Kowalczyk, and Y.T. Lee, "Ozone Photolysis: A Determination of the Electronic and Vibrational State Distributions of Primary Products," J. Chem. Phys., 72, 1401 (1980), and references therein.

61. M.C. Sauer, Jr. and L.M. Dorfman, "Pulse Radiolysis of Gaseous Argon-Oxygen Solutions," J. Am. Chem. Soc., 87, 3801 (1965).

62. C.J. Hochanadel, J.A. Ghormley, and J.W. Boyle, "Vibrationally Excited Ozone in the Pulse Radiolysis and Flash Photolysis of Oxygen," J. Chem. Phys., 48, 2416 (1968).

63. J.A. Ghormley, C.J. Hochanadel, and J.W. Boyle, "Yield of Ozone in the Pulse Radiolysis of Gaseous Oxygen at Very High Dose Rate," J. Chem. Phys., 50, 419 (1969).

64. M.C. Sauer, Jr., "A Pulse Radiolysis Study of the Dependence of the Reaction of Atomic Oxygen with Oxygen on the Nature of the Third Body," J. Phys. Chem., 71, 3311 (1967).

65. F. Kaufmann and J.R. Kelso, "M Effect in the Gas Phase Recombination of O with O_2," J. Chem. Phys., 46, 4541 (1967).

66. F. Kaufmann and J.R. Kelso, "Rate Constant of the Reaction $O + 2O_2 = O_2 + O_3$," Disc. Faraday Soc., 37, 26 (1964).

67. J.R. McNesby and H. Okabe, "Vacuum Ultraviolet Photochemistry," in Advances in Photochemistry, W.A. Noyes, Jr., G.S. Hammond, and J.N. Pitts, Jr., Eds., Vol. 3 , John Wiley & Sons, NY, 1964.

68. D.H. Volman, "Photochemical Gas Phase Reactions," ibid., Vol. 1, 1963.

69. A. Mathias and H.I. Schif, "Mass Spectrometric Studies of Atom Reactions," Discuss. Faraday Soc., 37, 38 (1964).

70. For reviews of early studies see references in Refs. 61,62,64,67, and 68.

71. G.M. Meaburn, D. Perner, J. LeCalve, and M. Bourene, "A Pulsed-Radiolysis Study of Atomic Oxygen Reactions in the Gas Phase," J. Phys. Chem., 72, 3920 (1968).

72. J.F. Riley and R.W. Cahill, "Absorption Spectrum of the Ozone Precursor," J. Chem. Phys., 52, 3297 (1970).

73. P.L.T. Bevan and G.R.A. Johnson, "Kinetics of Ozone Formation in the Pulsed Radiolysis of Oxygen Gas," J. Chem. Soc. Faraday Trans.I, 69, 216 (1973).

74. C.W. von Rosenberg, Jr. and D.W. Trainor, "Vibrational Excitation of Ozone Formed by Recombination," J. Chem. Phys., 61, 2442 (1974).

75. C.W. von Rosenberg, Jr. and D.W. Trainor, "Excitation of Ozone Formed by Recombination," J. Chem. Phys., 63, 5348 (1975).

76. T. Kleindienst, J.B. Burkholder, and E.J. Bair, "The Spectrum of Ozone During Formation by Recombination," Chem. Phys. Lett., 70, 117 (1980).

77. T. Kleindienst, J.R. Locker, and E.J. Bair, "Metastable Intermediates in the Formation of Ozone by Recombination," J. Photochem., 12, 67 (1980).

78. R.E. Huie, J.T. Herron, and D.D. Davis, "Absolute Rate Constants for the Reaction O + O_2 + M Over the Temperature Range 200-346 ^oK," J. Phys. Chem., 76, 2653 (1972).

79. E.C.Y. Inn and Y. Tanaka, "Absorption Coefficient of Ozone in the UV and Visible Regions," J. Opt. Soc. Am., 43, 870 (1953).

80. W.B. DeMore and O. Raper, "Hartley Band Extinction Coefficients of Ozone," J. Phys. Chem., 68, 412 (1964).

81. L.M. Dorfman, "Pulse Radiolysis," in Techniques of Chemistry, G.G. Hammes, Ed., Vol. 6, Pt. 2, John Wiley & Sons, NY, 1974.

82. a. Y. Hatano, private communication.
b. Y. Hatano, S. Takao, and T. Ueno, "Phosphorescence of Biacetyl Sensitized by Benzene in Gas Phase Pulse Radiolysis," Chem. Phys. Lett., 30, 429 (1975).

83. a. J.A. Irvin, private communication.
b. T.I Quickenden, J.A. Irvin, and D.F. Sangster, "Time-Resolved Emission from OH Produced by the Pulse Radiolysis of Water Vapor," J. Chem. Phys., 69, 4395 (1978).

84. S. Kinsman, Radiological Health Handbook, U.S. Dept. of Health, Education, and Welfare, 1957, p. 53.

85. J.W. Boag, "Physical Methods in Radiation Chemistry and Radiobiology," in Ations Chimiques et Biologuiques des Radiations, M. Haissinsky, Ed., Vol. 6 , Masson, Paris, 1963.

86. W. Braun and M. Lenzi, "Resonance Fluorescence Method for Kinetics of Atomic Reactions," Disc. Faraday Soc., 44, 256 (1967).

87. D.D. Davis, W. Braun, and A.M. Bass, "Reactions of the Ground State Chlorine Atom," J. Chem. Kinet, 2, 101 (1970).

88. J.U. White, "Long Optical Paths at Large Aperature," J. Opt. Soc. Am,, 32, 285 (1942).

89. D.D. Davis and W. Braun, "Intense Vacuum Ultraviolet Atomic Line Sources," Appl. Optics, 7, 2071 (1968).

90. F.C. Fehsenfeld, K.M. Evenson, and H.P. Broida, "Microwave Discharge Cavities Operating at 2450 MHz," Rev. Sci. Instrum., 36, 294 (1965).

91. J.W. Hunt, C.L. Greenstock, and M.J. Bronskill, "Design Considerations for Nanosecond Pulse Radiolysis Studies," Int. J. Rad. Phys. Chem., 4, 87 (1972).

92. A. Fenster, J.C.LeBlanc, W.B. Taylor, and H.E. Johns, "Linearity and Fatigue in Photomultipliers," Rev. Sci. Instrum., 44, 689 (1973).

93. P. Hartek, R.R. Reeves, and B.A. Thompson, "The Iodine Lamp: A Light Source for Selective Excitation of CO," Z. Naturforschg., 19a, 2 (1964).

94. C.C. Kiess and C.H. Corliss, "Description and Analysis of the First Spectrum of Iodine," J. Res. Nat. Bur. Stand., 63a, 1 (1959).

95. A.N. Zaidel and E.Y. Shreider, Vacuum Ultraviolet Spectroscopy, Ann Arbor-Humphery Science Publishers, Ann Arbor, MI, 1970.

96. W. Braun and T. Carrington, "Line Emission Sources for Concentration Measurements and Photochemistry," J. Quant. Spec. Radiat. Transfer, 9, 1133 (1969).

97. E.A. Ogryzlo, "Halogen Atom Reactions," Can. J. Chem., 39, 2556 (1961).

98. J.A. Blake and G. Burns, "Kinetics of Iodine Atom Recombination Between 300 and 1164 °K," J. Chem. Phys., 54, 1480 (1971).

99. T. Carrington and H.P. Broida, "Wall Effects on Rotational Populations of OH in a Microwave Discharge," J. Molec. Spec., 2, 273 (1958).

100. F.M. Charbonnier, J.P. Barbour, and J.L. Brewster, "Electron Source for Pulse Radiolysis," in Fast Processes in Radiation Chemistry and Biology, G.E. Adams, E.M. Fielden, and B.D. Michael, Eds., John Wiley & Sons, NY, 1975.

101. Hewlett-Packard, McMinnville Division, Bulletin No. 5952-6730.

102. Hewlett-Packard, McMinnville Division, Model 706 System Instruction Manual.

103. S. Gordon, K.H. Schmidt, and J.E. Martin, "A TV Scanning Method for Recording Time-Resolved Optical Spectra of Transients Produced by a Single Pulse of Electrons," Rev. Sci. Instrum., 45, 552 (1974).

104. Biomation, Model 610B Manual, Part No. 0610-0051, Cupertino, CA.

105. The author was not involved with the IMSAI 8080 system design, construction, or initial software.

106. T. Barret, D. Lunney, A.D. Salt, and M. Walter, "A Microcomputer-Controlled Transient Recorder," J. Chem. Ed., 56, 67 (1979).

107. L.F. Fiser and M. Fieser, Reagents for Organic Synthesis, John Wiley & Sons, NY, 1967, p. 17.

108. D. Husain and J.R. Wiesenfeld, "Time-Resolved Emission Studies of Electronically Excited Iodine Atoms," Trans. Faraday Soc., 63, 1349 (1967).

109. R.J. Donovan and D. Husain, "Deactivation of Excited Iodine Atoms," Trans. Faraday Soc., 62, 11 (1966).

110. G.M. Lawrence, "Resonance Transition Probabilities in Intermediate Coupling for Some Neutral Non-Metals," Astrophys. J., 148, 261 (1967).

111. R.J. Donovan, E.G.M. Hathorn, and D. Husain, "Reaction of Electronically Excited Iodine Atoms with Methyl Iodide," J. Chem. Phys., 49, 953 (1968).

112. D. Detar, "A Computer Program for Making Steady State Calculations," J. Chem. Ed., 44, 193 (1967).

113. A.J. Frank, "The Radiation Chemistry and Photochemistry of Ethyl Bromide in the Gas Phase," Ph. D. Dissertation, University of Florida, 1975.

114. T. Hsieh, "The Radiation Chemistry and Mass Spectrometry of Trifluoromethyl Iodide and Pentafluoroethyl Iodide in the Gas Phase," Ph. D. Dissertation, University of Florida, 1976.

115. J.M. Hoffman, E.L. Patterson, and R.A. Gerber, "Energy Extraction from a Large-Volume HF Laser Amplifier," J. Appl. Phys., 50, 3861 (1979).

116. G.C. Tisone and J.M. Hoffman, "Effect of Rare-Gas Diluents on the Performance of an XeCl Laser Pumped by a High-Intensity Electron Beam," Appl. Phys. Lett., 39, 145 (1981).

117. R. Marcotte, "The Radiation Chemistry of Gas Phase Carbon Tetrachloride-Carbon Tetrafluoride Mixtures," Ph. D. Dissertation, p.87, University of Florida, 1968.

118. R.A. Young and G. Block, "Deactivation of $O(^1D)$," J. Chem. Phys., 47, 2311 (1967).

119. P.J. Hay and T.H. Dunning, "Geometries and Energies of the Excited States of O_3 from ab initio Potential Energy Surfaces," J. Chem. Phys., 67, 2290 (1977).

BIOGRAPHICAL SKETCH

Jorge E. Ramirez was born in Belize, British Honduras, on March 18, 1952. He moved with his family to Merida, Yucatan, Mexico, in 1955 and to Miami, Florida, in 1959.

He received the Bachelor of Science degree in chemistry at the Florida State University in 1974.

During Graduate School at the University of Florida he held graduate teaching and research assistantships in the Department of Chemistry.

Jorge is the youngest son of Luis and Anita. His brothers are Miguel, Juan, and Luis.

I certify that I have read this study and that in my opinion it conforms to acceptable standards of scholarly presentation and is fully adequate, in scope and quality, as a dissertation for the degree of Doctor of Philosophy.

Robert J Hanrahan

Robert J. Hanrahan, Chairman
Professor of Chemistry

I certify that I have read this study and that in my opinion it conforms to acceptable standards of scholarly presentation and is fully adequate, in scope and quality, as a dissertation for the degree of Doctor of Philosophy.

M Luis Muga

M. Luis Muga
Professor of Chemistry

I certify that I have read this study and that in my opinion it conforms to acceptable standards of scholarly presentation and is fully adequate, in scope and quality, as a dissertation for the degree of Doctor of Philosophy.

Phillip M. Achey

Phillip M. Achey
Professor of Microbiology

This dissertation was submitted to the Graduate Faculty of the Department of Chemistry in the College of Liberal Arts and Sciences and to the Graduate Council, and was accepted as partial fulfillment of the requirements for the degree of Doctor of Philosophy.

December 1981

Dean, Graduate School

UNIVERSITY OF FLORIDA
3 1262 08553 5242